UNIVERSITY OF CALIFORNIA, SAN DIEGO

Structural details and mechanism of filamentous actin organization by the isoforms vinculin and metavinculin

A dissertation submitted in partial satisfaction of the

requirements for the degree of Doctor of Philosophy

in

Molecular Pathology

by

Maria Elisabeth Janssen

Committee in charge:
- Professor Dorit Hanein, Chair
- Professor Sanford Shattil, Co-Chair
- Professor Timothy Baker
- Professor Mark Ginsberg
- Professor Robert Liddington
- Professor Robert Ross

2010

The dissertation of Maria Elisabeth Janssen is approved, and it is acceptable in quality and form for publication on microfilm and electronically:

_____

_____

_____

_____

_____
Co-Chair

_____
Chair

University of California, San Diego

2010

Table of Contents

List of Abbreviations

ABP	actin binding protein
ADP	adenosine diphosphate
ATP	adenosine triphosphate
F-actin	filamentous actin
G-actin	monomeric actin
CCD	charge coupled device
CD	α-catenin domain
CTF	contrast transfer function
FRET	forster resonance energy transfer
IEF	isoelectric focussing
HSP	high speed pellet
LSP	low speed pellet
Sup	supernatant
Vh	vinculin head
(M)Vt	(meta)vinculin tail domain
Vfl	full length vinculin
VBS	vinculin binding site
2D	two-dimensional
3D	three-dimensional

List of Figures

Movies related to the Molecular Cell article (chapter 3) can be found online via Sciencedirect:

Movie S1. Fit of Vinculin Tail Crystal Structure into Corresponding Difference Density

Movie S2. Fit of Vinculin Tail F-Actin Model into Corresponding Reconstruction

List of Tables

Acknowledgements

I would like to thank my advisor, Dr. Dorit Hanein, for the opportunity she gave me to work on my thesis in her laboratory and for her encouragement to continue my graduate studies three years ago. Her support and guidance through the past five and a half years have been invaluable. In addition I would like to thank my thesis committee members, Dr. Timothy Baker, Dr. Mark Ginsberg, Dr. Robert Liddington, Dr. Robert Ross and Dr. Sanford Shattil for their advice and encouraging comments as I advanced towards the dissertation. I would like to thank Dr. Andrey Bobkov for his advice and help with DSC and AUC experiments. Thanks to Dr. Niels Volkmann for all the times he evaluated and advised on the image reconstruction and analysis part, and his help on the projects that are not included in this dissertation.

I would like to thank Dr. Ya Chen for generating the VBS3-peptide, Dr. R. Liddington for providing some of the vinculin and metavinculin constructs and the CD3 construct, and Dr. D. Critchley for providing the talin VBS2 and VBS3 constructs.

Thanks to Scott Snipas for performing the N-terminal sequencing and to Allen Liu for helping me out with the TIRF experiments at Scripps Institute. Although these experiments did not work out, your enthusiasm was definitely contagious and our discussions helped me advancing the last part of this work!

I have had the pleasure to work with many wonderful people over the past few years and I would like to thank them for their friendship as well as their advice and support during my time in lab. I would like to acknowledge all the members of the Hanein lab and Volkmann lab, especially Larnele for her help and making the lab a

happy workplace with her positive view on everything! Many thanks to Robert, Eldar, Dalaver and Wendy for all their support and advice.

Many thanks to all my friends, especially Morgan, Nisha, Linda, Emi, Manja and Bartosz, not only for discussing research or practicing talks, but also for the numerous dinners and fun hiking, skiing and climbing trips. Good luck with finishing your thesis! Thanks to my friends back home who cared for me every time I visited the Netherlands and made me feel close even when I am here in San Diego.

I would like to thank my family, Harry, Marion, Bram, Jojanneke and Jeroen, for their enormous support. You thought me to keep things in perspective and remind me of what is important in life. That means the world to me!

And last but definitely not least to Brandon: although you often did not entirely understand what I was working on, you were always interested and supportive. Thanks for your patience and your love. Thank you for being my best friend, Brando!

Chapter 3, in full is a reprint of the material as it appears in Molecular Cell, January 2006, Mandy E.W. Janssen, Eldar Kim, Hongjun Liu, L. Miya Fujimoto, Andrey Bobkov, Niels Volkmann and Dorit Hanein, 21(2): 271-281. The dissertation author was the primary investigator and the co-authors listed in this publication provided significant scientific input or supervised the research which forms the basis for this chapter.

Chapter 5, in part is currently being prepared for submission for publication of the material. Mandy Janssen, Hongjun Liu, Robert Jeng, Larnele Hazelwood, Niels Volkmann and Dorit Hanein. The dissertation author was the primary investigator and author of this material.

Vita

2001	Bachelor of Science, Department of Biomedical Engineering, University of Technology, The Netherlands
2003	Master of Science, Department of Biomedical Engineering, University of Technology, The Netherlands
2002-2003	Teaching assistant, Department of Biomedical Engineering, University of Technology, The Netherlands
2003-2010	Research assistant, Sanford-Burnham Medical Research Institute, La Jolla, USA
2010	Doctor of Philosophy, University of California, San Diego, USA

Publications

Mandy E.W. Janssen, Eldar Kim, Hongjun Liu, L.Miya Fujimoto, Andrey Bobkov, Niels Volkmann, Dorit Hanein. “Three-dimensional structure of vinculin bound to actin filaments”, *Molecular Cell*. 2006 Jan 20; **21**: 271-281.

Mandy E.W. Janssen, Hongjun Liu, Robert Jeng, Larnele Hazelwood, Niels Volkmann, Dorit Hanein. “A 68aa insert changes a bundling protein into a severing protein: actin organization by vinculin and metavinculin*”. In preparation*.

Field of study

Major Field: Molecular Pathology

Studies in Cell Adhesion & Migration

Dr. Dorit Hanein

ABSTRACT OF THE DISSERTATION

Structural details and mechanism of filamentous actin organization by the isoforms vinculin and metavinculin

by

Maria Elisabeth Janssen

Doctor of Philosophy in Molecular Pathology

University of California, San Diego, 2010

Professor Dorit Hanein, Chair

Professor Sanford Shattil, Co-Chair

Vinculin and its splice variant metavinculin are actin binding proteins involved in the organization of actin filaments, which is necessary in cellular processes such as cell migration, division and differentiation. Vinculin is essential in formation of a stable link between the actin cytoskeleton and the cell membrane via proteins such as talin and α-catenin. A lack of vinculin causes cells to adhere less and have a higher motility, while *in vivo* this results in impaired neuronal development and heart malfunction causing early death. In this dissertation, I characterized the structural details of how vinculin and metavinculin organize actin filaments.

Transmission electron microscopy is the only technique to obtain high resolution structural information on actin-vinculin assemblies, since these are too large to solve with NMR and are non-crystallizable. A near-atomic model generated by electron

microscopy, computational docking and biochemistry reveals the structural details of the actin-vinculin tail interaction. Furthermore, binding to actin filaments causes a conformational change in the vinculin tail domain which exposes its dimerization site and subsequently induces actin bundling. A combinatorial input of two or more ligands has been proposed to activate vinculin. In the presence of F-actin, full length vinculin is activated by α-catenin's CD3 domain and several talin domains. CD3 turns out to be the most efficient activator. A slightly smaller, constituently active vinculin construct binds F-actin similar to the vinculin tail. In addition, the smaller construct induces formation of comparable actin bundles except that it leads to a larger spacing between filaments owing to the presence of the head domain.

Despite an additional 68aa insert in the metavinculin tail domain, both vinculin isoforms bind actin filaments similarly. Interestingly, biochemical and biophysical techniques indicate that the metavinculin tail does not bundle, but instead severs actin filaments in a dose dependent manner. This severing activity is not affected by a cardiomyopathy related mutation in the metavinculin tail insert. However, this mutation might influence the affinity between the head and tail domains.

These studies have lead to a molecular model for actin organization by vinculin in adhesion sites and describe a new function for the isoform metavinculin.

Chapter 1

Background: Vinculin and metavinculin

Macromolecular organization of actin filaments is important for many cellular processes such as cell motility, division, shape, and differentiation. The isoforms vinculin and metavinculin (Fig 1-1) are essential actin binding proteins that regulate the formation of stable actin filament assemblies. They are present in cell structures like adhesion junctions, dense plaques, intercalated disks and costameres. These structures are able to confer mechanical strength to tissue and they need to be highly dynamic and coordinated. A primary motivation for the current study was to characterize the molecular details of how activated vinculin and metavinculin organize actin filaments in these cellular structures.

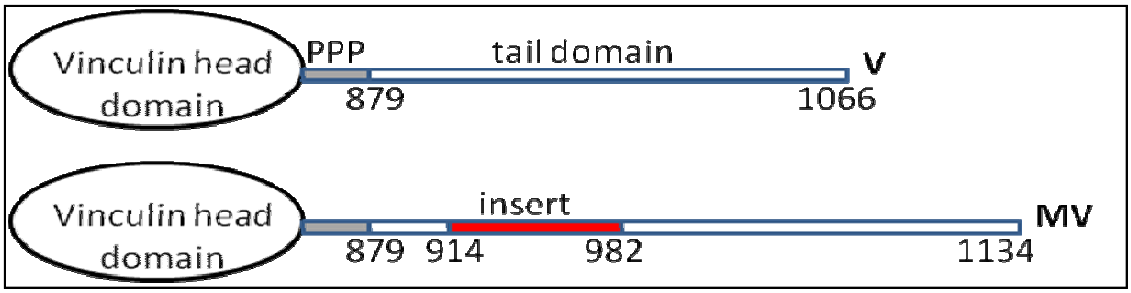

Fig 1-1. Schematic representation of Vinculin and Metavinculin. Both C-terminal tail domains start at amino acid 879. Metavinculin shows the position of the insert in the tail domain. PPP: proline-rich region, V: Vinculin, MV: Metavinculin.

Localization and function *in-vivo*

Vinculin plays a major role in connecting the ends of actin filaments to the cytoplasmic domains of either cadherins via α-catenin in cell-cell adhesions (Weiss, Kroemker et al. 1998) or of integrins via talin in cell-matrix adhesions (Burridge and

Mangeat 1984). It was one of the first proteins discovered to be part of focal adhesions, Fig. 1-2 (Geiger, Tokuyasu et al. 1980), but many other cytoplasmic plaque proteins were revealed since. Vinculin interacts with several different proteins, such as VASP (Brindle, Holt et al. 1996), vinexin (Kioka, Sakata et al. 1999), ponsin (Mandai, Nakanishi et al. 1999), α-actinin (Kroemker, Rudiger et al. 1994), talin (Johnson and Craig 1994), PIP2 (Johnson, Niggli et al. 1998) and paxillin (Turner, Glenney et al. 1990). Interestingly, talin and α-actinin both couple actin filaments to integrins and they also both bind the vinculin head domain via helical bundle conversion. Binding both actin and talin or α-actinin is one way in which vinculin could stabilize focal adhesions. Another way involves modulation of FAK and paxillin signaling by vinculin. The C-terminal tail region of vinculin resembles the C-terminal focal adhesion targeting region of FAK and they both bind overlapping sequences in paxillin (Bakolitsa, de Pereda et al. 1999). Vinculin moderates the FAK-paxillin interaction, which in turn causes decreased paxillin phosphorylation and leads to reduced cell motility and survival mediated by ERK1/2 (Subauste, Pertz et al. 2004). Phosphorylation of two tyrosines (Y100 and Y1065) in vinculin by Src kinases decreases cell spreading (Zhang, Izaguirre et al. 2004). Y1065 phosphorylation enhances the exchange dynamics of vinculin, enabling the focal adhesion junction to grow upon external force application. During maturation vinculin gets dephosphorylated and stably incorporated into these junctions, which then become highly mechanically resistant (Diez, Kollmannsberger et al. 2009; Mohl, Kirchgessner et al. 2009).

Vinculin has been studied extensively over the last two decades, but not much is known about its isoform, metavinculin. The vinculin gene contains an exon that codes

for the metavinculin-specific insert, which is alternatively spliced to obtain both vinculin and metavinculin mRNA (Byrne, Kaczorowski et al. 1992; Koteliansky, Ogryzko et al. 1992). Vinculin is expressed ubiquitously, whereas metavinculin is only found in platelets (Turner and Burridge 1989) and muscle tissue (Saga, Hamaguchi et al. 1985; Glukhova, Kabakov et al. 1986; Belkin, Ornatsky et al. 1988; Belkin, Ornatsky et al. 1988; Gimona M. 1988). Muscle specific isoforms of actin regulating proteins are common in mammals. UNC-60B, an ADF/cofilin family actin binding protein of *Caenorhabditis elegans*, is specific for muscle tissue, yet its splice variant UNC-60A is expressed in various tissues. UNC-60B has a stronger actin severing activity and induces faster pointed-end depolymerization than UNC-60A (Yamashiro, Mohri et al. 2005). Also, the expression of twinfilin isoform Twf2b is restricted to striated muscle, butTwf2a is expressed in most non-muscle tissues. The difference between these isoforms is a higher affinity for ADP-G-actin of Twf2a. (Nevalainen, Skwarek-Maruszewska et al. 2009). However, the reason for a muscle specific isoform of vinculin remains to be elucidated.

Metavinculin co-localizes with vinculin in membrane-associated dense plaques of smooth muscle and in intercalated disks and costameres of cardiac muscle (Belkin, Ornatsky et al. 1988; Witt, Zieseniss et al. 2004). The amount of metavinculin varies depending on the muscle type. In skeletal muscle metavinculin accounts for ~6-8% of the total vinculin pool, in smooth muscle ~40-50%, and in cardiac muscle ~20% (Belkin, Ornatsky et al. 1988). Human fetal aortas contain ~5-7% metavinculin, a two month old child aorta contains 10%, after six months this is increased up to 31% and a 1.5 year old child aorta contains as much as 39% (Glukhova, Frid et al. 1990). Expression of metavinculin in vivo is closely related to the differentiation of muscle

cells, whereas vinculin expression is equally high during embryogenesis (Saga, Hamaguchi et al. 1985; Glukhova, Frid et al. 1990). During the cultivation of smooth muscle cells in vitro the amount of metavinculin decreases in time. Metavinculin is present in all focal contacts when the cells just finish spreading, but then disappears when cells no longer contract (Glukhova, Kabakov et al. 1986; Belkin, Ornatsky et al. 1988; Sobue, Hayashi et al. 1999). This suggests a role for metavinculin in force transduction.

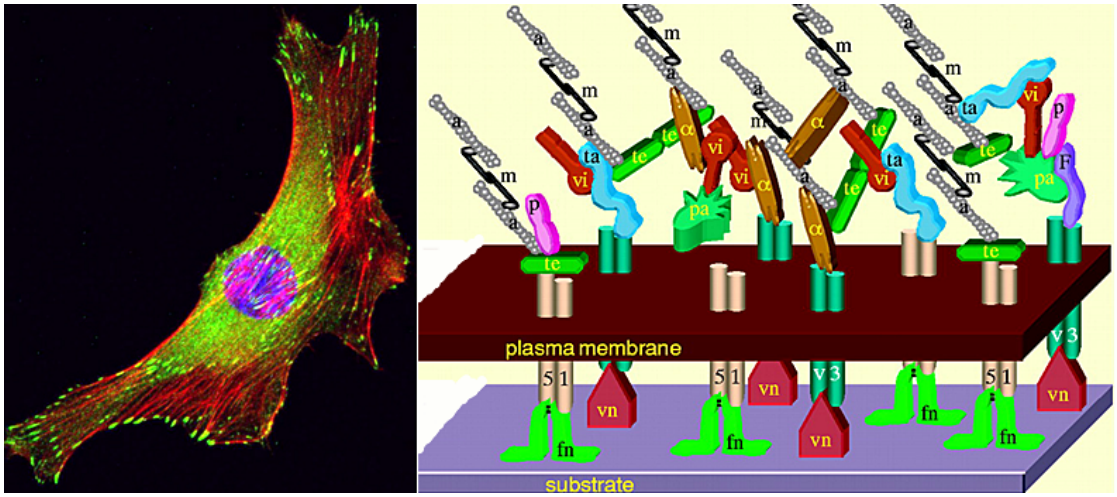

Fig. 1-2 Vinculin localizes at the ends of actin bundles at focal adhesion sites. (Left) Fluorescently labeled F-actin (red) running through a C2C12 myoblast cell and fluorescently labeled vinculin (green) associated with focal adhesion sites. (Imaged by Z. Al-Rekabi, webpage Pelling laboratory). (Right) Hypothetical molecular model of a focal adhesion contact (Zamir and Geiger 2001).

The biological significance of vinculin and metavinculin

The importance of vinculin has been shown by vinculin knock-out F9 embryonic mouse carcinoma cells and mouse embryonic fibroblasts that were less adhesive, had less and smaller focal adhesions, and had increased motility on 2D substrates

and had a rounder shape (Xu, Baribault et al. 1998). They also exhibited higher talin and paxillin concentrations and FAK activity compared to wild-type cells. Over-expression of vinculin induces stronger adhesion and less motility (Rodriguez Fernandez, Geiger et al. 1992). This protein in fact has been shown to act as a tumor suppressor (Rodriguez Fernandez, Geiger et al. 1992). In addition, vinculin null mice (lacking both vinculin and metavinculin) do not survive beyond embryonic day 10 due to heart malfunction and impaired development of the neuronal system. Heterozygous inactivation of vinculin (and thus metavinculin) induces stress-induced heart problems. Although talin is the key regulator of integrin regulation, vinculin is suggested to be essential for focal adhesion growth by recruiting other focal adhesion components and forming a stable link to the actin cytoskeleton (Humphries, Wang et al. 2007).

Besides the structural role that vinculin plays in connecting the actin cytoskeleton to cell adhesion associated proteins, there is evidence that vinculin also has important regulatory roles. For example, vinculin binds Arp2/3 without F-actin binding being involved and this interaction is stimulated by induction of lamellipodia formation (DeMali, Barlow et al. 2002). Binding to vinculin recruits Arp2/3 to the leading edge of migrating cells and is suggested to localize actin assembly to newly engaged integrins (DeMali, Barlow et al. 2002). In addition, vinculin recruits paxillin to focal adhesions and thereby regulates cell survival and migration (Subauste, Pertz et al. 2004).

Structure of vinculin and metavinculin

Vinculin is a 116kD protein, that has been shown by early electron microscopy and biochemical studies to consist of a globular head (residues 1-835) and a tail domain (residues 896-1066), connected by a flexible proline-rich region (Winkler, Lunsdorf et al. 1996). The crystallographic model of vinculin shows that the head domain consists of four subdomains (D1-4), the first three of them comprise two, four-helix bundles in which a central helix traverses the length of the subdomain. Domain 4 is a four-helix bundle that packs end to end with the vinculin tail domain (domain 5) and is linked via a proline-rich region, see Fig. 1-1 (Bakolitsa, Cohen et al. 2004; Borgon, Vonrhein et al. 2004).

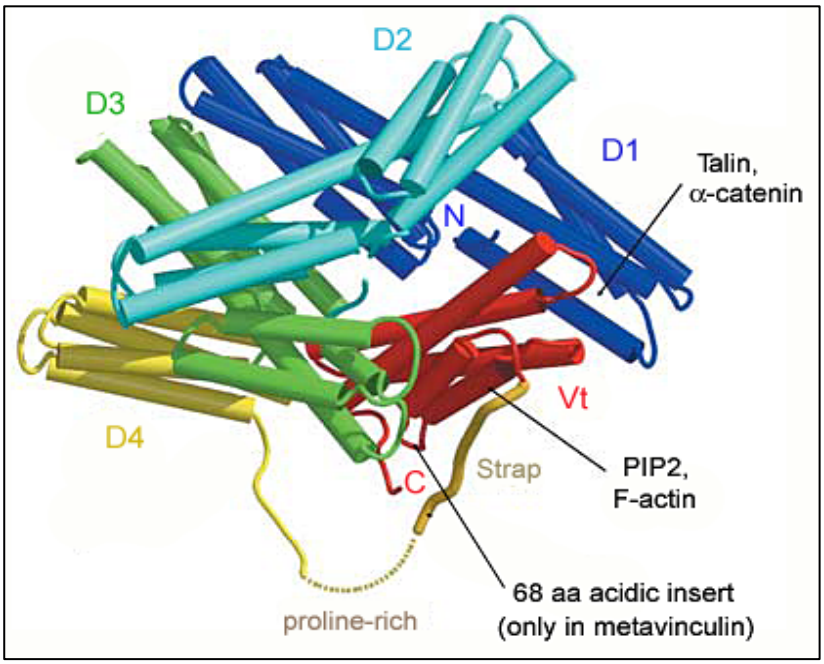

Fig. 1-3 Crystallographic model of vinculin in its auto-inhibited state. The vinculin tail domain is shown in red. (Bakolitsa, Cohen et al. 2004). The insert in metavinculin is located between helix I and II of Vt.

Vinculin is highly conserved among species and the sole difference between vinculin and metavinculin is a 68 amino acid acidic insert in the tail domain. The insert is located between helix I and II of the tail domain, just after amino acid 914 (Fig. 1-1). It is flanked on both sides by a KWSSK-motif and the C-terminal part of the insert contains a repeat of a region located just N-terminal of the insert. It is striking that the second half of the insert containing this repeat is highly conserved between species (Fig. 1-4). No atomic model of metavinculin is available yet, but some predict the insert to consist of two α-helices interspaced by three coil regions (Gimona, Small et al. 1988), or of three α-helical regions interspaced by two loops (Olson, Illenberger et al. 2002).

```
human           MAARQLHDEARKWSSK-PGI---PAAEVGIGV--------VAEADAADA
chicken         MAARQLHDEARKWSSK-PVT---VINEAAEAV-------DIDEEDDAD-
pig             MAARQLHDEARKWSSK-PGN---PAAKVGIGV--------VAEADAADA
frog            -----------KWSSKSPGNYDYPAPQGREAVISEVEQAQEEEEEEA-S
                           ***** *        :   .*          * : *

human           DYEPELLLMPSNQPVNQPILAAAQSLHREATKWSSKG aGFPVPPDMED
chicken         DYEPELLLMPTNQPVNQPILAAAQSLHREATKWSSKG VEFSLPSDIED
pig             DYEPELLLMPSSQPVNQPILAAAQSLHREATKWSSKG VGFPVPSDMED
frog            DYEPELLLVPEGQPVNQPMLAAAQSLHREATKWSSKG VEFALSSDIED
                ********:* .******:****************** . *.:..*:**
```

Fig. 1-4 Alignment of the Metavinculin insert region among several species. Residues 898-993 are shown. (CLUSTAL FORMAT for T-COFFEE Version_7.71 [http://www.tcoffee.org] [MODE: regular], CPU=0.21 sec, SCORE=88, Nseq=4, Len=97).

Vinculin and metavinculin activation

As described earlier, numerous vinculin binding ligands have been characterized. Examples are talin, α-actinin, α- and β-catenin binding the vinculin head domain, Arp2/3, VASP, ponsin and vinexin binding the proline-rich region, and PIP2, paxillin

and actin binding the tail domain (Zamir and Geiger 2001; Zamir and Geiger 2001; DeMali, Barlow et al. 2002). However, most of these ligand binding sites are masked by an intramolecular interaction between the vinculin head and tail domain. In this state vinculin is called inactive. Vinculin is active when it is rendered in an open conformation and can bind its ligands. Forster resonance energy transfer (FRET) was used to show that vinculin is in an inactive state in the cell cytoplasm, but that it undergoes a conformational change resulting in the active vinculin form at the focal adhesion sites (Chen, Cohen et al. 2005).

As seen in the crystallographic structure (Fig. 1-3), the tail domain is held in an auto-inhibited state by Domains 1 and 3. The top of the vinculin tail five-helix bundle structure makes an extensive hydrophobic contact with Domain 1. Two additional contacts with the top of Domain 4 and a mostly polar interaction with Domain 3 increase the binding affinity from 20-50 nM between Domain 1 and Vt to less than 1 nM between the complete head domain and Vt in the full length protein (Bakolitsa, Cohen et al. 2004). The vinculin tail domain binds F-actin with an affinity of about 1 μM (Johnson and Craig 1995) and its interactions with talin or α-actinin are even weaker. This leads to the proposal of a vinculin activation mechanism that describes the necessity of a combinatorial input of two or multiple vinculin binding ligands (Bakolitsa et al. 2004). Vinculin is not unique in exploiting such an auto-inhibitory mechanism. Myosin II, Src kinase and ezrin are also proteins that need to be activated in order to expose their otherwise cryptic binding sites (Chambers and Bretscher 2005; Ozkirimli and Post 2006; Vicente-Manzanares, Ma et al. 2009). However, these proteins are activated upon phosphorylation, whereas vinculin is suggested to be activated synergistically by multiple ligands. Binding of an

appropriate ligand has to induce dramatic movements, rearrangements and distortions in the N-terminal vinculin head domain, thereby disrupting the vinculin head-tail interaction from a distance. Provoking these dramatic changes in the conformation of α-helices is referred to as helical bundle conversion (Izard, Evans et al. 2004).

Metavinculin exhibits a similar head-tail interaction (Witt, Zieseniss et al. 2004), but one that is weaker owing to the acidic nature of the insert in the tail domain (Witt, Zieseniss et al. 2004). Metavinculin has an extra tyrosine phosphorylation site and has been reported to be phosphorylated ~8-fold higher than vinculin in vivo (Siliciano and Craig 1987; Gimona M. 1988). The functional significance for this is not yet understood, but phosphorylation could potentially influence the head-tail interaction.

Vinculin and Metavinculin in Dilated- and Hyper Cardio-Myopathy

Cardiomyopathy is the most common cause of sudden cardiac death. Dilated and Hypertrophic Cardiomyopathy (DCM and HCM) are the two most common types of cardiomyopathy in the U.S. affecting about 1 in every 500 people. In dilated cardiomyopathy the heart cavity is enlarged and stretched, impeding the normal pumping activity. DCM is frequently associated with arrhythmias, which eventually leads to heart failure. In hypertrophic cardiomyopathy the muscle mass of the left ventricle is enlarged, which can obstruct the blood flow, cause leakage of heart valves, or cause arrhythmias, that can also lead to sudden death. Both diseases are attributed to multiple factors, such as valvular heart or coronary artery disease, excessive alcohol use, pregnancy, viral infections etc, but genetics also play a role (www.americanheart.com). Both cardiomyopathies have been associated with

mutations involving a number of cytoskeletal proteins, such as actin, β-myosin heavy chain, myosin-binding protein C, troponin T, titin, α-tropomyosin, etc. (Towbin 1998). Recently, three different mutations in metavinculin were found to be associated with both cardio-myopathies (Olson, Illenberger et al. 2002; Vasile, Will et al. 2006). It is interesting to note that these three mutations, A934V, L954del and R975W, all occur in the insert region. The R975W substitution is the most dramatic mutation and was shown to disrupt intercalated disks significantly (Olson, Illenberger et al. 2002; Vasile, Will et al. 2006). However, this observation was made in an explanted heart which had in-stage heart failure. Metavinculin deficiency was also linked to dilated cardio-myopathy and heart failure (Maeda, Holder et al. 1997), as was vinculin deficiency (Xu, Baribault et al. 1998; Zemljic-Harpf, Ponrartana et al. 2004; Vasile, Edwards et al. 2006; Zemljic-Harpf, Miller et al. 2007). Recently, a missense mutation in vinculin, L277M, was found to be involved in hypertrophic cardiomyopathy (Vasile, Ommen et al. 2006).

Determining how vinculin and metavinculin organize actin filaments

The preceding sections gave a brief overview of what is known about vinculin and metavinculin and the roles they serve in cell adhesion. It is clear that significantly more research has been conducted on vinculin than metavinculin; nevertheless there are still many unanswered questions. The observation that vinculin is essential in formation of a stable link between the actin cytoskeleton and the cell membrane via proteins like talin and α-catenin, led me to study the structural details of this interaction. Vinculin's actin binding site is known to be located in its tail domain. However, the tail domain shows no resemblance to other actin binding domains

(Puius, Mahoney et al. 1998). So, what is the exact location of this site in the tail domain? And does vinculin binding to F-actin introduce any conformational changes in the actin filament, or in vinculin itself? Its dimerization site was shown to be located in the tail domain as well (Huttelmaier, Bubeck et al. 1997). But how exactly does vinculin dimerize in order to induce actin bundling? There is no evidence for large conformational changes in the vinculin tail domain upon actin binding (Bakolitsa, de Pereda et al. 1999). In addition, vinculin is a monomer in solution, but vinculin not only binds to actin filaments, it also bundles them. Since vinculin has only one actin binding domain, it must be able to homodimerize when it is bound to actin in order to crosslink filaments. A smaller, more subtle conformational change may be introduced in the vinculin tail domain upon F-actin binding, allowing it to form homodimers only when bound to actin. Transmission electron microscopy in combination with helical reconstruction, docking of atomic models into the obtained electron density maps and mutagenesis are the preferred techniques to help answer such questions. It is the only way to obtain high resolution structural information on actin-vinculin assemblies, because these structures are to large to solve with NMR and they do not crystallize for x-ray diffraction analysis.

The questions raised in the preceding paragraph were initially addressed (in chapter 3) using the vinculin tail domain. This is possible as this domain contains the actin binding domain and the dimerization site, but also because the structure of the isolated tail domain is identical to the tail domain in the full length protein structure (Bakolitsa, de Pereda et al. 1999; Bakolitsa, Cohen et al. 2004). However, how does full length vinculin crosslink actin filaments? The full length vinculin protein has to be activated in order to bind F-actin. The hypothesis, which will be tested in this work

(chapter 4), is that vinculin can be activated by combinatorial binding of F-actin and a second ligand, such as talin and α-catenin (Bakolitsa, Cohen et al. 2004). Since the actin binding sites are known and are similar for both the vinculin tail domain and full length vinculin, full length vinculin is expected to bind F-actin like the vinculin tail domain. However, due to the presence of the large head domain, dimerization and thus crosslinking might be different.

The third part of this work (chapter 5) addresses questions concerning vinculin's isoform metavinculin. As described earlier, vinculin is expressed ubiquitously, but the expression of metavinculin is restricted to muscle tissue and platelets. This leads to the question of why is there a muscle (and platelet) specific vinculin isoform? Like the actin binding domain, the insert is located in metavinculin's tail domain. This means that actin binding of vinculin and metavinculin might differ and hence potentially affect actin organization differently. Conversely, the insert might affect dimerization and thereby prevent metavinculin from crosslinking actin filaments. Again, transmission electron microscopy and helical reconstruction techniques were used to elucidate this mechanism. Once the normal function of the metavinculin tail is known, one can ask a second question, namely how does the R975W mutation, associated with cardiomyopathy, affect metavinculin's function? This mutation possibly affects the way in which metavinculin organizes actin filaments. If metavinculin turns out not to crosslink F-actin, the mutant could actually restore this bundling activity. Chapter 2 provides background regarding actin and actin binding proteins and explains how actin assemblies are visualized and analyzed using transmission electron microscopy and image reconstruction techniques.

References

Avnur, Z., J. V. Small, et al. (1983). "Actin-independent association of vinculin with the cytoplasmic aspect of the plasma membrane in cell-contact areas." J Cell Biol **96**(6): 1622-30.

Bakolitsa, C., D. M. Cohen, et al. (2004). "Structural basis for vinculin activation at sites of cell adhesion." Nature **430**(6999): 583-6.

Bakolitsa, C., J. M. de Pereda, et al. (1999). "Crystal structure of the vinculin tail suggests a pathway for activation." Cell **99**(6): 603-13.

Belkin, A. M., O. I. Ornatsky, et al. (1988). "Immunolocalization of meta-vinculin in human smooth and cardiac muscles." J Cell Biol **107**(2): 545-53.

Belkin, A. M., O. I. Ornatsky, et al. (1988). "Diversity of vinculin/meta-vinculin in human tissues and cultivated cells. Expression of muscle specific variants of vinculin in human aorta smooth muscle cells." J Biol Chem **263**(14): 6631-5.

Borgon, R. A., C. Vonrhein, et al. (2004). "Crystal structure of human vinculin." Structure **12**(7): 1189-97.

Brindle, N. P., M. R. Holt, et al. (1996). "The focal-adhesion vasodilator-stimulated phosphoprotein (VASP) binds to the proline-rich domain in vinculin." Biochem J **318 (Pt 3)**: 753-7.

Burridge, K. and P. Mangeat (1984). "An interaction between vinculin and talin." Nature **308**(5961): 744-6.

Byrne, B. J., Y. J. Kaczorowski, et al. (1992). "Chicken vinculin and meta-vinculin are derived from a single gene by alternative splicing of a 207-base pair exon unique to meta-vinculin." J Biol Chem **267**(18): 12845-50.

Chambers, D. N. and A. Bretscher (2005). "Ezrin mutants affecting dimerization and activation." Biochemistry **44**(10): 3926-32.

Chen, H., D. M. Cohen, et al. (2005). "Spatial distribution and functional significance of activated vinculin in living cells." J Cell Biol **169**(3): 459-70.

DeMali, K. A., C. A. Barlow, et al. (2002). "Recruitment of the Arp2/3 complex to vinculin: coupling membrane protrusion to matrix adhesion." J Cell Biol **159**(5): 881-91.

Diez, G., P. Kollmannsberger, et al. (2009). "Anchorage of vinculin to lipid membranes influences cell mechanical properties." Biophys J **97**(12): 3105-12.

Geiger, B., K. T. Tokuyasu, et al. (1980). "Vinculin, an intracellular protein localized at specialized sites where microfilament bundles terminate at cell membranes." Proc Natl Acad Sci U S A **77**(7): 4127-31.

Gimona, M., J. V. Small, et al. (1988). "Porcine vinculin and metavinculin differ by a 68-residue insert located close to the carboxy-terminal part of the molecule." Embo J **7**(8): 2329-34.

Gimona M., S. J. V., Moeremans M., van Damme J., Puype M., Vandekerckhove J. (1988). "Molecular domain structure of porcine vinculin and metavinculin." protoplasma **145**: 133-140.

Glukhova, M. A., M. G. Frid, et al. (1990). "Developmental changes in expression of contractile and cytoskeletal proteins in human aortic smooth muscle." J Biol Chem **265**(22): 13042-6.

Glukhova, M. A., A. E. Kabakov, et al. (1986). "Meta-vinculin distribution in adult human tissues and cultured cells." FEBS Lett **207**(1): 139-41.

Humphries, J. D., P. Wang, et al. (2007). "Vinculin controls focal adhesion formation by direct interactions with talin and actin." J Cell Biol **179**(5): 1043-57.

Huttelmaier, S., P. Bubeck, et al. (1997). "Characterization of two F-actin-binding and oligomerization sites in the cell-contact protein vinculin." Eur J Biochem **247**(3): 1136-42.

Izard, T., G. Evans, et al. (2004). "Vinculin activation by talin through helical bundle conversion." Nature **427**(6970): 171-5.

Johnson, R. P. and S. W. Craig (1994). "An intramolecular association between the head and tail domains of vinculin modulates talin binding." J Biol Chem **269**(17): 12611-9.

Johnson, R. P., V. Niggli, et al. (1998). "A conserved motif in the tail domain of vinculin mediates association with and insertion into acidic phospholipid bilayers." Biochemistry **37**(28): 10211-22.

Kioka, N., S. Sakata, et al. (1999). "Vinexin: a novel vinculin-binding protein with multiple SH3 domains enhances actin cytoskeletal organization." J Cell Biol **144**(1): 59-69.

Koteliansky, V. E., E. P. Ogryzko, et al. (1992). "An additional exon in the human vinculin gene specifically encodes meta-vinculin-specific difference peptide. Cross-species comparison reveals variable and conserved motifs in the meta-vinculin insert." Eur J Biochem **205**(3): 1218.

Kroemker, M., A. H. Rudiger, et al. (1994). "Intramolecular interactions in vinculin control alpha-actinin binding to the vinculin head." FEBS Lett **355**(3): 259-62.

Maeda, M., E. Holder, et al. (1997). "Dilated cardiomyopathy associated with deficiency of the cytoskeletal protein metavinculin." Circulation **95**(1): 17-20.

Mandai, K., H. Nakanishi, et al. (1999). "Ponsin/SH3P12: an l-afadin- and vinculin-binding protein localized at cell-cell and cell-matrix adherens junctions." J Cell Biol **144**(5): 1001-17.

Mohl, C., N. Kirchgessner, et al. (2009). "Becoming stable and strong: the interplay between vinculin exchange dynamics and adhesion strength during adhesion site maturation." Cell Motil Cytoskeleton **66**(6): 350-64.

Nevalainen, E. M., A. Skwarek-Maruszewska, et al. (2009). "Two biochemically distinct and tissue-specific twinfilin isoforms are generated from the mouse Twf2 gene by alternative promoter usage." Biochem J **417**(2): 593-600.

Olson, T. M., S. Illenberger, et al. (2002). "Metavinculin mutations alter actin interaction in dilated cardiomyopathy." Circulation **105**(4): 431-7.

Ozkirimli, E. and C. B. Post (2006). "Src kinase activation: A switched electrostatic network." Protein Sci **15**(5): 1051-62.

Puius, Y.A., N.M.Mahoney, et al. (1998). “The modular structure of actin-regulatory proteins.” Curr Opin Cell Biol **10**(1): 23-34.

Rodriguez Fernandez, J. L., B. Geiger, et al. (1992). "Suppression of tumorigenicity in transformed cells after transfection with vinculin cDNA." J Cell Biol **119**(2): 427-38.

Saga, S., M. Hamaguchi, et al. (1985). "Expression of meta-vinculin associated with differentiation of chicken embryonal muscle cells." Exp Cell Res **156**(1): 45-56.

Siliciano, J. D. and S. W. Craig (1987). "Properties of smooth muscle meta-vinculin." J Cell Biol **104**(3): 473-82.

Sobue, K., K. Hayashi, et al. (1999). "Expressional regulation of smooth muscle cell-specific genes in association with phenotypic modulation." Mol Cell Biochem **190**(1-2): 105-18.

Subauste, M. C., O. Pertz, et al. (2004). "Vinculin modulation of paxillin-FAK interactions regulates ERK to control survival and motility." J Cell Biol **165**(3): 371-81.

Towbin, J. A. (1998). "The role of cytoskeletal proteins in cardiomyopathies." Curr Opin Cell Biol **10**(1): 131-9.

Turner, C. E. and K. Burridge (1989). "Detection of metavinculin in human platelets using a modified talin overlay assay." Eur J Cell Biol **49**(1): 202-6.

Turner, C. E., J. R. Glenney, Jr., et al. (1990). "Paxillin: a new vinculin-binding protein present in focal adhesions." J Cell Biol **111**(3): 1059-68.

Vasile, V. C., W. D. Edwards, et al. (2006). "Obstructive hypertrophic cardiomyopathy is associated with reduced expression of vinculin in the intercalated disc." Biochem Biophys Res Commun **349**(2): 709-15.

Vasile, V. C., S. R. Ommen, et al. (2006). "A missense mutation in a ubiquitously expressed protein, vinculin, confers susceptibility to hypertrophic cardiomyopathy." Biochem Biophys Res Commun **345**(3): 998-1003.

Vasile, V. C., M. L. Will, et al. (2006). Identification of a metavinculin missense mutation, R975W, associated with both hypertrophic and dilated cardiomyopathy. Mol Genet Metab. **87:** 169-74.

Vicente-Manzanares, M., X. Ma, et al. (2009). "Non-muscle myosin II takes centre stage in cell adhesion and migration." Nat Rev Mol Cell Biol **10**(11): 778-90.

Weiss, E. E., M. Kroemker, et al. (1998). "Vinculin is part of the cadherin-catenin junctional complex: complex formation between alpha-catenin and vinculin." J Cell Biol **141**(3): 755-64.

Winkler, J., H. Lunsdorf, et al. (1996). "The ultrastructure of chicken gizzard vinculin as visualized by high-resolution electron microscopy." J Struct Biol **116**(2): 270-7.

Witt, S., A. Zieseniss, et al. (2004). "Comparative biochemical analysis suggests that vinculin and metavinculin cooperate in muscular adhesion sites." J Biol Chem **279**(30): 31533-43.

Xu, W., H. Baribault, et al. (1998). "Vinculin knockout results in heart and brain defects during embryonic development." Development **125**(2): 327-37.

Yamashiro, S., K. Mohri, et al. (2005). "The two Caenorhabditis elegans actin-depolymerizing factor/cofilin proteins differently enhance actin filament severing and depolymerization." Biochemistry **44**(43): 14238-47.

Zamir, E. and B. Geiger (2001). "Components of cell-matrix adhesions." J Cell Sci **114**(Pt 20): 3577-9.

Zamir, E. and B. Geiger (2001). "Molecular complexity and dynamics of cell-matrix adhesions." J Cell Sci **114**(Pt 20): 3583-90.

Zemljic-Harpf, A. E., J. C. Miller, et al. (2007). "Cardiac-myocyte-specific excision of the vinculin gene disrupts cellular junctions, causing sudden death or dilated cardiomyopathy." Mol Cell Biol **27**(21): 7522-37.

Zemljic-Harpf, A. E., S. Ponrartana, et al. (2004). "Heterozygous inactivation of the vinculin gene predisposes to stress-induced cardiomyopathy." Am J Pathol **165**(3): 1033-44.

Zhang, Z., G. Izaguirre, et al. (2004). "The phosphorylation of vinculin on tyrosine residues 100 and 1065, mediated by SRC kinases, affects cell spreading." Mol Biol Cell **15**(9): 4234-47.

Chapter 2

Background: Actin and actin binding proteins and their analysis using transmission electron microscopy and image reconstruction techniques

Tight regulation of actin dynamics is at the heart of important cellular processes such as cell migration, adhesion, division, transport, signaling, and maintaining cell shape. The diversity of these processes requires the existence of multiple filamentous actin structures with distinct properties. For example, an activity like cell migration, which plays a key role during embryonic development, cancer, wound healing and immune responses, is a highly orchestrated, multistep process. In a characteristic polarized cell, a morphology is adopted with extended protrusions in the direction of extracellular cues. These protrusions are broad lamellipodia or spike-like filopodia that serve as traction sites as the cell moves forward, and they are disassembled at the cell rear allowing the cell to detach. The type of actin assembly depends on the protrusion: filopodia are formed of large actin bundles, whereaslamellipodia consist of a branching actin network. Formation and disassembly of these actin structures is controlled by numerous actin-regulatory proteins that function in binding, cross-linking, capping, severing, depolymerization, and nucleation of actin (Pollard and Borisy 2003; Le Clainche and Carlier 2008).

Structural details on monomeric and filamentous actin

Actin is the major component of the microfilament system in the cell. It is an abundant, highly conserved, globular, 42kD protein and *in vivo* exists in roughly equal amounts as monomeric actin (G-actin) and filamentous actin (F-actin). G-actin,

which contains one molecule of non-covalently bound ATP, is polymerized to F-actin and ATP is hydrolyzed to bound ADP and free inorganic phosphate, P_i, under physiological conditions (dependent on pH, temperature, Mg^{2+} concentration, ionic strength, etc). Polymerization starts slowly due to the small unstable oligomers, but once filaments are formed polymerization is fast and almost complete. Even after polymerization has reached a steady-state condition, addition and loss of actin monomers at F-actin ends continues. This process is called treadmilling. Net polymerization is higher at the barbed end of the filament, while net depolymerization is higher at the pointed end of the filament. Overall (de)polymerization depends on the concentration of free actin monomers in the cell (Korn, Carlier et al. 1987; Steinmetz, Stoffler et al. 1997; Pollard and Cooper 2009).

Approximately 25 crystal structures of monomeric actin have been published. All these structures were complexed with other proteins such as DNAseI (Kabsch, Mannherz et al. 1990) or vitamine D binding protein (Otterbein, Cosio et al. 2002) or were chemically modified (Otterbein, Graceffa et al. 2001; Kudryashov, Sawaya et al. 2005) in order to prevent polymerization and make crystallization possible. Subsequently, an ECP32-cleaved actin was crystallized, and this form of actin retains many features of the intact protein, including its ability to polymerize in its Mg-ATP bound form. In its Ca-ATP bound form it is virtually non-polymerizable (Klenchin, Khaitlina et al. 2006) (Fig. 2-1).

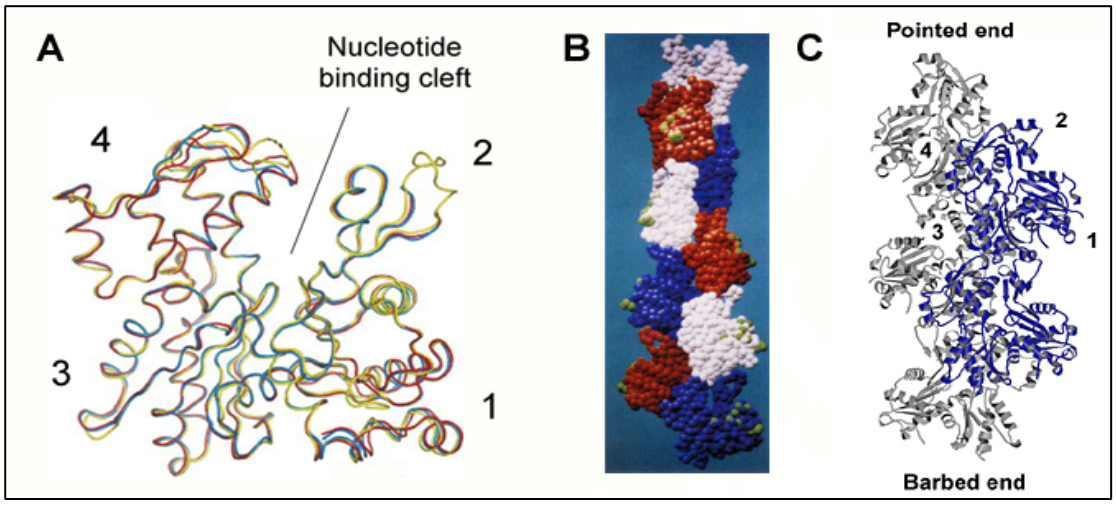

Fig. 2-1 Structure of monomeric and filamentous actin. (A) Main chain structures of ECP monomers A and B (red and blue) are superimposed on the structure of actin in complex with DNAseI (yellow). The nucleotide binding cleft is indicated in the center of the molecule and actin subdomains 1-4 are labeled. (Klenchin, Khaitlina et al. 2006) (B) Holmes model of F-actin including 9 actin subunits (Holmes, Popp et al. 1990). (C) Structure of five neighboring actin residues after fitting them to electron density maps (Holmes, Tirion et al. 1993).

These crystal structures all display a relatively consistent model of monomeric actin, consisting of a 'large' domain (left side) and a' small' domain (right side) (Fig. 2-1A). Each domain can be further divided into two subdomains that are held together by salt bridges and hydrogen bonds to the phosphate group of the bound nucleotide and to its divalent cation at the bottom of the cleft, in the center of the molecule. Subdomain 2 is significantly less massive than the other domains and renders the molecule polar in the direction from subdomain 1 and 3 (barbed end) toward subdomains 2 and 4 (pointed end) (Fig. 2-1A). An F-actin filament is build up from these actin subunits and consists of two intertwined, "long pitch", right-handed helical strands. One helical turn in the filament contains 13 actin subunits and the axial subunit repeat is 2.75nm, resulting in a pitch of 71.5nm. The two helical strands are

axially staggered by half the axial subunit spacing, meaning that they cross each other every 35.75nm. The F-actin filament can also be described as a structure with a single, left-handed, “shallow pitch” helical strand with 13 subunits per 6 turns, resulting in a similar cross-over distance of 35.75nm (Bremer and Aebi 1992; Lorenz, Popp et al. 1993; Steinmetz, Stoffler et al. 1997).

Since actin filaments cannot be crystallized due to their varying lengths and complexes larger than ~100kD cannot be characterized by NMR, no high resolution structure of F-actin is available. However, several models exist for F-actin. The original (‘Holmes’) model assumes that there are no large conformational changes between G-actin as a monomer and G-actin incorporated into the helical strand of an actin filament (Fig. 2-1). The only change is a movement of a hydrophobic loop from the body of the actin subunit to form a contact with subunits on the opposite long-pitch strand. This model was generated using a translational and rotational search for placement of the monomeric actin crystal structure into a helical filament so that it fits the observed x-ray fiber diffraction pattern from an oriented F-actin gel (~8Å resolution) (Holmes, Popp et al. 1990). The ‘Lorenz model’ emerged a couple of years later and is a refinement of the ‘Holmes model’ (Lorenz, Popp et al. 1993). The earlier Holmes model was adjusted to fit high resolution EM density maps of F-actin and showed that the G- to the F-actin transition introduces some substantial conformational changes (Holmes, Tirion et al. 1993). In this model a crystal structure of G-actin (Otterbein, Graceffa et al. 2001) was used in which subdomain 4 was rotated inwards by 15^{o} and subsequently flattened to give the best fit. This is also the F-actin model that was used for docking into EM density maps in my studies (chapter 3 and 5). A more recent F-actin model (‘Oda model’) is based on x-ray fiber diffraction

studies at a resolution of 3.3-5.6Å (Oda, Iwasa et al. 2009). This higher resolution was obtained by controlling filament length by adding gelsolin and controlling filament orientation using a superconductive magnet. This model shows a relative rotation of the two major domains of ~20^{o}, giving the subunits in F-actin a flatter structure compared to G-actin. A second difference is the open loop conformation of the DNAseI binding loop in subdomain 2. Recently, molecular dynamics simulations were used to compare the structure and properties of filamentous actin according to the Holmes and Oda models (Pfaendtner, Lyman et al. 2009). This study suggested that the Oda model better describes the interactions between subunits and gives rise to more stable filament dynamics. In addition, it describes how polymerization-induced flattening of actin subunits promotes ATP hydrolysis by locating one of the side chains closer to the γ-phosphate of ATP and that dissociation of γ-phosphate induces changes in the DNAse I-binding loop, which leads to destabilization of the filament.

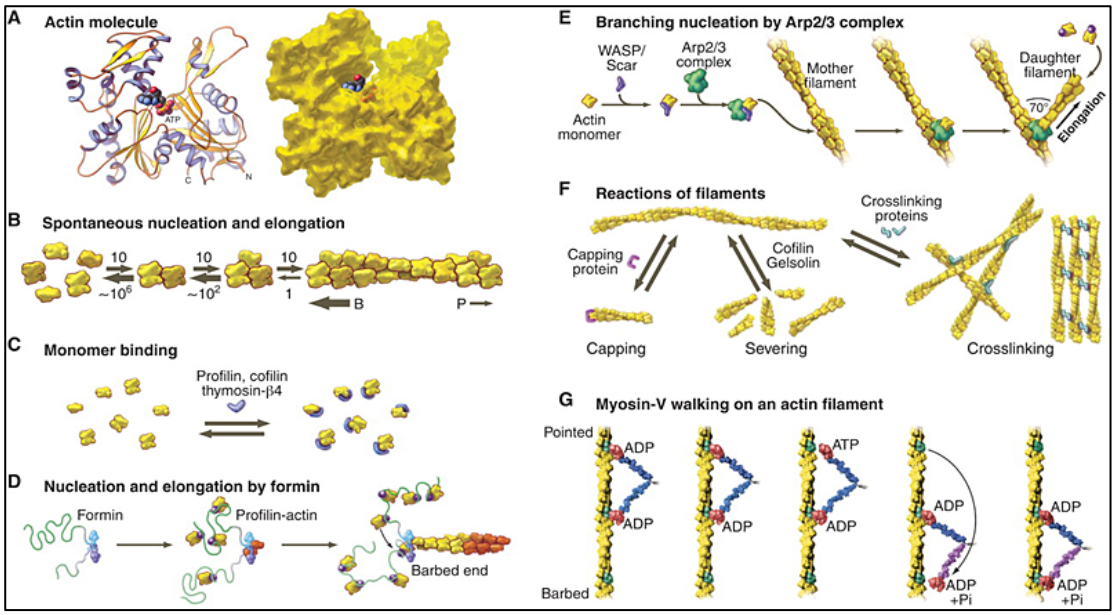

Fig. 2-2 Structures of actin and diagrams of fundamental reactions. (A) Ribbon and space filling model of G-actin (pdb: 1ATN). (B) Spontaneous nucleation and elongation. Dimers and trimers are unstable, rapid growth at barbed ends and slow growth at pointed ends. (C) G-actin binding proteins. (D) Nucleation and elongation. (E) Nucleation of new filaments. (F) Reactions of actin filaments: capping, severing and cross-linking. (G) Transportation along actin filament. (Pollard and Cooper 2009).

Regulation of the actin cytoskeletal organization

Assembly and function of actin are controlled by numerous actin-regulatory proteins. Many of these proteins bind F-actin in similar ways, namely by interacting with actin subdomains 1 and 2, which form the ‘outer’-domain of the filament helix and is more readily accessible for binding than subdomains 3 and 4. In addition, a ‘hot spot’ (the hydrophobic pocket at the front end of the hydrophobic cleft in actin) exists for binding of actin regulatory proteins (Dominguez 2004). Actin binding proteins (ABPs) are multi-domain proteins consisting of an actin binding domain, and often also signaling and other protein-protein interaction domains. The large numbers of ABPs are classified into different structural families according to their actin binding

domains, such as the gelsolin homology fold, profilin-homology domain, calponin-homology domain, myosin motor domain, and Wasp-homology domain (Hanein, Volkmann et al. 1998; Van Troys, Vandekerckhove et al. 1999; Kureishy, Sapountzi et al. 2002; Dominguez 2004). These ABPs regulate actin in a number of ways (Fig. 2-2). For example, thymosin-β4 can bind to monomeric actin and decrease the critical concentration for actin polymerization, preventing spontaneous polymerization (Fig. 2-2c). Thymosin-β4 competes for G-actin binding with profilin. By creating a large pool of G-actin, it co-operates with profilin and promotes rapid filament assembly. As opposed to thymosin-β4, profilin does not block all assembly reactions. It inhibits actin polymerization from the pointed end, but promotes nucleotide exchange that facilitates polymerization at the barbed end (Sun, Kwiatkowska et al. 1995). However, Cofilin, yet another example of a G-actin binding protein (Fig. 2-2c), sequesters G-actin to prevent polymerization and nucleotide exchange. Cofilin also severs F-actin to further promote disassembly of filaments. This in turn increases the number of filaments and might increase profilin-driven polymerization. A tight regulation of activities is necessary to control the assembly of required actin structures. This is often achieved by factors such as protein concentration or pH (Maciver, Zot et al. 1991; Blanchoin and Pollard 1999; Andrianantoandro and Pollard 2006). Another actin regulatory mechanism is the initiation of polymerization from free G-actin by formins (Fig. 2-2d). Formins remain associated with the growing barbed end and cause partial inhibition of barbed end elongation (Harris, Li et al. 2004; Papp, Bugyi et al. 2006). In addition, mouse formins sever actin filaments (although not very efficiently) (Harris, Li et al. 2004) and formins in yeast, bundle actin filaments (Lew 2002). At the leading edges of the cell, actin filament branching is initiated by the

actin-related protein 2/3 (Arp2/3) complex (Fig.2-2e) (Rouiller, Xu et al. 2008). Cofilin, in turn, competes with arp2/3 for the binding sites on actin and can subsequently dissociate the Arp2/3 complex and branches (Chan, Beltzner et al. 2009). Other reactions include capping by proteins such as capping protein (Fig. 2-2f), and severing and cross-linking as described in more detail below.

F-actin severing proteins

F-actin severing proteins are important for rapid turnover of actin filaments, especially at the leading edge of motile cells. Filaments need to be disassembled to recycle G-actin for polymerization of new F-actin. Also, severing can increase the number of filament ends on which new actin can be nucleated. Filament length is regulated by severing, and also by filament end capping and acceleration of F-actin depolymerization or polymerization. Most severing proteins exhibit one of these activities in addition to severing. Based on their sequences, these proteins have been grouped into distinct categories or families such as the gelsolin family, which includes proteins such as gelsolin, villin, and severin (containing 3-6 gelsolin-like domains) (Ono 2007). These proteins bind, sever, and cap the barbed end, and depend on pH, calcium concentration, phosphorylation and nucleotide state (Yin and Stossel 1979; Brown, Yamamoto et al. 1982; Khurana and George 2008). For example, gelsolin's stoichiometric severing activity is stimulated by Ca^{2+}. When gelsolin's tail domain binds Ca^{2+} a conformational change is induced that exposes the actin binding sites in gelsolin. After severing, gelsolin remains attached to the barbed end of the filament and functions as a cap. On the other hand, gelsolin severing is inhibited by binding to phophophoinositide 4,5-biphosphate (PIP_2) (Sun, Yamamoto et al. 1999). Villin in this

family bundles actin filaments in addition to severing (Hampton, Liu et al. 2008). The ADF/Cofilin family represents a second group of severing proteins, which are smaller in size than the first group of F-actin severing proteins and contain a single ADF-homology domain, and includes proteins such as cofilin, actophorin, and twinfillin. These proteins also bind actin, sever, and influence actin (de)polymerization, and depend on protein concentration and pH (Maciver, Zot et al. 1991; Blanchoin and Pollard 1999; Andrianantoandro and Pollard 2006; Moseley, Okada et al. 2006; Pavlov, Muhlrad et al. 2006). Cofilin severs and promotes disassembly of F-actin from the pointed end. It works together with the Arp2/3 complex in reorganizing the actin filaments by increasing the amount of barbed ends while simultaneously increasing the G-actin pool. This provides free barbed ends for further polymerization and nucleation by the Arp2/3 complex (Ichetovkin, Grant et al. 2002).

Severing mechanisms differ for each severing protein. Gelsolin initiates severing after binding to the sides of the actin filament (Sun, Yamamoto et al. 1999). Electron cryomicroscopy and helical reconstruction showed that gelsolin bridges two longitudinally associated monomers in F-actin, causing large conformational changes in both gelsolin and actin, leading to a kink in the actin filament (McGough, Chiu et al. 1998). This only happens when F-actin is freely available in solution (Dawson, Sablin et al. 2003). Another severing mechanism is that of cofilin, which binds substoichiometriccally to F-actin. By sparsely binding to the filament, cofilin changes the filament twist, causing strain and fragmentation (McGough, Pope et al. 1997; Andrianantoandro and Pollard 2006). Opposite from gelsolin, actin filament flexibility has to be restricted for optimal severing by cofilin, probably because of the higher strains that can be reached in the filament (Pavlov, Muhlrad et al. 2006). Actophorin

belongs to the same group as cofilin, but its severing mechanism is different. Severing by actophorin mainly occurs at pre-existing bends in the filament. F-actin is mechanically disrupted by intercalation of actophorin between two adjacent actin monomers in the filament. This mechanism is dependent on the bending-flexibility of F-actin, which is in turn dependent on the bound divalent cation (Ca^{2+} or Mg^{2+}) and nucleotide (ATP or ADP) (Maciver, Zot et al. 1991; Rebello and Ludescher 1998).

Actin crosslinking proteins

Actin bundling represents another form of actin organization. Actin bundles are prominent in filopodia, but large tightly organized actin bundles are also found around the nucleus and form the cellular geodome, in microvilli, and stressfibers. Bundle characteristics, such as packing, flexibility, and polarity, depend on the size and bundling strategy of the type of ABP that is involved. A large ABP that is capable of self-association, like α-actinin (~100kD), induces the formation of loose bundles (Meyer and Aebi 1990; Tseng, Fedorov et al. 2001). On the other hand, an ABP that has two suitable actin binding domains, such as fimbrin (~67kD) or fascin (~55kD), induces tight unipolar bundles dependent on the distance between the two actin binding sites (Volkmann, DeRosier et al. 2001; Kureishy, Sapountzi et al. 2002).

Actin crosslinking proteins, like severing proteins, are also regulated by external factors. For example, within the α-actinin family the non-muscle isoforms are regulated by Ca^{2+}, whereas the muscle-specific isoforms are Ca^{2+}-insensitive. Fimbrin is also regulated by Ca^{2+}. Fimbrin only induces actin bundling in absence of Ca^{2+} and does not crosslink actin filaments in the presence of Ca^{2+}. Another way of regulating actin bundling is through phosphorylation. The bundling activity of fascin is inhibited

by phosphorylation at residue Ser-39 by protein kinase C (Yamakita, Ono et al. 1996). The length of actin bundles and their growth rate are subsequently determined by capping, severing, and nucleating proteins such as the ones described above.

While both α-actinin and fimbrin are both members of the same spectrin superfamily and both their actin binding domains (ABDs) consist of two consecutive, calponin homology domains, their bundling mechanism is different. α-Actinin, which is composed of one ABD linked to a C-terminal calmodulin-like domain via four spectrin repeats, forms an antiparallel homodimer. As a result, this dimer has an actin binding domain at both ends, allowing it to crosslink actin filaments into bundles. Due to the flexibility of the linker domain, α-actinin is able to arrange actin filaments in diverse arrays. It can induce highly ordered anti-parallel actin arrays or variable orientations of filaments in an actin network. (Taylor and Taylor 1993; Hampton, Taylor et al. 2007; Sjoblom, Salmazo et al. 2008). Fimbrin, like α-actinin, is composed of a C-terminal calmodulin-like domain, a spectrin linker and, unlike α-actinin, two tandem pairs of ABDs at the N-terminus. These ABDs are arranged on the same polypeptide chain, without any spacers and this enables fimbrin to organize actin filaments into densely packed bundles (Volkmann, DeRosier et al. 2001). Fascin belongs to the β-trefoil family of proteins and contains two actin binding sites, one at the N-terminus and the second about 300 amino acids C-terminal of the first binding site. This allows fascin to bundle actin filaments into highly ordered, tightly-packed, parallel bundles (Kureishy, Sapountzi et al. 2002). Vinculin is an actin crosslinking protein, which organizes filaments into bundles (Jockusch and Isenberg 1981; Huttelmaier, Bubeck et al. 1997). As described in chapter 1, the mechanism of actin bundling by vinculin and the subsequent bundle characteristics are not yet known.

Analysis of crosslinked actin arrays

Three-dimensional F-actin bundles are often disordered and polymorphic and hence difficult to analyze. I used a method that helps constrain disorder and polymorphism to two dimensions and facilitates detailed structural studies on actin-protein crosslinking interactions (Ward, Menetret et al. 1990). Positively-charged lipid layers were used as a substrate for formation of highly-organized two-dimensional (2D) F-actin arrays ('rafts'). Actin filaments bind these lipid monolayers and allow intercalation of the actin bundling protein between them. Although actin bundles *in vivo* have more constrains due to their crosslinking in three-dimensions, the better ordered 2D actin rafts have the potential to yield higher resolution structural information on actin bundling. These 2D rafts allow for the visualization and analysis of individual filaments and crossbridges by electron microscopy.

The analysis of these two-dimensional actin rafts is described in (Sukow and Derosier 1998). Optical diffraction patterns obtained from electron micrographs provide information about the geometrical arrangements of subunits in the specimen, in this case the actin filaments and their crossbridges. The diffraction patterns of electron microscopy images of highly organized, paracrystalline actin-crosslinker arrays provide information on interfilament spacing and rotation, axial translation, polarity of the filaments ,and crosslinker spacing. A diffraction pattern of crosslinked actin arrays (Fig. 2-3) consists of horizontal lines (layer lines) that arise from the helical symmetry of the actin filaments. A single filament would give rise to continuous lines, but because of the paracrystalline nature of the filaments in the raft, the layer lines appear as sharper spots. The distance between these spots correlates with the reciprocal distance between the filaments. Doubling of row line sampling means that

the repeat distance is twice the distance between filaments, indicating that neighboring filaments in the array have opposite polarity. The repetition within the filament due to its pitch and the distance between successive crosslinkers gives rise to spots on the vertical lines (row lines). The angle and position of these spots shows the spatial relationship (axial shift, rotation) between neighboring filaments in the raft, see Fig. 2-3. (Sukow and DeRosier 1998; Volkmann, DeRosier et al. 2001). In addition to providing information on the specimen itself, diffraction patterns also provide information on the image quality, such as resolution, radiation damage, astigmatism, focus, and drift.

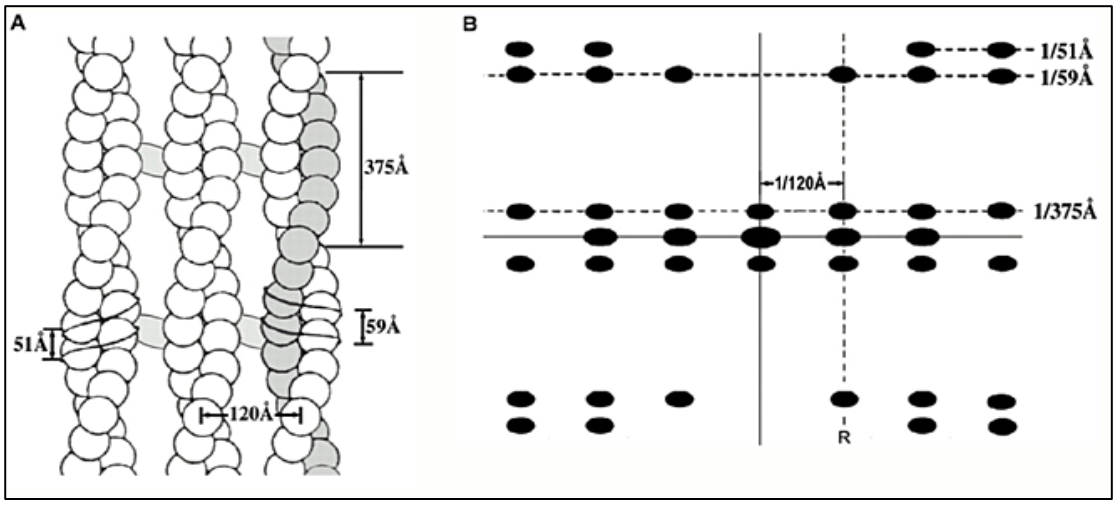

Fig. 2-3 Example of a two-dimensional F-actin array crosslinked by an actin bundler and its diffraction pattern (Volkmann, DeRosier et al. 2001). (A) F-actin raft indicating the distances between repetitive units and showing the crosslinker in grey. (B) Diffraction pattern of the raft in A.

Although a large amount of data can be derived form these diffraction patterns, they don not provide all information. Visualizing the actin assemblies by imaging and

subsequently using the appropriate reconstruction technique will provide additional information how the crosslinkers are positioned in the actin monolayers.

Helical reconstruction technique

Due to the size and the helical nature of filamentous actin, conventional methods such as NMR spectroscopy and x-ray crystallography respectively are not suitable for studying actin complexes. However, transmission electron microscopy combined with image reconstruction techniques is an excellent tool to determine the structure of these large molecular assemblies. In contrast to single particles, one image of a helical polymer often provides all the different orientations needed to reconstruct the three-dimensional (3D) structure to moderate resolution. For the analysis of helical structures, such as actin filaments bound by the vinculin or metavinculin tail domain in this work, reconstructions can be generated using standard helical reconstruction techniques (Owen, Morgan et al. 1996). The Brandeis Helical Package is a group of programs used for analysis of electron micrographs of helical objects using the Fourier-Bessel method. First, single filaments have to be boxed out from a digitized image. Filaments are then rotated to a standard orientation, straightened, and images more tightly boxed and apodized (smoothening of the sharp box edges). These images are then Fourier transformed and layer line data are extracted. At this stage, filtering and CTF-correction can be applied, as well as phase origin correction. CTF stands for contrast-transfer-function and arises form artifacts generated by the microscope system such as lens aberration and defocus. Layer line data are either separated into near- and far-side data (resulting from the 2 helices), after which all

files are merged, aligned, averaged, and 3D maps are generated by Fourier Bessel inversion.

A more recent development in helical reconstruction techniques is a hybrid procedure that combines single particle reconstruction approaches with helical symmetry (Egelman 2000). The filament straightening as described for conventional helical reconstruction has the potential to introduce artifacts, for example, by assuming there is no coupling between bending and twisting or by assuming the filament undergoes a merely elastic, normal mode of bending, etc. In addition, F-actin does not have a precisely defined helical symmetry. To avoid these difficulties, single particle methods can be applied to helical filaments. In this real-space reconstruction method, small overlapping segments of actin filaments are selected from digitized electron micrographs. These segments are aligned against reference projections that were generated from a helically-symmetric reference structure. The aligned images are subsequently used to generate a 3D reconstruction by back projection. Helical symmetry of the volume is determined and imposed to generate a new helically-symmetric reference volume. This procedure is iteratively refined until convergence is reached with no further improvements in the 3D reconstruction. (Egelman 2000; Egelman 2007).

Using these procedures, helical reconstructions can be obtained from cryo-EM data with a resolution around 10Å (Galkin, Orlova et al. 2008; Low, Sachse et al. 2009). For comparison: at low resolution (~20-30Å) individual proteins can be detected in a multiprotein complex and its shape can be determined. At ~8-9Å α-helices are just visible, at ~5Å β-strands are visible, and at a resolution of ~3-4Å densities of individual amino acid side chains can be detected (Auer 2000). However,

most biological specimens do not reach this kind of resolution. Nevertheless, atomic models can be generated using high resolution structures of individual molecules in a macromolecular complex that are obtained using techniques such as NMR or x-ray crystallography combined with the lower resolution structure of the entire complex that was obtained by electron microscopy (Baker and Johnson 1996). The atomic structures have to be docked into the density provided by electron microscopy. This can provide information on intermolecular interfaces and large conformational changes of individual molecules upon complex formation.

Electron tomography

The reconstruction methods described in the preceding section are not useful for 2D actin arrays crosslinked by ABPs. Although the actin arrays contain information from all orientations of F-actin due to its helical symmetry, the crosslinkers in between the filaments are fixed in one orientation due to their constriction by the monolayer. A powerful tool to obtain 3D reconstructions of the actin-crosslinker arrays is electron tomography. Electron tomography is the only technique that can provide structural information of larger complexes and supramolecular assemblies, whether they are ordered or not. In this technique images of the sample are recorded under different orientations of the object with respect to the electron beam and are then computationally merged to obtain a 3D reconstruction (Fig. 2-4). The resolution of tomograms is ~20 (Lučić, Förster et al. 2005) and is dependent on the number of projections and their alignment. The degree of rotation that can be achieved is dependent on physical constrains imposed by the specimen holder and the sample itself and causes nonisotropic resolution. Full structural information on a sample can

be obtained by tilting the specimen over an angular range of 180^{o}. However, in general the sample can only be physically tilted from -70^{o} to 70^{o} with respect to the electron beam. This limited tilt range results in missing data in a wedge-shaped region and causes distortions in the 3D reconstruction. In order to improve reconstruction quality, a second set of data can be collected after rotating the specimen by 90^{o} about the optic axis of the microscope. The pyramidal-shaped region of missing data is smaller than the wedge-shaped region and this data collection strategy improves the quality of the 3D reconstruction. This missing data is especially visible in single tilt tomography of helical assemblies: filaments that lay perpendicular to the tilt axis will be strongly affected by the missing wedge, and will not appear in the reconstruction. In double tilt tomography this information will be added from the second tilt series. In addition, the tilt increment also determines the quality of the image reconstruction. Small tilt increments improve final resolution (Fig. 2-4d).

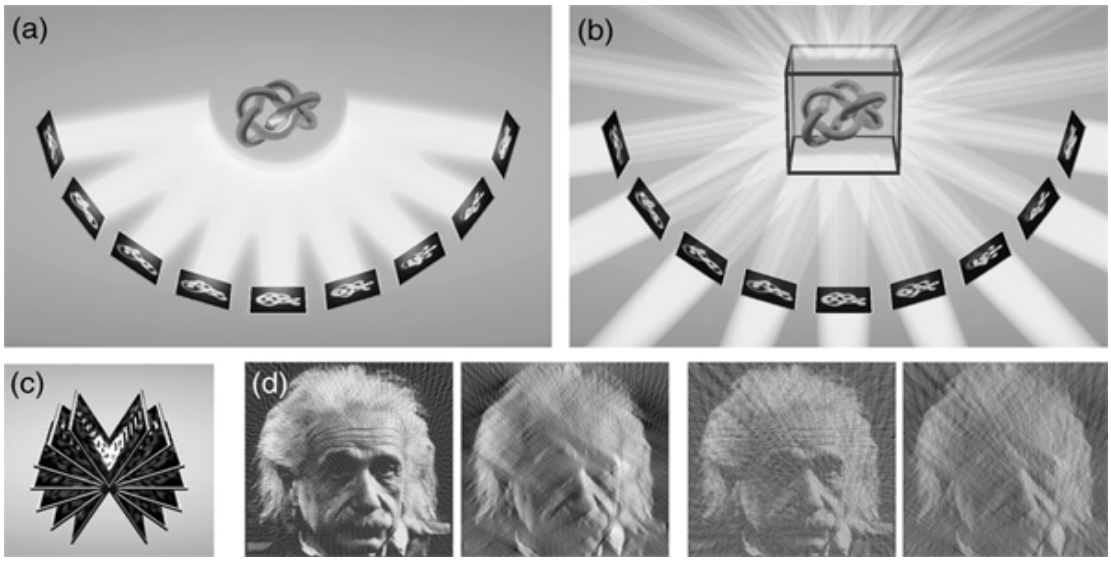

Fig. 2-4 The principal of single axis tomography (Baumeister, Grimm et al. 1999). (a) Two-dimensional projection images are recorded while tilting the sample with respect to the electron beam. (b) The backprojection body for each image is calculated after which all backprojections are combined to calculate the 3D reconstruction. (c) The specimen cannot be tilted over the full range of 180^{o} due to technical constraints. Various kinds of distortions in the 3D reconstruction are caused by the absence of data in this wedge-shaped region, often referred to as missing-wedge artifacts. (d) The quality of the 3D reconstruction depends on tilt angle and increment as shown by these four images. The first image (left) demonstrates a nearly perfect reconstruction obtained with a ±90^{o} tilt range and 2^{o} tilt increment. In the second image the maximum tilt angle was ±60^{o}. The details in the reconstruction perpendicular to the z-direction are smeared out due to the missing wedge. The two reconstructions on the right were obtained by recording images with tilt increments of 5^{o} over a tilt angle of ±90^{o} and ±60^{o}, respectively. Compared with the first two images, the resolution is lower, and the images are more degraded.

Another point of caution in electron tomography is the large amount of images that need to be collected. The electron dose should be minimized and this results in a very low signal-to-noise ratio in each projection image. Electron tomography, however, has the advantage that the signal-to-noise ratio will increase after combining the data in all projections. Further improvement of data quality involves the sample preparation technique. A commonly used method is staining the sample with heavy metals to increase the contrast in electron microscopy. In negative staining,

these metals are deposited around the molecules of the specimen and in cavities. Thus, the specimen appears light, while it is surrounded by a dark envelope of heavy metals. What is seen is not biological material but stain. In addition, the stain causes artifacts like flattening or collapsing of the specimen due to the stain deposit and dehydration. To avoid staining artifacts, specimens can be prepared by cryofixation. In this technique, samples are rapidly frozen under cryogenic temperatures in liquid ethane. This causes the proteins to be embedded in a vitrified layer of water, which preserves the protein's native environment. Using cryo-electron tomography, the specimen can be investigated in its frozen-hydrated state. Low-dose techniques, high electron voltage and energy filters are aids that are commonly used to protect the specimen against too much radiation damage. For a review see (Lučić, Förster et al. 2005).

References

Andrianantoandro, E. and T. D. Pollard (2006). "Mechanism of actin filament turnover by severing and nucleation at different concentrations of ADF/cofilin." Mol Cell **24**(1): 13-23.

Baker, T. S. and J. E. Johnson (1996). "Low resolution meets high: towards a resolution continuum from cells to atoms." Curr Opin Struct Biol **6**(5): 585-94.

Blanchoin, L. and T. D. Pollard (1999). "Mechanism of interaction of Acanthamoeba actophorin (ADF/Cofilin) with actin filaments." J Biol Chem **274**(22): 15538-46.

Bremer, A. and U. Aebi (1992). "The structure of the F-actin filament and the actin molecule." Curr Opin Cell Biol **4**(1): 20-6.

Brown, S. S., K. Yamamoto, et al. (1982). "A 40,000-dalton protein from Dictyostelium discoideum affects assembly properties of actin in a Ca2+-dependent manner." J Cell Biol **93**(1): 205-10.

Chan, C., C. C. Beltzner, et al. (2009). "Cofilin dissociates Arp2/3 complex and branches from actin filaments." Curr Biol **19**(7): 537-45.

Dawson, J. F., E. P. Sablin, et al. (2003). "Structure of an F-actin trimer disrupted by gelsolin and implications for the mechanism of severing." J Biol Chem **278**(2): 1229-38.

Dominguez, R. (2004). "Actin-binding proteins--a unifying hypothesis." Trends Biochem Sci **29**(11): 572-8.

Egelman, E. H. (2000). "A robust algorithm for the reconstruction of helical filaments using single-particle methods." Ultramicroscopy **85**(4): 225-34.

Egelman, E. H. (2007). "The iterative helical real space reconstruction method: surmounting the problems posed by real polymers." J Struct Biol **157**(1): 83-94.

Galkin V. E., A. Orlova, et al. (2008). “High-resolution cryo-EM structure of the F-actin-fimbrin/plastin ABD2 complex.” Proc Natl Acad Sci USA **105**(5): 1494-8.

Hampton, C. M., J. Liu, et al. (2008). "The 3D structure of villin as an unusual F-Actin crosslinker." Structure **16**(12): 1882-91.

Hampton, C. M., D. W. Taylor, et al. (2007). "Novel structures for alpha-actinin:F-actin interactions and their implications for actin-membrane attachment and tension sensing in the cytoskeleton." J Mol Biol **368**(1): 92-104.

Hanein, D., N. Volkmann, et al. (1998). "An atomic model of fimbrin binding to F-actin and its implications for filament crosslinking and regulation." Nat Struct Biol **5**(9): 787-92.

Harris, E. S., F. Li, et al. (2004). "The mouse formin, FRLalpha, slows actin filament barbed end elongation, competes with capping protein, accelerates polymerization from monomers, and severs filaments." J Biol Chem **279**(19): 20076-87.

Holmes, K. C., D. Popp, et al. (1990). "Atomic model of the actin filament." Nature **347**(6288): 44-9.

Holmes, K. C., M. Tirion, et al. (1993). "A comparison of the atomic model of F-actin with cryo-electron micrographs of actin and decorated actin." Adv Exp Med Biol **332**: 15-22; discussion 22-4.

Huttelmaier, S., P. Bubeck, et al. (1997). "Characterization of two F-actin-binding and oligomerization sites in the cell-contact protein vinculin." Eur J Biochem **247**(3): 1136-42.

Ichetovkin, I., W. Grant, et al. (2002). "Cofilin produces newly polymerized actin filaments that are preferred for dendritic nucleation by the Arp2/3 complex." Curr Biol **12**(1): 79-84.

Jockusch, B. M. and G. Isenberg (1981). "Interaction of alpha-actinin and vinculin with actin: opposite effects on filament network formation." Proc Natl Acad Sci U S A **78**(5): 3005-9.

Kabsch, W., H. G. Mannherz, et al. (1990). "Atomic structure of the actin:DNase I complex." Nature **347**(6288): 37-44.

Khurana, S. and S. P. George (2008). "Regulation of cell structure and function by actin-binding proteins: villin's perspective." FEBS Lett **582**(14): 2128-39.

Klenchin, V. A., S. Y. Khaitlina, et al. (2006). "Crystal structure of polymerization-competent actin." J Mol Biol **362**(1): 140-50.

Korn, E. D., M. F. Carlier, et al. (1987). "Actin polymerization and ATP hydrolysis." Science **238**(4827): 638-44.

Kudryashov, D. S., M. R. Sawaya, et al. (2005). "The crystal structure of a cross-linked actin dimer suggests a detailed molecular interface in F-actin." Proc Natl Acad Sci U S A **102**(37): 13105-10.

Kureishy, N., V. Sapountzi, et al. (2002). "Fascins, and their roles in cell structure and function." Bioessays **24**(4): 350-61.

Le Clainche, C. and M. F. Carlier (2008). "Regulation of actin assembly associated with protrusion and adhesion in cell migration." Physiol Rev **88**(2): 489-513.

Lew, D. J. (2002). "Formin' actin filament bundles." Nat Cell Biol **4**(2): E29-30.

Lorenz, M., D. Popp, et al. (1993). "Refinement of the F-actin model against X-ray fiber diffraction data by the use of a directed mutation algorithm." J Mol Biol **234**(3): 826-36.

Low H. H., C. Sachse, et al. (2009). "Structure of a bacterial dynamin-like protein lipid tube provides a mechanism for assembly and membrane curving." Cell **139**(7): 1342-52.

Lučić, V., F. Förster, W. Baumeister (2005). "Structural studies by electron tomography: from cells to molecules." Annu Rev Biochem **74**: 833-865.

Maciver, S. K., H. G. Zot, et al. (1991). "Characterization of actin filament severing by actophorin from Acanthamoeba castellanii." J Cell Biol **115**(6): 1611-20.

McGough, A., W. Chiu, et al. (1998). "Determination of the gelsolin binding site on F-actin: implications for severing and capping." Biophys J **74**(2 Pt 1): 764-72.

McGough, A., B. Pope, et al. (1997). "Cofilin changes the twist of F-actin: implications for actin filament dynamics and cellular function." J Cell Biol **138**(4): 771-81.

Meyer, R. K. and U. Aebi (1990). "Bundling of actin filaments by alpha-actinin depends on its molecular length." J Cell Biol **110**(6): 2013-24.

Moseley, J. B., K. Okada, et al. (2006). "Twinfilin is an actin-filament-severing protein and promotes rapid turnover of actin structures in vivo." J Cell Sci **119**(Pt 8): 1547-57.

Oda, T., M. Iwasa, et al. (2009). "The nature of the globular- to fibrous-actin transition." Nature **457**(7228): 441-5.

Ono, S. (2007). "Mechanism of depolymerization and severing of actin filaments and its significance in cytoskeletal dynamics." Int Rev Cytol **258**: 1-82.

Otterbein, L. R., C. Cosio, et al. (2002). "Crystal structures of the vitamin D-binding protein and its complex with actin: structural basis of the actin-scavenger system." Proc Natl Acad Sci U S A **99**(12): 8003-8.

Otterbein, L. R., P. Graceffa, et al. (2001). "The crystal structure of uncomplexed actin in the ADP state." Science **293**(5530): 708-11.

Owen, C. H., D. G. Morgan, et al. (1996). "Image analysis of helical objects: the Brandeis Helical Package." J Struct Biol **116**(1): 167-75.

Papp, G., B. Bugyi, et al. (2006). "Conformational changes in actin filaments induced by formin binding to the barbed end." Biophys J **91**(7): 2564-72.

Pavlov, D., A. Muhlrad, et al. (2006). "Severing of F-actin by yeast cofilin is pH-independent." Cell Motil Cytoskeleton **63**(9): 533-42.

Pfaendtner, J., E. Lyman, et al. (2009). "Structure and Dynamics of the Actin Filament." J Mol Biol.

Pollard, T. D. and G. G. Borisy (2003). "Cellular motility driven by assembly and disassembly of actin filaments." Cell **112**(4): 453-65.

Pollard, T. D. and J. A. Cooper (2009). "Actin, a central player in cell shape and movement." Science **326**(5957): 1208-12.

Rebello, C. A. and R. D. Ludescher (1998). "Influence of tightly bound Mg2+ and Ca2+, nucleotides, and phalloidin on the microsecond torsional flexibility of F-actin." Biochemistry **37**(41): 14529-38.

Rouiller, I., X. P. Xu, et al. (2008). "The structural basis of actin filament branching by the Arp2/3 complex." J Cell Biol **180**(5): 887-95.

Sjoblom, B., A. Salmazo, et al. (2008). "Alpha-actinin structure and regulation." Cell Mol Life Sci **65**(17): 2688-701.

Steinmetz, M. O., D. Stoffler, et al. (1997). "Actin: from cell biology to atomic detail." J Struct Biol **119**(3): 295-320.

Sukow, C. and D. DeRosier (1998). "How to analyze electron micrographs of rafts of actin filaments crosslinked by actin-binding proteins." J Mol Biol **284**(4): 1039-50.

Sun, H. Q., K. Kwiatkowska, et al. (1995). "Actin monomer binding proteins." Curr Opin Cell Biol **7**(1): 102-10.

Sun, H. Q., M. Yamamoto, et al. (1999). "Gelsolin, a multifunctional actin regulatory protein." J Biol Chem **274**(47): 33179-82.

Taylor, K. A. and D. W. Taylor (1993). "Projection image of smooth muscle alpha-actinin from two-dimensional crystals formed on positively charged lipid layers." J Mol Biol **230**(1): 196-205.

Tseng, Y., E. Fedorov, et al. (2001). "Micromechanics and ultrastructure of actin filament networks crosslinked by human fascin: a comparison with alpha-actinin." J Mol Biol **310**(2): 351-66.

Van Troys, M., J. Vandekerckhove, et al. (1999). "Structural modules in actin-binding proteins: towards a new classification." Biochim Biophys Acta **1448**(3): 323-48.

Volkmann, N., D. DeRosier, et al. (2001). "An atomic model of actin filaments cross-linked by fimbrin and its implications for bundle assembly and function." J Cell Biol **153**(5): 947-56.

Ward, R. J., J. F. Menetret, et al. (1990). “Method for forming two-dimensional paracrystals of biological filaments on lipid monolayers.” J Electron Microsc Tech **14**(4): 335-41.

Yamakita, Y., S. Ono, et al. (1996). "Phosphorylation of human fascin inhibits its actin binding and bundling activities." J Biol Chem **271**(21): 12632-8.

Yin, H. L. and T. P. Stossel (1979). "Control of cytoplasmic actin gel-sol transformation by gelsolin, a calcium-dependent regulatory protein." Nature **281**(5732): 583-6.

Chapter 3 Janssen et al. (2006)

Three-dimensional structure of vinculin bound to actin filaments.

Molecular Cell, 2006 Jan; 21(2): 271-281.

Three-Dimensional Structure of Vinculin Bound to Actin Filaments

Mandy E.W. Janssen,[1] Eldar Kim,[1] Hongjun Liu,[1] L. Miya Fujimoto,[1] Andrey Bobkov,[1] Niels Volkmann,[1,*] and Dorit Hanein[1,*]
[1] Program on Cell Adhesion
The Burnham Institute for Medical Research
10901 North Torrey Pines Road
La Jolla, California 92037

Summary

Vinculin plays a pivotal role in cell adhesion and migration by providing the link between the actin cytoskeleton and the transmembrane receptors, integrin and cadherin. We used a combination of electron microscopy, computational docking, and biochemistry to provide an atomic model of how the vinculin tail binds actin filaments. The vinculin tail actin binding site comprises two distinct regions. One of these regions is exposed in the full-length autoinhibited conformation of vinculin, whereas the second site is sterically occluded by vinculin's N-terminal domain. The partial accessibility of the F-actin binding site in the autoinhibited full-length vinculin structure suggests that F-actin can act as part of a combinatorial input framework with other binding partners such as α-catenin or talin to induce vinculin head-tail dissociation, thus promoting vinculin activation. Furthermore, binding to F-actin potentiates a local rearrangement in the vinculin tail that in turn promotes vinculin dimerization and, hence, formation of actin bundles.

Introduction

Vinculin is a conserved component of cell morphology and migration and is central to brain and heart development (Xu et al., 1998), integrity of cardiomyocytes, and preservation of normal muscle function (Barstead and Waterston, 1991; Maeda et al., 1997; Olson et al., 2002; Zemljic-Harpf et al., 2004). Electron microscopy studies of isolated molecules showed that vinculin comprises a globular head domain (Vh), a short tail (Vt), and a flexible neck connecting the two (Winkler et al., 1996). In the cytosol, vinculin adopts a default autoinhibited conformation in which Vh and Vt form intramolecular interactions. When these interactions are relieved, binding sites for several molecules are exposed (Jockusch and Rudiger, 1996). In this activated state, α-catenin, α-actinin, and talin can bind to the Vh domain; actin, paxillin, and phosphatidylinositol (4,5)-biphosphate (PIP_2) can bind to the Vt domain; and vasodilator-stimulated phosphoprotein (VASP), actin-related protein complex (Arp2/3), vinexin and ponsin (DeMali et al., 2002; Zamir and Geiger, 2001) can bind to a proline-rich region in the flexible neck.

The recently solved crystal structures of vinculin (Bakolitsa et al., 2004; Borgon et al., 2004) reveal the molecule in its compact autoinhibited form. These studies show that Vh contains four distinct domains (D1–D4), in which D1 and D3 hold the Vt domain like a pair of pincers in the autoinhibited configuration (Bakolitsa et al., 2004). D4 packs end-to-end with Vt and is believed to correspond to the neck region. The interactions between D4 and vinculin were recently shown to play a pivotal role in regulating binding between vinculin domain D1 and talin (Cohen et al., 2005). The conformation of Vt observed in the full-length crystal structure is virtually identical to that of the isolated tail and contains a five-helix bundle (H1–H5) (Bakolitsa et al., 1999). A flexible linker, containing the proline-rich region and connecting D4 and Vt, is mostly disordered in the crystal structures with the exception of residues 879–893 that form a strap, which packs against helices H1 and H2 of the Vt domain. The binding site for PIP_2, which is contained in Vt, is partially occluded by the strap in the full-length structure. Thus, the strap was postulated to be freed to fully expose the PIP_2 binding site when the intramolecular interaction between Vt and Vh are disrupted (Bakolitsa et al., 2004).

Binding to talin recruits vinculin to integrin-mediated extracellular-matrix adhesion sites (Burridge and Mangeat, 1984), whereas localization to cell-cell contacts occurs by binding to α-catenin (Weiss et al., 1998). In both cases, vinculin provides a link between actin filaments (F-actin) and the membrane. However, the precise mechanism remains unclear. Although it is clear that the actin binding site resides in Vt and is deactivated in the autoinhibited form of the full-length molecule (Johnson and Craig, 1995), little is known of its nature. Binding studies of recombinant fragments (Huttelmaier et al., 1997) identified two peptides that can bind F-actin independently, but mapping onto the Vt crystal structure reveals that these peptides do not correspond to coherent separate binding sites. Full-length vinculin was shown to promote actin bundling (Jockusch and Isenberg, 1981), and the existence of a cryptic dimerization site in Vt, which is activated upon binding to F-actin, was demonstrated (Johnson and Craig, 2000). In addition, changes in protease sensitivity and tryptophane fluorescence (Bakolitsa et al., 1999) support a conformational change in Vt upon actin binding, but the details and extent of this change and the location of the dimerization site are not yet established.

We used electron microscopy, image analysis, and computational docking to obtain a detailed model of the F-actin-Vt complex at near-atomic resolution. We find that the overall five-helix bundle structure of Vt is preserved upon F-actin binding. There are two distinct binding sites in Vt, interacting with two separate actin monomers along the filament. One binding site is located close to the top and one close to the bottom of H3. Despite the lack of sequence or structural homology with other known actin binding proteins, the Vt interface on F-actin is similar to that of the calponin-homology domain family, which includes α-actinin and fimbrin (Hanein et al., 1998; McGough et al., 1994). In the full-length vinculin structure, one of the F-actin binding sites is

*Correspondence: niels@burnham.org (N.V.); dorit@burnham.org (D.H.)

partially occluded by domain D1 of Vh, but the second binding site is fully exposed to solvent. Steric hindrance between F-actin and D1 prevents the second binding site to make full contact with the filament, explaining the low affinity of full-length vinculin to F-actin.

To unravel the molecular mechanism of Vt dimerization, we employed electron tomography to F-actin arrays crosslinked by Vt. Computational docking of the F-actin-Vt model into the three-dimensional (3D) structure reconstructions of Vt-crosslinked F-actin filaments extracted from these tomograms revealed severe clashes between the C-terminal loop at the base of the helical bundle of one Vt and the N-terminal strap of another. Biochemical analysis of recombinant Vt fragments that lacked the N-terminal strap and the C-terminal loop, respectively, confirm the involvement of these two structural elements in dimer formation.

Our results implicate a two-step process for F-actin crosslinking in which actin binding of Vt in its intact, five-helix bundle conformation triggers conformational changes in the strap and the C-terminal loop that in turn potentiate dimerization. The partial accessibility of the F-actin binding site in the autoinhibited full-length structure suggests that F-actin, analogous to what was proposed for PIP_2 (Bakolitsa et al., 2004), can act as part of a combinatorial input framework with other binding partners such as α-catenin or talin that also cannot activate vinculin by themselves. Our observation that mixtures of α-catenin's actin binding domain and F-actin show higher binding affinities for full-length vinculin than either of these alone clearly supports this notion.

Results

3D Reconstruction of F-Actin-Vt Complex

To obtain information about the F-actin-Vt interface at near-atomic resolution, we first sought experimental conditions in which to observe recombinant Vt (residues 879–1066) bound to single actin filaments. Whereas Vt almost exclusively crosslinks actin into higher-order structures at a wide range of molar ratios, according to our actin binding assays (data not shown), we detected small fractions of decorated actin filaments pelleting down in the high-speed pellet at low protein concentrations. We increased the population of single actin filaments decorated with Vt and collected data of Vt bound to F-actin in negative stain (Figure 1). Four independent three-dimensional reconstructions were obtained for crossvalidation purposes by using two different image processing approaches (see Experimental Procedures). The 0.5 Fourier shell correlation criterion indicates a resolution of about 2 nm for these reconstructions. Two reconstructions of negatively stained undecorated actin filaments were also obtained. Comparison of images and optical diffraction patterns clearly indicate the presence of Vt (Figures 1A and 1B). After alignment, difference maps were obtained by subtracting each reconstruction of undecorated F-actin from each reconstruction of Vt-decorated filaments. The resulting eight difference maps each represent the density attributable to the bound Vt and can be used to crossvalidate results (see the Supplemental Data available with this article online). An atomic model of actin was docked into the undecorated actin filament reconstructions by using the correlation statistics-based docking algorithm CoAn (Volkmann and Hanein, 1999). The analysis indicated an uncertainty of 0.2 nm for the actin docking. The difference peaks attributed to Vt correspond in volume and shape to a single Vt monomer. Four crystal structures of Vt that differed slightly in the conformation

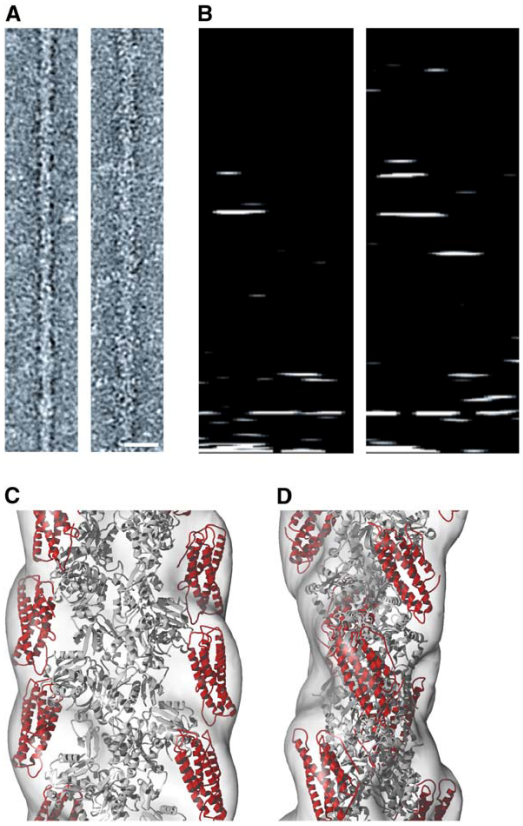

Figure 1. 3D Reconstruction of Actin Filaments Decorated with Vinculin Tail

(A) Representative images of decorated (right) and undecorated (left) actin filaments. There is a clear difference in width caused by vinculin tail binding. The bar is 20 nm.

(B) Optical diffraction patterns of the filaments in (A). The organization of the diffraction pattern into distinct layer lines at distinct heights is a consequence of the helical symmetry. The diffraction patterns of vinculin-tail decorated (right) and undecorated actin (left) show similar layer-line positions, indicating that the helical symmetry of the two structures is the same. The differences in intensity along the layer lines is a consequence of the differences in structure (decorated versus undecorated). Only one quarter of the respective diffraction pattern is shown for clarity, the meridian is on the left side of each pattern, and the equator is at the bottom.

(C) 3D reconstruction of Vt-decorated actin filaments at 2 nm resolution (transparent surface) with atomic models of the actin filament (gray cartoon representation) and vinculin tail (red) docked into the density. The pointed end of the filament is at the top of the figure.

(D) Same as (C), rotated by 90° clockwise around the filament axis. The high quality of the fit clearly demonstrates that there are no large-scale conformational changes when the vinculin tail binds to actin. See also Movie S2, which shows a rotation of the density map and the fit around the filament axis. Movie S1 shows the fit of the Vt structure into the Vt-actin difference map.

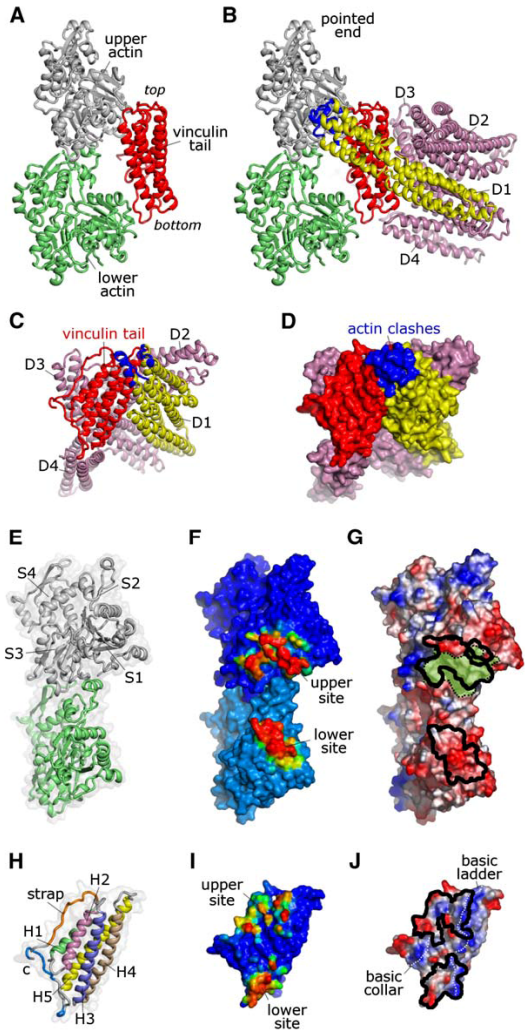

Figure 2. Actin and Vinculin-Tail Docking and Interaction Analysis

(A) Docked model of a vinculin tail molecule (red cartoon representation) and the two actin monomers along the filament (gray and green cartoons) that are in contact with the vinculin tail molecule. The top and the bottom of the Vt helix bundle are labeled. The orientation is the same as in Figure 1C.

(B) Same as (A), with the full-length vinculin structure superimposed by using the docked position of the vinculin tail (red). This arrangement generates severe clashes between the N-terminal vinculin head and subdomain 3 (S3) of the upper actin monomer. The clashing vinculin residues are colored in blue. D1 is shown in yellow and D2–D4 of vinculin are shown in pink.

(C) Full-length vinculin structure shown in an orientation turned 90° counter clockwise around the filament axis. This corresponds to the view that the actin filament would see. Coloring is as in (B), cartoon representation.

(D) Same as in (C), space-filling solvent-exposed surface representation.

(E) The two docked actin monomers are shown as cartoon representations turned 90° clockwise around the filament axis from the orientation in (A). This corresponds to the view that the vinculin tail would see. Subdomains 1–4 are marked as S1-4 on the upper actin (gray). A transparent space-filling surface model is also shown.

(F) Atomic interaction probability as resulting from the docking analysis mapped onto the solvent-exposed surface of the two actin monomers. Red corresponds to highest probability, and blue is zero. There are two spatially distinct sites of interaction: one at the top of subdomain 1 of the lower actin (lower site) and the other on the bottom of subdomain 1 and peripheral to residues of subdomain 3 of the upper actin (upper site). The orientation is the same as (E).

(G) Electrostatic potential mapped onto the solvent-exposed surface of the two actin monomers. Blue corresponds to positive and red to negative. The patches with high interaction probabilities are outlined in black, and the large hydrophobic patch is shaded green and delimited by a dotted line. The orientation is the same as (E).

(H) Vinculin tail in cartoon representation rotated 90° counter clockwise from the orientation in (A) or 180° from (E). This corresponds to the view in (C). The N-terminal strap, the five (color-coded) helices, and the C terminus are marked. The two areas that generate clashes in the dimer model (see Figure 5) are colored in orange (N-terminal strap region) and blue (C-terminal region). A transparent solvent-exposed surface is also shown.

(I) Atomic interaction probability as resulting from the docking analysis mapped onto the solvent-exposed surface of the vinculin-tail model. Red corresponds to highest probability, and blue is the lowest (zero). There are two sites of interaction: one at the top of H2 and H3 (upper site) and the other at the bottom of H3 and the C-terminal loop (lower site). Orientation is the same as in (H).

(J) Electrostatic potential mapped onto the solvent-exposed surface of the vinculin tail. Blue corresponds to positive, and red corresponds to negative. The patches with high interaction probabilities are outlined in black. The basic ladder and the basic collar are outlined as white dotted lines. The orientation is the same as in (H).

of their flexible loops (Bakolitsa et al., 1999) and the Vt portion of the full-length structure (Bakolitsa et al., 2004) were docked into the eight difference maps for crossvalidation. The statistical analysis of these 40 independent docking experiments yielded a single set of fits with positioning uncertainty of only 0.4 nm at a confidence level of 99.9%. The high correlation of the docked Vt structure with the corresponding density in the reconstructions (91.4% ± 0.2), the fact that most of the docked Vt structure is confined in the corresponding reconstruction density (Movie S1), and that there are no severe clashes between the docked Vt and F-actin molecules (Figures 1C and 2A and Movie S2) all indicate that there are no large-scale conformational changes in Vt upon filament binding. The lack of large-scale conformational changes is further supported by the recent results of FRET experiments (Chen et al., 2005) that showed a decrease of FRET efficiency from 46% to 32% upon actin binding, putting an upper bound of ~1 nm on the change in distance between the N and C termini of Vt.

When the full-length vinculin molecule is superimposed on our F-actin-Vt model by aligning the Vt segments, the N-terminal portion of Vh domain D1 (mostly residues 25–40, marked in blue in Figures 2B–2D) clashes severely with subdomain 3 of the upper actin monomer. This explains why full-length vinculin does not bind strongly to F-actin and shows how head-tail dissociation would relieve this steric hindrance.

The Molecular Details of the Actin-Vinculin Interface

We analyzed the interactions between actin and Vt at the near-atomic level by using the interaction probability concept, a probabilistic scoring scheme for the residues involved in binding that arises from a statistical analysis of the docking results (Volkmann and Hanein, 1999, 2003). Analysis of the docking surface identifies two major binding sites (upper and lower interface) at the top

and bottom of the Vt helix bundle that interact with two separate actin monomers along the long-pitch helix of the actin filament (Figure 2). The fact that Vt contacts two monomers in the filament explains its preference for F-actin rather than actin monomers. Differential scanning calorimetry (Figure S3) as well as pyrene fluorescence experiments (Figure S4) both indicate a significant stabilization of F-actin by Vt binding, consistent with Vt bridging between actin monomers along the long-pitch helix of the filament.

Most residues of the "basic ladder," a set of positively charged patches along Vt helix H3 implicated in PIP_2 binding (Bakolitsa et al., 1999), are contained in one of the two interaction sites (Figure 2J), explaining why PIP_2 and F-actin binding are mutually exclusive (Steimle et al., 1999). Although Vt does not share structural or sequence homology with other types of actin binding domains, the actin residues participating in Vt binding substantially overlap with those involved in binding to members of the calponin-homology-domain superfamilies, which includes fimbrin (Hanein et al., 1998) and α-actinin (McGough et al., 1994). This overlap suggests that members of the superfamily cannot bind simultaneously with vinculin to F-actin.

The Upper Interface

This interface buries a total area of 745 $Å^2$ and contains 49.7% polar atoms. Both of these values are well within the range of standard protein-protein interfaces compiled from the crystal structures of heterodimers (Jones et al., 2000). The upper interaction surface of Vt is at the top of helices H2 and H3 and also includes residues 883–890 in the strap (Figures 2I and 2J). This binding site interacts with the upper actin monomer at the bottom of subdomain 1. This region largely coincides with a large hydrophobic pocket on the actin filament, indicating that the interactions of the upper interface region have a substantial hydrophobic component. This hydrophobic pocket on actin was implicated in the interactions with several actin binding proteins (Hanein et al., 1998; McGough et al., 1994; Milligan, 1996; Volkmann et al., 2000; Volkmann et al., 2005) and is thought to be a major target for specific interactions (Dominguez, 2004).

The Lower Interface

This interface buries an area of 533 $Å^2$ and contains 57.2% polar atoms, a percentage significantly higher than that of a typical heterodimer interface (Jones et al., 2000), thus indicating that polar interactions are a significant component of this interface. The lower interaction surface of Vt is at the base of helix H3 and also includes a stretch of residues close to the C terminus (Figures 2I and 2J). The site interacts with an acidic region at the top of subdomain 1 of the lower actin monomer. Two of the interacting Vt residues (R1049 and T1050 in the C-terminal loop) make contact with D4 in the full-length crystal structure (Figure 3A) but at the back face of the molecule, so these interactions do not directly interfere with the actin binding interface. The fact that full-length vinculin can crosslink F-actin (Jockusch and Isenberg, 1981) and that the back faces of Vt residues R1049 and T1050 are likely involved in dimer formation (see below and Figure 3A) suggests that the D4 contacts are released from Vt upon actin binding.

Comparison with Previous Mutagenesis Experiments

Clustered charge-to-alanine mutagenesis experiments were inconclusive in regards to actin binding sites and showed only small effects on actin binding with a maximum decrease of ~20% for any single mutation cluster (Cohen et al., 2005). However, by using our Vt-actin interface model, a clear picture emerges: except for one (containing R978 in H4), all alanine mutation clusters that contain at least one of the seven charged residues in the lower Vt interface (Figures 3A and 3D) result in maximum decrease in actin affinity of Vt. This decrease suggests that a significant part of the interaction of the lower region is electrostatic in nature, consistent with the charge complementarity of the interacting surfaces (Figures 2F and 2I) and the high content of polar atoms in the interface. The single cluster that contains a charged residue of the lower interface (R978) that did not show a significant decrease in actin binding efficiency was shown to have a major effect on vinculin head-tail affinity (Cohen et al., 2005).

Only a single-mutation cluster (K924, R925) that contains a residue (R925) in the upper Vt interface has a marked effect on actin binding. However, here the removal of the charge actually increases actin affinity by ~50%, suggesting that R925 or K924 generate unfavorable charge repulsion at the interface. It was shown previously that the charge at K924 is necessary for PIP_2 interactions (Bakolitsa et al., 1999), rationalizing its existence despite the negative effect on actin binding. There is little change in affinity between wild-type and the mutations of the charged residues in the strap region, supporting the notion that this region may rearrange upon actin binding and these residues move away from the interface. No significant changes occur for the cluster containing interface residues E932 and R935. These findings further support the notion that electrostatic forces are only a minor component of the upper interface interactions and are consistent with the report that significant binding of Vt to F-actin is maintained even in 1 M KCl (Huttelmaier et al., 1997) and with binding of this interface to F-actin's hydrophobic pocket.

Binding of F-Actin and α-Catenin to Vinculin

Isolated Vt binds with micromolar affinity to actin (~1 μM) (Bakolitsa et al., 1999), but full-length vinculin binds only weakly. Similarly, a domain-size fragment (CD3) of α-catenin that contains the vinculin binding site was previously shown to bind D1 of Vh with nanomolar affinity (~80 nM) but bound very weakly to full-length vinculin (Bakolitsa et al., 2004). If F-actin and the α-catenin fragment are simultaneously mixed with full-length vinculin, the affinity of F-actin as well as α-catenin to vinculin increases significantly (Figure 4A). This finding clearly shows that vinculin's actin binding activity is enhanced by the presence of α-catenin and vice versa, supporting the combinatorial input hypothesis.

F-Actin Arrays Crosslinked by Vt and Vt-Dimer Model

It was shown previously that full-length vinculin can induce 3D crosslinked actin bundles (Jockusch and Isenberg, 1981) and that the dimerization site is contained within Vt (Johnson and Craig, 2000). Consistent with previous results (Johnson and Craig, 2000), we did not

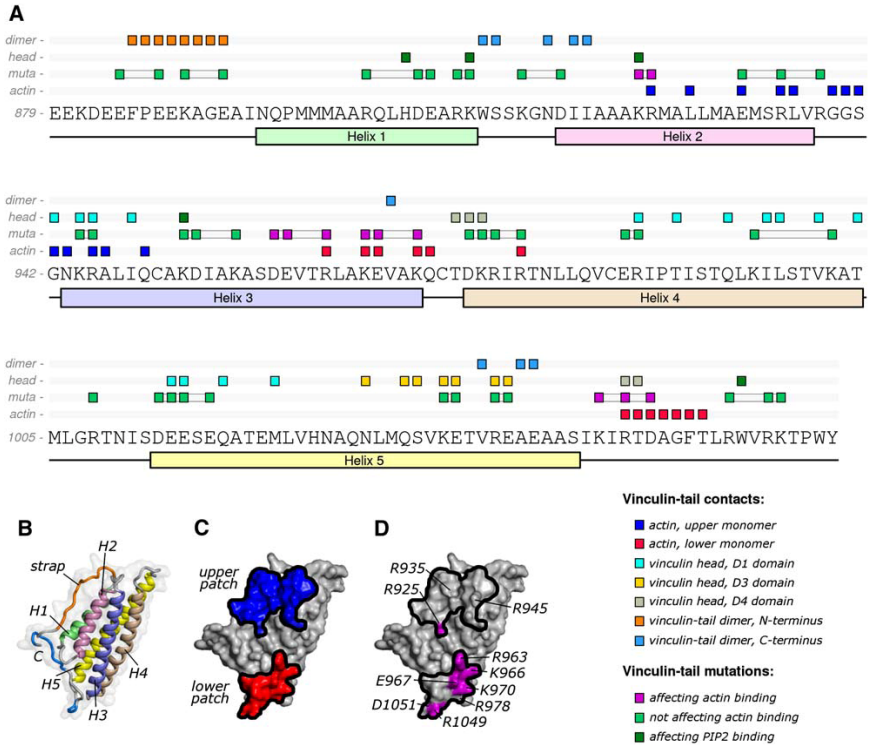

Figure 3. Correlation between Interaction Probabilities, Mutations, Head-Tail Contacts, and Dimer Contacts

(A) Mapping of contacts and mutations onto the Vt sequence. The head contacts are taken from the full-length crystal structure (Bakolitsa et al., 2004). The actin contacts correspond to residues that had atoms with more than 15% interaction probability. The dimer contacts are taken from the analysis of the VtΔs and VtΔC mutants. The charge-to-alanine mutation clusters (Cohen et al., 2005) are indicated by connecting lines. Decreases of ~20% and increases of more than 30% in actin affinity were marked as affecting actin binding. Mutations that affect PIP_2 binding (Bakolitsa et al., 1999) are marked in dark green in the "head" rows.

(B) Vinculin tail structure in cartoon representation. The five color-coded helices, the N-terminal strap, and the C terminus are marked. The residues clashing in the crosslink model are colored, matching with the colors in Figures 5E and 5F. Orientation is as in Figure 1H.

(C) Solvent-exposed surface representation of vinculin tail mapped with the actin-contacting residues. Colors are the same as in (A), and orientation is as in (B).

(D) Solvent-exposed surface with mapping of residues that were assigned to contact actin by the docking analysis and, at the same time, to affect actin binding by charge-to-alanine mutagenesis (magenta). The areas assigned to interact by the docking analysis are outlined in black. Each group of mutations that affects actin binding has at least one residue within these areas. All these residues are indicated; in addition R935, R945, and R978 are marked.

find any evidence for dimerization of Vt in solution with differential scanning calorimetry (Figure S3) or differential centrifugation (data not shown). In contrast, light scattering (Figure S2) as well as pyrene fluorescence (Figure S4) experiments indicate actin-induced dimerization of Vt, implying that Vt can only dimerize after it is bound to actin.

To investigate the molecular mechanism of vinculin dimerization, we extended our structural analysis to actin filaments crosslinked by Vt. We restricted the assembly process in the third dimension by using a lipid monolayer that attracts actin filaments to its surface. In contrast to 3D bundles, the corresponding crosslinked, ordered arrays are suitable for high-resolution analysis (Sukow and DeRosier, 1998; Volkmann et al., 2001). The actin filaments were first polymerized in the presence of Vt in solution and then subsequently attracted to the positively charged lipid layer suspended at the air water interface, thus only generating one monolayer of ordered actin-Vt assemblies. These samples were then transferred to electron microscope grids and imaged in negative stain.

Two-Dimensional Image Analysis

Analysis of the micrographs of actin filament arrays in the presence of Vt clearly show crosslinking between the filaments (Figures 5A and 5B). In the crosslinked arrays, crossbridges appear as regularly spaced bands perpendicular to the axis of the actin filaments (Figure 5A). Diffraction analysis confirms the paracrystalline order of the arrays, which is comparable in quality and resolution to other crosslinked actin arrays previously investigated by us and others (Sukow and DeRosier, 1998; Taylor et al., 2000; Volkmann et al., 2001). The diffraction patterns of the Vt-actin arrays show only a single meridonal reflection at a height corresponding to the actin crossover repeat (~1/38 nm). This finding confirms that there is only one crosslinking site per actin crossover (Figure 5A). A combination of Fourier and real-space analysis (Sukow and DeRosier, 1998; Volkmann et al., 2001) shows that the average distance between

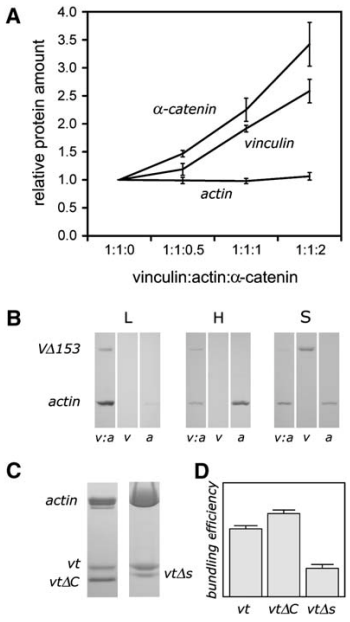

Figure 4. Analysis of Cosedimentation Experiments

Crosslinked or bundled actin-filaments were detected with low-speed pelleting, and filaments were detected with high-speed pelleting.

(A) Enhancement of full-length vinculin binding to F-actin by addition of α-catenin vinculin binding domain CD3 (see Figure S1 for additional data). Amounts were quantified (in arbitrary units) with densitometry of the gels and computer analysis. Material of the same protein detected in low-speed and high-speed pelleting was added up, corresponding to the complete material bound to actin. Actin and vinculin were normalized to 1 by using the amounts at a concentration of 1:1 for vinculin:actin. CD3 was normalized to 1 by using the amount at a concentration of 1:1 for CD3:actin. Error bars were compiled from independent experiments. When CD3 is added to the solution, full-length vinculin binds F-actin more efficiently.

(B) Binding of VΔ153 to F-actin. Abbreviations are as follows: L, low-speed pellet; H, high-speed pellet; S, supernatant; V:a, a 1:1 mix of actin and VΔ153; v, VΔ153 only; a, actin only. These gels show that VΔ153 efficiently crosslinks F-actin.

(C) Actin-bundling competition experiments between Vt and Vt deletion mutants lacking the C-terminal loop (VtΔC, left) and the N-terminal strap (VtΔs, right). Vt and the respective mutant construct were first mixed in equimolar ratios and then added to the F-actin sample. Gels after low-speed pelleting are shown.

(D) Quantified bundling efficiency of Vt versus VtΔC and VtΔs. The relative amounts of Vt, VtΔC, and VtΔs implicated in actin bundling (in arbitrary units) shown were estimated from the gels in (C) by densitometry and computer analysis. The error bars were compiled from independent gels. The average effect of the deletion of the C-terminal loop was an increase of 23% in bundling efficiency, indicating that the loop obstructs a cryptic dimerization site. The effect of the strap deletion was a decrease of 60%, implicating that a cryptic dimerization site in wild-type Vt is contained in the strap.

the crosslinked filaments is about 10.5 nm, which is significantly larger than the 9 nm average distance between adjacent actin filaments in arrays without the crosslinker (Volkmann et al., 2001). By comparison, the distance in actin-fimbrin arrays is 12 nm (Volkmann et al., 2001) and in actin-α-actinin arrays it is 39 nm (Taylor et al., 2000). Actin filaments are polar in nature, and the distance of the diffraction spots in relation to the filament distance (Sukow and DeRosier, 1998; Volkmann et al., 2001) indicates that the filaments in the Vt-crosslinked arrays have the same polarity. This unipolarity of the arrays is consistent with observations in cells, wherein actin fibers close to vinculin-containing adhesion sites are also unipolar (Geiger et al., 1995).

Tomographic 3D Reconstructions

We obtained a tomographic tilt series of the negatively stained samples and calculated 3D reconstructions of the entire arrays (Figure 5A). Tomographic reconstructions are much noisier and generally of lower resolution than reconstructions that involve averaging of many motifs. Tomograms are not easily interpreted at high resolution for this reason. To ease interpretation, a 3D watershed segmentation algorithm (Volkmann, 2002) was applied to analyze the size and shape of the crosslinker (Figures 5B and 5C). The analysis showed consistently over a variety of data sets that the crosslinker is composed of two separate units (Figure 5C), each of which has the approximate shape and size of a Vt monomer. We obtained a model of the crosslink by computationally docking atomic models of the F-actin-Vt complex into appropriate segments of the tomographic reconstructions (Figures 5C–5F). The spatial relationships between the actin filaments in the arrays as determined by two-dimensional (2D) image analysis (see above) were used as constraints to enhance robustness of the docking.

The docking experiments bring the N-terminal Vt region of one monomer close to the C terminus of the second one, leading to severe steric clashes between the strap and the C-terminal end of the molecule (Figure 5F). This observation suggests that one or both of these structural elements need to change conformation in order to expose cryptic dimerization sites. Several of the clashing residues are also implicated in interacting with actin. These residues are 883–890 in the strap and 1049–1051 in the C-terminal loop. Residue F885 locks the strap into place in the crystal structures by inserting into a hydrophobic crevice between H1 and H2 (Bakolitsa et al., 1999). It is interesting to note that the four immediately adjacent strap residues (E883, E884, E887, and E888) are negatively charged, making it energetically unfavorable to contact the negatively charged actin surface and thus providing a plausible trigger for the conformational change in this area by disrupting the F885 interactions that anchor the strap to the rest of the molecule. The yellow fluorescent protein (YFP) used as a reporter for the conformation of full-length vinculin in the context of FRET (Chen et al., 2005) is inserted between residues E883 and E884. Upon actin binding, the distance between this YFP and a cyan fluorescent protein (CFP) at the C terminus (residue 1066) increases by ~1 nm, further supporting the notion that the strap is released but no large-scale refolding or unfurling of the molecule occurs. Residues 1049–1051 in the C-terminal loop are implicated in the interface between Vt and the head domain D4 (Bakolitsa et al., 2004). This area of Vt was identified by charge-to-alanine mutagenesis to provide a significant portion of the affinity necessary for autoinhibition of vinculin in regards to talin (Cohen et al., 2005).

Biochemical Analysis of Vinculin Deletion Mutants

To further refine and validate our structural findings, we synthesized and characterized three vinculin deletion

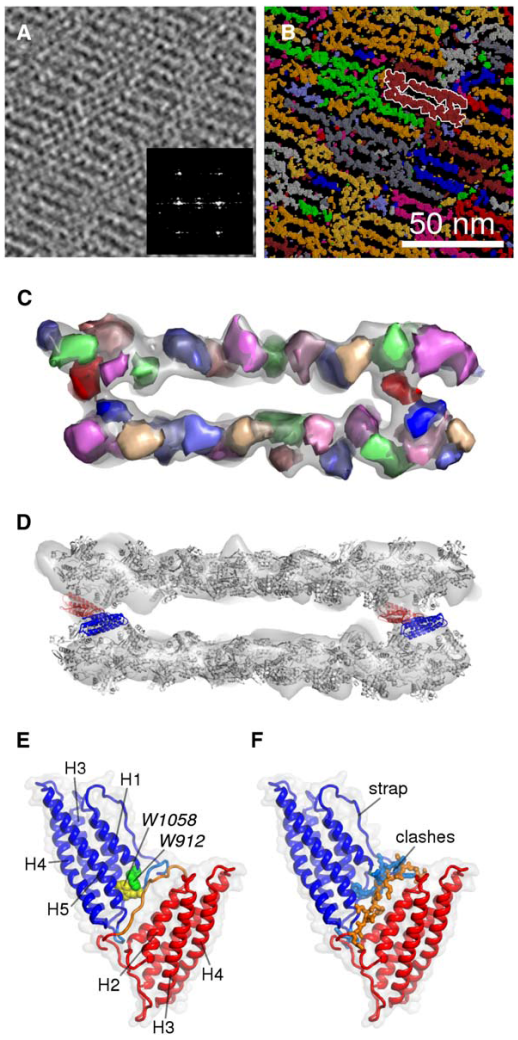

Figure 5. Analysis of Actin Arrays Crosslinked by the Vinculin Tail

(A) Central slice of a tomographic reconstruction showing actin filaments running from the top left corner to the lower right corner. Bands of crosslinks can be seen perpendicular to the filament direction. The insert shows an optical diffraction pattern used for determining polarity, distance, and relative rotation of the filaments in the array. The meridian and the equator intersect in the center of the diffraction pattern.

(B) Results of coarse-grained watershed segmentation that isolates and highlights connected areas of interest. A representative area is outlined in white.

(C) Surface representation (transparent) of outlined area in (B) and results of fine-grained watershed segmentation of this area (solid surfaces, slightly lower contour level for clarity). Monomers can be identified as segments in the two filament areas. The densities that connect the filaments (crosslinks) can be segmented into two entities (red and blue) that correspond to one vinculin tail molecule each.

(D) Two actin filaments (gray cartoon representation) with attached vinculin-tail molecules (red and blue) docked into the outlined area from (B).

(E) Enlarged view of the vinculin-tail dimer extracted from (D). One vinculin tail is shown in red and the other one in blue cartoon representation. The red molecule is in the same orientation as that in Figure 2H. Helices H2–H4 are marked for the red molecule. Helices H1, H3–H5, and tryptophans W912 (green space-filling atom representation) and W1058 (yellow) are marked for the blue molecule.

(F) The clashes between the C-terminal loop of the blue molecule (light-blue stick representation) and the N-terminal strap region of the red molecule (orange stick representation).

mutants. These were constructs containing residues 154–1066 (VΔ153), residues 893–1066 (VtΔs, s for strap), and residues 879–1051 (VtΔC). All residues that obscure the actin binding sites in full-length autoinhibited vinculin are within the first 153 residues. Thus, VΔ153 should exhibit similar actin binding behavior as Vt because both actin binding sites are fully accessible. Indeed, cosedimentation experiments show that VΔ153 binds actin with similar efficiency as Vt (Figure 4B). This finding fully supports our interface model and the proposed mechanism of actin binding autoinhibition by interference of domain D1 of the vinculin head.

Actin cosedimentation experiments show that Vt and the deletion mutant VtΔs exhibit no significant difference in actin binding (data not shown), indicating that the strap residues implicated in actin binding by the docking have no effect on binding affinity. This finding supports the notion that the strap rearranges upon actin binding and moves away from the interface. In contrast, actin-bundling efficiency of VtΔs is decreased by 60% in comparison to Vt (Figures 4C and 4D). This finding implies that a significant portion of the dimerization site resides in the strap (namely residues 886–891) and that the strap needs to change conformation from the solution structure in order to expose its dimerization site. For the VtΔC mutant, a 23% increase in bundling efficiency is observed (Figures 4C and 4D). This result indicates that the C-terminal loop is not directly involved in dimerization but obscures a dimerization site in the solution structure and needs to change conformation in order to allow access. Residues with significantly increased exposed surface area upon removal of the C-terminal loop are located in the loop between H1 and H2 and at the bottom end of H5 (see also Figure 3A). In conclusion, both the N-terminal strap and the C-terminal loop need to change conformation in order to expose cryptic dimerization sites in Vt. Whereas the C-terminal loop merely obscures the corresponding dimerization site, the strap is actively involved in crosslink formation.

Discussion

Mechanism of Actin-Vinculin Binding

The structural similarity between Vt and the exchangeable apolipoproteins taken together with evidence for conformational changes in Vt upon phospholipid binding led to the proposal that Vt may unfurl its five-helix bundle when it binds to phospholipids (Bakolitsa et al., 1999). Because tryptophan fluorescence and increase of protease sensitivity support a conformational change in Vt upon actin binding, an unfurling of the bundle was proposed as part of the actin binding mechanism as well (Bakolitsa et al., 1999). However, our data are incompatible with unfurling of the five-helix bundle upon actin binding and clearly show that there are no large-scale changes upon binding. The nature of the conformational change triggered by actin binding is more subtle,

involving local rearrangements in the strap and C-terminal loop regions.

Our results identify two spatially separate actin binding sites at the top and at the bottom of the Vt helix bundle. The two recombinant peptides previously shown to bind actin individually (Huttelmaier et al., 1997) do not coincide with these two sites, but both peptides encompass parts of both sites, thus rationalizing their binding behavior. One of the actin binding sites identified in our study is partially occluded by Vh-Vt interactions in the autoinhibited form, and steric clashes between the Vh domain D1 and F-actin prevent the second binding site, which is almost fully exposed, to make full contact with F-actin. Thus D1-Vt interactions need to be released to allow full access to the two binding sites of Vt, explaining why autoinhibited full-length vinculin binds actin only weakly. The notion of D1-Vt interactions playing a major role for regulation of F-actin binding is supported by our results with the recombinant fragment VΔ153 that has the N-terminal 153 residues of D1 removed and, thus, does not contain the residues that occlude one of the Vt actin binding sites or the residues that would clash with F-actin. The VΔ153 construct binds and crosslinks actin in a similar manner as the isolated Vt domain.

Each of the two actin binding surfaces of Vt contacts a different actin monomer along the filament. The binding surface at the bottom of the helix bundle, which is exposed in the autoinhibited form, contacts a highly charged area on top of subdomain 1 of actin, indicating that this interaction is dominated by electrostatic interactions. The second Vt binding surface, at the top of the bundle and partially occluded in the autoinhibited full-length structure, contacts a prominent hydrophobic pocket on F-actin that was previously assigned in binding of a variety of actin binding proteins. Recent clustered charge-to-alanine experiments (Cohen et al., 2005) are fully consistent with the binding sites and support the structural conclusions that the site at the top is mostly hydrophobic in nature, whereas the one at the bottom contains a significant amount of electrostatic interactions. Many of the residues implicated in PIP_2 binding (Bakolitsa et al., 1999) are contained in one of the binding sites, explaining why PIP_2 and F-actin binding are mutually exclusive (Steimle et al., 1999).

Mechanism of Vinculin Dimerization

Vt is monomeric in solution, and decorated actin filaments contain monomeric Vt, but Vt crosslinks consist of dimers. These observations indicate that dimerization occurs subsequent to actin binding. One plausible mechanism for crosslinking is that actin binding triggers a local conformational change in Vt that exposes a dimerization surface. Crosslinking experiments have also suggested the existence of a cryptic dimerization site for Vt that only gets exposed after actin binding (Johnson and Craig, 2000). Our data identifies one of the dimerization sites in the N-terminal strap and the other close to the C-terminal loop of Vt.

Release of the strap from the surface of Vt is strongly implicated in the conformational transitions during opening of the full-length molecule (Bakolitsa et al., 2004), and the actin binding behavior of the strap deletion mutant indicates that the strap moves away from the actin interface. Additional supportive evidence for strap release comes from marked changes in trytophan fluorescence and increased protease sensitivity upon F-actin binding (Bakolitsa et al., 1999). The three tryptophans in Vt that can participate in fluorescence all occur in this region (Figure 5E), and the proteolytic cleavage sites that are buried in the crystal structure (residues 900 and 912) will get exposed if the strap is released. The strap is well structured in crystals of recombinant Vt as well as in full-length vinculin. In both structures, the strap is packed against the Vt body obscuring the dimerization site, which explains why Vt and vinculin are monomeric in solution. Results from FRET experiments (Chen et al., 2005) limit the increase of distance between the Vt C terminus (residue 1066) and the strap (883 and 884) upon actin binding to ~1 nm. Thus, the combined body of data suggests that binding of vinculin to F-actin potentiates dimerization not by triggering a large-scale conformational change in Vt such as bundle unfurling but by presenting two monomers on apposing filaments into the correct position and orientation.

Activation by Combinatorial Input

It was previously suggested that spatial clustering of vinculin binding partners at focal adhesions provides the mechanism for vinculin activation if the thermodynamic additivity of binding energies exceeds the affinity of the intramolecular head-tail interaction (Bakolitsa et al., 2004). Such combinatorial input (Figures 6A–6E) would provide an efficient, localized mechanism of activation. Only if all required binding partners are present does vinculin get activated.

Consistent with this model, the low binding affinity of actin to full-length vinculin is insufficient to trigger head-tail dissociation to fully expose the occluded actin binding site and to eliminate the steric clashes of the actin filament and the N-terminal Vh residues. This steric occlusion prevents the formation of a stable Vinculin-F-actin complex. However, the fact that the lower actin binding site is fully exposed to solvent opens the possibility for transient interactions with F-actin that might impact interactions with other binding partners. Interactions of full-length vinculin with α-catenin (Bakolitsa et al., 1999), talin (Cohen et al., 2005), and IpaA, a *Shigella flexneri* protein that binds to D1 and competes with talin (Bourdet-Sicard et al., 1999), are all weaker than the respective interactions with Vh. This implicates that full head-tail dissociation does not generally occur for the binding of these ligands alone. This notion of combinatorial input and a cooperative role of F-actin in the process are directly supported by the fact that binding of IpaA to full-length vinculin does not induce the fully activated conformation, which is only observed after F-actin is added (Chen et al., 2005).

In the case of talin, it was shown that the release of a contact between the bottom of the Vt helix bundle and domain D4 of Vh is necessary to allow release of the D1-Vh interactions by talin (Cohen et al., 2005). Interestingly, the critical residues for the D4-Vt interactions are exposed at the opposite side of D4 and are contained in the exposed lower actin binding site of Vt. Some of those residues are contained in the C-terminal loop of Vt, which we showed to change conformation upon actin binding, most likely disrupting the interaction

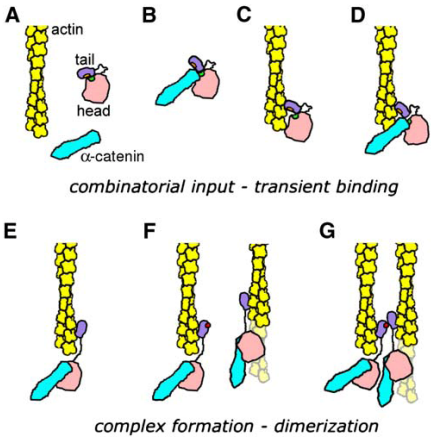

Figure 6. Hypothetical Model of Combinatorial Activation and Subsequent Dimerization of Vinculin

(A) Vinculin exists in the cytoplasm in its autoinhibited form where the head (pink) and the tail (purple) are attached to each other in a way that the binding sites for its binding partners are not fully accessible. For example, we show in this study that the actin binding site (orange) in the vinculin tail is not fully accessible, and it was shown previously (Bakolitsa et al., 2004) that the α-catenin binding site (green) in the head is not fully accessible either. An actin filament is shown in yellow, and α-catenin is shown in cyan.

(B) α-catenin can bind to vinculin only with low affinity (Bakolitsa et al., 2004), indicating that α-catenin is not capable of dissociating the vinculin head from the tail. However, α-catenin triggers some change in vinculin that increases the affinity of F-actin to vinculin.

(C) Although binding of vinculin to actin is very weak, its presence increases the affinity of vinculin to α-catenin.

(D and E) Only if both actin and α-catenin (and possibly other components) are present is the combined effect shown in (B) and (C) large enough to result in a stable complex between actin, vinculin, and α-catenin (E), most likely by full head-tail dissociation (D), as previously shown for IpaA and F-actin.

(F and G) Once the vinculin tail is bound to actin (F), a conformational change takes place within the tail that exposes cryptic dimerization sites (red dot), allowing formation of crosslinks between actin filaments (G).

with D4. A compelling model for cooperation between F-actin and talin entails that transient interactions between F-actin and the exposed actin binding site of Vt weaken interactions between Vt and D4, which, in turn, would increase the probability for talin to disrupt the D1-Vt interactions. Our results that the affinity of full-length vinculin to F-actin is significantly increased in the presence of the vinculin binding fragment of α-catenin and vice versa lends further support to such cooperation between F-actin and other vinculin binding partners.

Experimental Procedures

Protein Preparation

Rabbit skeletal muscle actin was kindly provided by Drs. S. Lowey and K. Trybus. It was generally used within 2–3 weeks of preparation. Chicken vinculin tail (residues 879–1066) was expressed in *E. coli* strain BL21(DE3), purified, and stored as described (Bakolitsa et al., 1999). GST-VΔ153 (residues 154–1066), GST-VtΔC (residues 879–1051), and GST-VtΔs (residues 893–1066) were expressed in pGEX plasmid (Amersham) and eluted from Glutathione Sepharose as a tag-free protein by overnight incubation at 4°C with GST-fused PreScission protease (Amersham). Full-length his-tagged vinculin pET-15b construct and α-catenin vinculin binding domain (CD3) were kindly provided by Dr. R. Liddington. Expression and the purification for full-length vinculin followed (Bakolitsa et al., 2004).

Cosedimentation Assays

Binding and crosslinking of actin filaments by vinculin, VtΔC, VtΔs, VΔ153, and CD3 were characterized in cosedimenation assays by using differential centrifugation in which the crosslinked actin filaments were recovered with low-speed pellets (20 krpm, 17,380 × g, 15 min), and filaments were recovered with high-speed pellets (80 krpm, 278,100 × g, 30 min). The samples were incubated with preformed actin filaments for 1 hr at 4°C. (1 concentration unit in Figure S1 is equal to 7 μM). All assays were performed in F-actin buffer (10 mM Tris [pH 7.5], 50 mM NaCl, 2 mM DDT, and 2 mM $MgCl_2$). Pellets and supernatants were recovered by using a Beckman TLA100 rotor at 4°C at the respective speed. For the cosedimentation assay of vinculin, actin, and CD3, the supernatants of the high-speed pellet were incubated for 1 hr at 4°C with fresh 7 μm F-actin. These samples were again assayed, generating a second set of high- and low-speed pellets and supernatants, removing bias generated by a portion of vinculin being either unfolded or denatured. The samples were analyzed on 4%–20% Tris-Glycine gels. Each experiment was repeated at least once to estimate the associated standard errors of the measurements. Relative intensities of the Coomassie blue-stained bands were quantified in arbitrary units with densitometry and computer processing. For Figure 4A, the quantified amount of protein recovered from the two low-speed and the two high-speed pellets were added up for each protein to give the total amount of material bound to F-actin. For Figures 4C and 4D only the amount recovered from the low-speed pellet, corresponding to the protein involved in actin bundling, was used for quantification.

Electron Microscopy

Actin-Vt Complexes

Actin was diluted to ~0.030 mg/ml with 50 mM Imidazole (pH 7.0), 100 mM NaCl, 10 mM $MgCl_2$, 10 mM EGTA, 0.5 mM DTT, and 0.2 mM ATP just prior to application to the glow-discharged 400-mesh copper grids coated with carbon film. After a 1 min incubation in a humid chamber, 5 μl of Vt diluted to 0.09 mg/ml with 20 mM Tris-HCl (pH 7.5), 50 mM NaCl, and 0.5 mM DTT was applied. After 1 min of incubation, the samples were stained with 2% uranyl acetate and air dried. Low-dose images were recorded with a Tecnai 12 electron microscope (FEI Electron Optics) at a nominal magnification of 52,000× (at 120 keV) and ~1.5 μm defocus (electron dose ~10 e^-/A^2). Thirty micrographs were digitized with a SCAI scanner (Z/I Imaging Corporation) with a pixel size of 0.3 nm on the sample.

Actin-Vt Arrays

Arrays were grown (24 hrs) at 4°C on positively charged lipid layers consisting of a 3:7 w/w solution of di-lauryl-phosphatidylinositol and didodecyldimethylammonium bromide dissolved in chloroform (Taylor and Taylor, 1992; Volkmann et al., 2001). The lipid and surfactant mixture was layered over the polymerization buffer prior to the injection of G-actin (~0.35 μg/μl) for producing the arrays. The polymerization buffer contains 20 mM Na_2PO_4, 50 mM KCl, 1 mM ATP, 2 mM $MgCl_2$, 1 mM EGTA, 1 mM DTT (pH 7.0) and ~0.9 μg/μl of Vt. The monolayers were transferred to 200-mesh copper grids coated with lacey carbon films. Specimens were stained with 2% uranyl acetate and air dried. Six tomographic tilt series were recorded at magnifications of 26,000× (low dose) with tilt angles ranging from −70° to +70° and increments of 1° (at 1.5 μm defocus) by using the FEI tomography package, the advanced tomography Holder from Fischione, PA, and a Gatan 1K CCD camera with a pixel size of 0.69 nm on the sample. A second tilt series rotated by ~90° was collected of each sample to minimize missing data due to the limited tilt range of the single tilt series.

Image Analysis of Filaments

A total of four reconstructions of actin decorated with Vt were obtained for crossvalidation purposes. Two of these maps were constructed by using standard helical reconstruction techniques (Owen et al., 1996), utilizing the fact that Fourier space methods allow separation of two independent diffraction patterns from each helix (far side and near side). Two additional reconstructions were obtained with a hybrid procedure (Volkmann et al., 2005) that

combines single-particle reconstruction approaches with helical symmetry (Egelman, 2000). For the reconstructions obtained by this method, 10,723 small overlapping segments of Vt-decorated actin filaments were selected from the micrographs. The data were then split into two arbitrary halves for independent analysis. Each set was phase corrected after fitting of the contrast transfer function with EMAN (Ludtke et al., 1999). In order to guard against bias from starting models, we calculated two different initial starting models with different helical parameters by using our atomic model for undecorated F-actin. For each of the starting models and each of the half-data sets, between 20 and 90 iterations were performed until convergence was achieved. An analysis of the Fourier shell correlation between the reconstructions from the independent half sets shows that the curve drops below 0.5 at a resolution of 2.02 (±0.06) nm. There were no statistically significant differences between the helical reconstructions and those calculated by the hybrid procedure. In addition, two three-dimensional reconstructions of undecorated actin for difference mapping were obtained by using standard helical reconstruction techniques. Eight difference maps were generated by using each of the four decorated maps with each of the two undecorated actin reconstructions.

Analysis of Tomograms

Tomographic reconstructions were generated with IMOD (Kremer et al., 1996). Two tilt series of the same data, rotated by 90°, were collected and merged to reduce reconstruction artifacts due to missing data. Two adjacent filament densities containing two cross-linking sites were segmented from the tomograms by using the three-dimensional watershed transform as described (Volkmann, 2002). Two actin filament models of 16 monomers with two Vt molecules attached in crossover distance each were docked into the segmented tomgraphic density with the CoAn package (Volkmann and Hanein, 1999). The known spatial relationship (in register, unipolar) between the filaments was enforced during the docking procedure.

Docking of Atomic Models

We docked an atomic model of F-actin (Volkmann et al., 2005) into each of the two undecorated actin filament reconstructions by using CoAn (Volkmann and Hanein, 1999). Next, we isolated single asymmetric units from the eight difference maps (see above) by using the watershed transform (Volkmann, 2002). The asymmetric unit represents the extra density that is attached to the actin filament and corresponds in size and shape to a single Vt molecule (see also Movie S1). We docked five alternative atomic models for Vt that differ slightly in the conformation of flexible loops into these maps and used a subsequent statistical analysis of the docking results to estimate the fitting uncertainty and the interaction probabilities as described in detail elsewhere (Volkmann and Hanein, 2003). Briefly, the method maps globally all docking possibilities that are compatible with the data and their inherent uncertainty. In contrast to other computational docking methods that provide only one single best fit, the final result of our docking study is a set of fits that are all compatible with the data in light of its associated error levels given a certain confidence level (we used 99.9% for this study). The confidence level can be interpreted as the probability of finding the correct fit in the solution set. The actual confidence intervals that define the solution set are determined by crossvalidation with independent reconstructions and multiple alternative models. Thus, errors (and noise) inherent to data collection, reconstruction technique, and minor variations in the search models are explicitly accounted for in the size of the confidence intervals. Parameters such as coordinate uncertainty or the probability of residues to partake in interactions can be derived as properties of these sets. For example, the root mean square deviation between models within the solution set (0.4 nm for Vt and 0.2 nm for F-actin in this study) gives a conceptual handle on the size of the confidence interval and can be used as an estimate for the uncertainty of the fitting. Representations of the solution sets for Vt and actin are available on the world wide web at http://coan.burnham.org.

Molecular Graphics

Molecular structure representations and density maps in the figures were created with Pymol (www.pymol.com).

Supplemental Data

Supplemental Data include four figures, two movies, and Supplemental References and can be found with this article online at http://www.molecule.org/cgi/content/full/21/2/271/DC1/.

Acknowledgments

We are grateful to Pamela Powers for technical assistance during the initial stages of the project. These studies were supported by the NIGMS Cell Migration Consortium (U54 GM646346) to D.H. and by the National Institutes of Health grant GM64473 to N.V.

Received: September 28, 2005
Revised: November 11, 2005
Accepted: November 17, 2005
Published: January 19, 2006

References

Bakolitsa, C., de Pereda, J.M., Bagshaw, C.R., Critchley, D.R., and Liddington, R.C. (1999). Crystal structure of the vinculin tail suggests a pathway for activation. Cell *99*, 603–613.

Bakolitsa, C., Cohen, D.M., Bankston, L.A., Bobkov, A.A., Cadwell, G.W., Jennings, L., Critchley, D.R., Craig, S.W., and Liddington, R.C. (2004). Structural basis for vinculin activation at sites of cell adhesion. Nature *430*, 583–586.

Barstead, R.J., and Waterston, R.H. (1991). Vinculin is essential for muscle function in the nematode. J. Cell Biol. *114*, 715–724.

Borgon, R.A., Vonrhein, C., Bricogne, G., Bois, P.R., and Izard, T. (2004). Crystal structure of human vinculin. Structure (Camb) *12*, 1189–1197.

Bourdet-Sicard, R., Rudiger, M., Jockusch, B.M., Gounon, P., Sansonetti, P.J., and Nhieu, G.T. (1999). Binding of the Shigella protein IpaA to vinculin induces F-actin depolymerization. EMBO J. *18*, 5853–5862.

Burridge, K., and Mangeat, P. (1984). An interaction between vinculin and talin. Nature *308*, 744–746.

Chen, H., Cohen, D.M., Choudhury, D.M., Kioka, N., and Craig, S.W. (2005). Spatial distribution and functional significance of activated vinculin in living cells. J. Cell Biol. *169*, 459–470.

Cohen, D.M., Chen, H., Johnson, R.P., Choudhury, B., and Craig, S.W. (2005). Two distinct head-tail interfaces cooperate to suppress activation of vinculin by talin. J. Biol. Chem. *280*, 17109–17117.

DeMali, K.A., Barlow, C.A., and Burridge, K. (2002). Recruitment of the Arp2/3 complex to vinculin: coupling membrane protrusion to matrix adhesion. J. Cell Biol. *159*, 881–891.

Dominguez, R. (2004). Actin-binding proteins–a unifying hypothesis. Trends Biochem. Sci. *29*, 572–578.

Egelman, E.H. (2000). A robust algorithm for the reconstruction of helical filaments using single-particle methods. Ultramicroscopy *85*, 225–234.

Geiger, B., Yehuda-Levenberg, S., and Bershadsky, A.D. (1995). Molecular interactions in the submembrane plaque of cell-cell and cell-matrix adhesions. Acta Anat. (Basel) *154*, 46–62.

Hanein, D., Volkmann, N., Goldsmith, S., Michon, A.M., Lehman, W., Craig, R., DeRosier, D., Almo, S., and Matsudaira, P. (1998). An atomic model of fimbrin binding to F-actin and its implications for filament crosslinking and regulation. Nat. Struct. Biol. *5*, 787–792.

Huttelmaier, S., Bubeck, P., Rudiger, M., and Jockusch, B.M. (1997). Characterization of two F-actin-binding and oligomerization sites in the cell-contact protein vinculin. Eur. J. Biochem. *247*, 1136–1142.

Jockusch, B.M., and Isenberg, G. (1981). Interaction of alpha-actinin and vinculin with actin: opposite effects on filament network formation. Proc. Natl. Acad. Sci. USA *78*, 3005–3009.

Jockusch, B.M., and Rudiger, M. (1996). Crosstalk between cell adhesion molecules: vinculin as a paradigm for regulation by conformation. Trends Cell Biol. *6*, 311–315.

Johnson, R.P., and Craig, S.W. (1995). F-actin binding site masked by the intramolecular association of vinculin head and tail domains. Nature *373*, 261–264.

Johnson, R.P., and Craig, S.W. (2000). Actin activates a cryptic dimerization potential of the vinculin tail domain. J. Biol. Chem. *275*, 95–105.

Jones, S., Marin, A., and Thornton, J.M. (2000). Protein domain interfaces: characterization and comparison with oligomeric protein interfaces. Protein Eng. *13*, 77–82.

Kremer, J.R., Mastronarde, D.N., and McIntosh, J.R. (1996). Computer visualization of three-dimensional image data using IMOD. J. Struct. Biol. *116*, 71–76.

Ludtke, S.J., Baldwin, P.R., and Chiu, W. (1999). EMAN: semiautomated software for high-resolution single-particle reconstructions. J. Struct. Biol. *128*, 82–97.

Maeda, M., Holder, E., Lowes, B., Valent, S., and Bies, R.D. (1997). Dilated cardiomyopathy associated with deficiency of the cytoskeletal protein metavinculin. Circulation *95*, 17–20.

McGough, A., Way, M., and DeRosier, D. (1994). Determination of the alpha-actinin-binding site on actin filaments by cryoelectron microscopy and image analysis. J. Cell Biol. *126*, 433–443.

Milligan, R.A. (1996). Protein-protein interactions in the rigor actomyosin complex. Proc. Natl. Acad. Sci. USA *93*, 21–26.

Olson, T.M., Illenberger, S., Kishimoto, N.Y., Huttelmaier, S., Keating, M.T., and Jockusch, B.M. (2002). Metavinculin mutations alter actin interaction in dilated cardiomyopathy. Circulation *105*, 431–437.

Owen, C.H., Morgan, D.G., and DeRosier, D.J. (1996). Image analysis of helical objects: the Brandeis Helical Package. J. Struct. Biol. *116*, 167–175.

Steimle, P.A., Hoffert, J.D., Adey, N.B., and Craig, S.W. (1999). Polyphosphoinositides inhibit the interaction of vinculin with actin filaments. J. Biol. Chem. *274*, 18414–18420.

Sukow, C., and DeRosier, D. (1998). How to analyze electron micrographs of rafts of actin filaments crosslinked by actin-binding proteins. J. Mol. Biol. *284*, 1039–1050.

Taylor, K.A., and Taylor, D.W. (1992). Formation of 2-D paracrytals of F-actin on phospholipid layers mixed with quarternary ammonium surfactants. J. Struct. Biol. *108*, 140–147.

Taylor, K.A., Taylor, D.W., and Schachat, F. (2000). Isoforms of alpha-actinin from cardiac, smooth, and skeletal muscle form polar arrays of actin filaments. J. Cell Biol. *149*, 635–646.

Volkmann, N. (2002). A novel three-dimensional variant of the watershed transform for segmentation of electron density maps. J. Struct. Biol. *138*, 123–130.

Volkmann, N., and Hanein, D. (1999). Quantitative fitting of atomic models into observed densities derived by electron microscopy. J. Struct. Biol. *125*, 176–184.

Volkmann, N., and Hanein, D. (2003). Docking of atomic models into reconstructions from electron microscopy. Methods Enzymol. *374*, 204–225.

Volkmann, N., Hanein, D., Ouyang, G., Trybus, K.M., DeRosier, D.J., and Lowey, S. (2000). Evidence for cleft closure in actomyosin upon ADP release. Nat. Struct. Biol. *7*, 1147–1155.

Volkmann, N., DeRosier, D., Matsudaira, P., and Hanein, D. (2001). An atomic model of actin filaments cross-linked by fimbrin and its implications for bundle assembly and function. J. Cell Biol. *153*, 947–956.

Volkmann, N., Liu, H., Hazelwood, L., Krementsova, E.B., Lowey, S., Trybus, K.M., and Hanein, D. (2005). The structural basis of myosin V processive movement as revealed by electron cryo-microscopy. Mol. Cell *19*, 595–605.

Weiss, E.E., Kroemker, M., Rudiger, A.H., Jockusch, B.M., and Rudiger, M. (1998). Vinculin is part of the cadherin-catenin junctional complex: complex formation between alpha-catenin and vinculin. J. Cell Biol. *141*, 755–764.

Winkler, J., Lunsdorf, H., and Jockusch, B.M. (1996). The ultrastructure of chicken gizzard vinculin as visualized by high-resolution electron microscopy. J. Struct. Biol. *116*, 270–277.

Xu, W., Baribault, H., and Adamson, E.D. (1998). Vinculin knockout results in heart and brain defects during embryonic development. Development *125*, 327–337.

Zamir, E., and Geiger, B. (2001). Molecular complexity and dynamics of cell-matrix adhesions. J. Cell Sci. *114*, 3583–3590.

Zemljic-Harpf, A.E., Ponrartana, S., Avalos, R.T., Jordan, M.C., Roos, K.P., Dalton, N.D., Phan, V.Q., Adamson, E.D., and Ross, R.S. (2004). Heterozygous inactivation of the vinculin gene predisposes to stress-induced cardiomyopathy. Am. J. Pathol. *165*, 1033–1044.

Supplemental Data

Three-Dimensional Structure of Vinculin Bound to Actin Filaments

Mandy E.W. Janssen, Eldar Kim, Hongjun Liu, L. Miya Fujimoto, Andrey Bobkov, Niels Volkmann, and Dorit Hanein

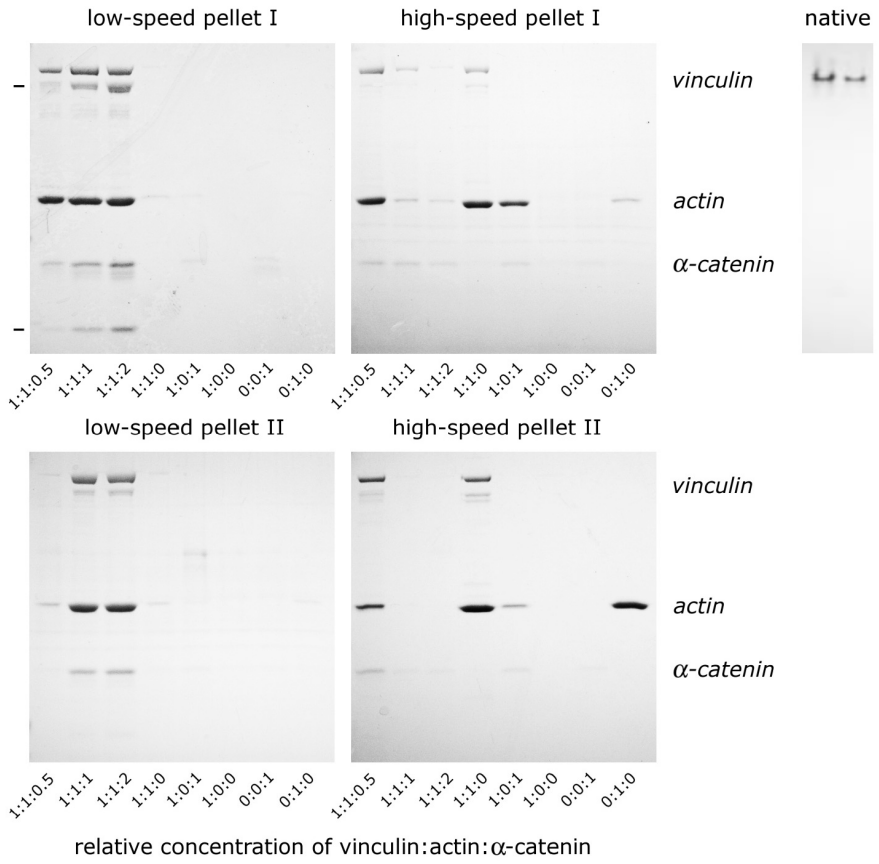

Figure S1. Cosedimentation Assays of Full-Length His-Tagged Vinculin, α-Catenin Vinculin-Binding Domain CD3, and F-Actin Show that F-Actin Binding Activity of Vinculin Is Enhanced in the Presence of CD3

These gels were quantified in arbitrary units for Figure 4b, the quantified amount of protein recovered from the two low-speed and the two high-speed pellets were added up for each protein to give the total

amount of material bound to F-actin. Relative concentration of 1 corresponds to 7 μM. The supernatant of high-speed pellet I was incubated with fresh F-actin and re-assayed (pellets II). This step was done to test for equilibrium effects and to remove bias from partially unfolded or denatured vinculin molecules. The second band and the lowest band in the gels (marked with -) correspond to cleavage products of full-length vinculin. The single band in the alkaline native gel (upper right of figure, concentration 14 μM on left, 7 μM on right) of the full-length vinculin construct after purification shows that all the material is fully folded and maintains its quaternary structure, indicating that the cleavage does not affect the structural integrity of the molecule. This is why both cleavage products are pelleted down with F-actin. Only after denaturation on the SDS gels, the cleavage products separate.

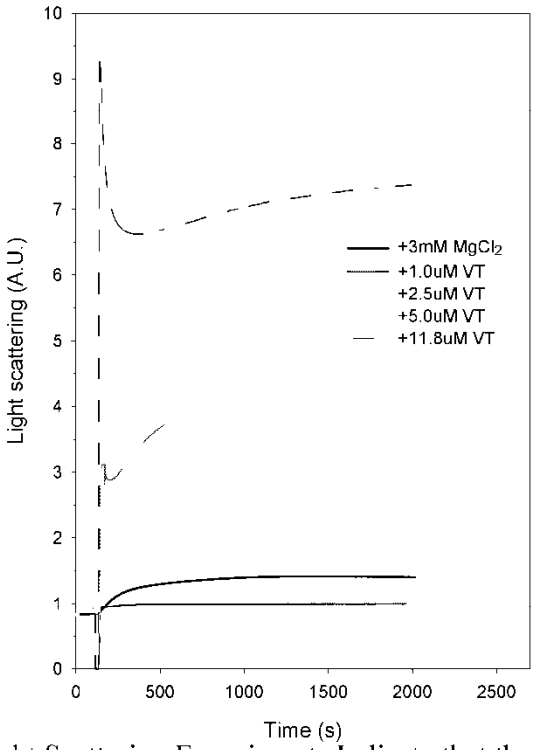

Figure S2. Light Scattering Experiments Indicate that the Interaction of Vt with Actin Is a Complex Multistep Process

In Figure S2, the black sigmoidal curve shows increase in the light scattering associated with polymerization of 12 μM G-actin induced by addition of 3.0mM $MgCl_2$. 1.0 μM Vt had no effect on the light scattering of 12 μM G-actin (blue curve). Upon addition of 2.5 μM Vt initial increase in light scattering was followed by decrease (green curve). At higher Vt concentrations, the initial jump in light scattering was followed by decrease and then increase (magenta and red curves). Clearly, all of the curves collected in the presence of Vt deviate from a typical polymerization curve (black line) and demonstrate the multi-step nature of the Vt-actin interactions. This complexity is most likely related to actin-induced dimerization of Vt and cross-linking of F-actin by Vt dimers.

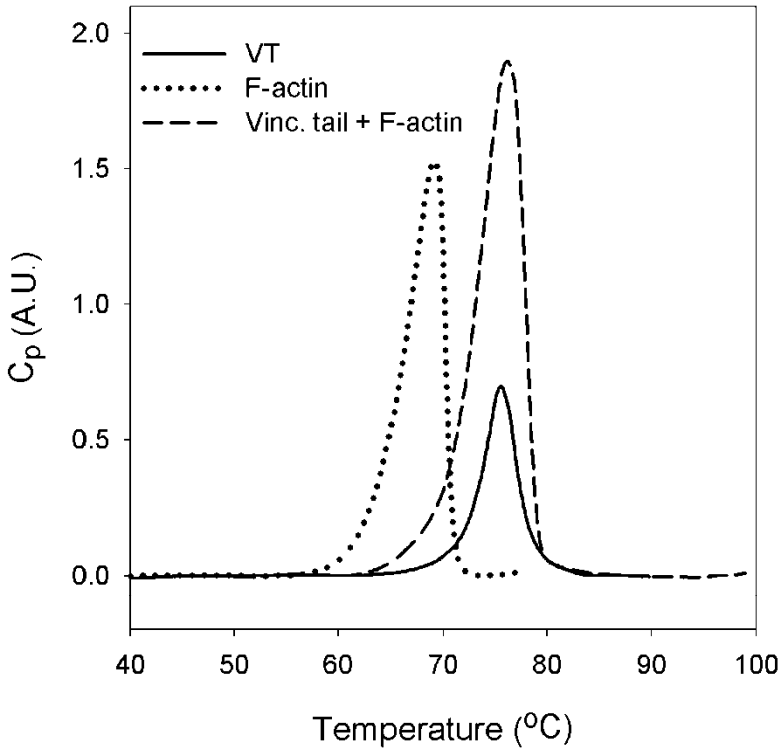

Figure S3. Differential Scanning Calorimetry (DSC) Probes Protein Conformations in Solution

Previous studies (Bertazzon et al., 1990; Le Bihan and Gicquaud, 1991; Levitsky et al., 1998) demonstrated that DSC is sensitive to the structural state of actin and to the conformation of the inter-protomer contacts in actin in particular. For instance, F-actin melts at a much higher temperature and more cooperatively than monomeric G-actin. This effect results from the interaction of actin monomers in the polymer. Also, ligands known to stabilize intermolecular contacts in F-actin (e.g., phalloidin, BeF_x) increase the melting temperature of F-actin (Le Bihan & Gicquaud, 1991; Levitsky et al., 1998). Fig. S3 shows DSC scans obtained for 33 μM F-actin (dotted line), 33μM Vt (solid line) and 1:1 Vt-F-actin complex (dashed line). While the melting temperature (T_m) of F-actin alone was 69.1 °C, the melting temperature of the Vt-F-actin complex was 76.2 °C. This ~7° increase in T_m indicates strong stabilization of F-actin by Vt. There is no evidence for the presence of Vt dimers in the DSC curve of Vt in solution (solid line).

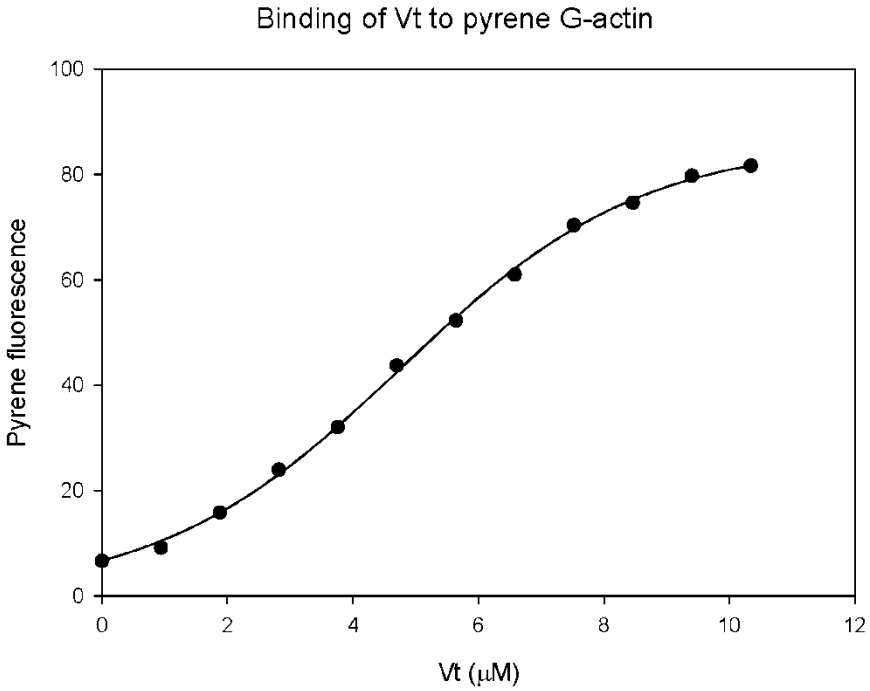

Figure S4. Pyrene Fluorescence Experiments of Labeled G-Actin in the Presence of Vt

The figure shows that Vt promotes actin polymerization (Fig. S4), again implicating that the F-actin structure is stabilized by Vt binding. In addition, binding of Vt to pyrene G-actin is cooperative, which is not consistent with regular 1:1 molar ratio, supporting the formation of actin induced Vt dimers.

Supplemental References

Bertazzon, A., Tian, G. H., Lamblin, A. & Tsong, T.Y. (1990). Enthalpic and entropic contributions to actin stability: calorimetry, circular dichroism, and fluorescence study and effects of calcium. Biochemistry *29*, 291-298.

Le Bihan, T. & Gicquaud, C. (1991). Stabilization of actin by phalloidin: a differential scanning calorimetric study. Biochem Biophys Res Comm *181*, 542-547.

Levitsky, D. I., Nikolaeva, O. P., Orlov, V. N., Pavlov, D. A., Ponomarev, M. A. & Rostkova, E. V. (1998). Differential scanning calorimetric studies on myosin and actin. Biochemistry (Moscow) *63*, 322-333.

Chapter 3, in full is a reprint of the material as it appears in Molecular Cell, January 2006, Mandy E.W. Janssen, Eldar Kim, Hongjun Liu, L. Miya Fujimoto, Andrey Bobkov, Niels Volkmann and Dorit Hanein, 21(2): 271-281. Janssen, Volkmann and Hanein conceived the project, designed the experiments, and wrote the paper. Janssen performed most of the experiments. Kim assisted and conducted in some of the biochemical molecular and cell biology studies Liu assisted and provided in the image analysis studies, Fujimoto and Bobkov assisted and performed some of the biophysical characterization studies.

Chapter 4

Structural details of vinculin activation

Summary

Binding of vinculin to F-actin and other ligands is mediated by an intramolecular head-tail interaction in vinculin. The auto-inhibited state of vinculin renders the protein inactive by masking its binding sides for other binding partners. A combinatorial input of F-actin and a second ligand is proposed to activate vinculin (Bakolitsa, Cohen et al. 2004). In this study, a combination of transmission electron microscopy and biochemical analysis was used to compare vinculin activation by F-actin in combination with constructs of talin and of α-catenin, which are part of the cell-matrix and cell-cell adhesion junctions respectively. None of the talin constructs was able to significantly activate vinculin *in-vitro*. However, the α-catenin construct (CD3) was able to induce considerable actin bundling by vinculin when present in low molar ratios.

In parallel, actin bundling by vinculin was assessed using a vinculin construct, VΔ153, which lacks the first 153 N-terminal amino acids and is therefore constituently active. Dual axis electron tomography and image analysis show that VΔ153 induces actin bundles like the vinculin tail, and that the head domain is flexible upon crosslinking and induce a larger interfilamental spacing.

Introduction

In order to activate vinculin a mechanism was proposed in which F-actin and a second ligand simultaneously bind the head and tail domain and subsequently disrupt the vinculin intermolecular interaction (Bakolitsa, Cohen et al. 2004). Talin is one of the proteins reported to bind the vinculin head domain (Vh) (residues1-258) (Izard, Evans et al. 2004) and in the presence of F-actin has been suggested to release the Vh-Vt interaction (Bakolitsa, Cohen et al. 2004). Talin is a 270kD, elongated antiparallel dimer, with a small globular N-terminal head domain and a flexible rod domain that contains 11 vinculin binding sites (Gingras, Ziegler et al. 2005). In this study I used isolated vinculin binding domains (VBSs) to activate vinculin instead of the full length talin protein or the talin rod domain. The reason for this is that the vinculin binding sites are not readily accessible in talin due to the inhibitory interaction between its rod and head domains (Goksoy, Ma et al. 2008).

Three of the talin VBSs have been described in detail and were previously used in assays to activate vinculin (Bass, Smith et al. 1999; Gingras, Ziegler et al. 2005). These include VBS1 (residues (607-636), VBS2 (residues 852-879), and VBS3 (residues 1944-1969). The vinculin binding site in talin is defined by a short peptide sequence that forms an amphipathic helix with basic and hydrophobic faces (Bass, Smith et al. 1999; Gingras, Ziegler et al. 2005). X-ray crystal structures have been determined for the VBSs of talin (Izard, Evans et al. 2004; Izard and Vonrhein 2004; Fillingham, Gingras et al. 2005), the VBS of α-actinin (Bois, Borgon et al. 2005), and of the IpaA invasion protein of *S. Flexneri* (Nhieu and Izard 2007), all interacting with the vinculin head domain. (Fillingham et al. 2005) determined what happens to the talin VBS2 domain (residues 755-889) upon binding to Vh (residues 1-258). VBS2 is

a left-handed, amphipathic, four-helix bundle in which the amino acids that are important for vinculin binding are buried in the core of the helical bundle. Therefore a significant conformational change is required upon binding the vinculin head domain. VBS2 helices H1, H3, and H4 are immobilized, whereas helix 2 completely unfolds and exposes the hydrophobic surfaces of H1, H3 and H4. This suggests that VBS2 is able to bind multiple vinculin head constructs simultaneously (Fillingham, Gingras et al. 2005).

A conformational change in Vh is introduced upon binding to talin VBSs (Izard, Evans et al. 2004; Izard and Vonrhein 2004). Talin VBS3 binds Vh (residues 1-258) in a 1:1 molar ratio. It does not activate vinculin by competing with Vt interaction, but it distorts the Vh-Vt interface from a distance. VBS3 is a single amphipathic α-helix that inserts between helices H1 and H2 of Vh, with its hydrophobic face contacting the hydrophobic core of the N-terminal helical bundle of Vh. This requires conformational changes in the vinculin head. The C-terminal helical bundle has a stable conformation and serves as an anchor, whereas helix H1, H2, and H4 of the N-terminal helical bundle undergo dramatic movements, rearrangements and distortions upon formation of the new five-helix bundle in the Vh-VBS3 complex. This process is referred to as helical bundle conversion in which dramatic changes occur in the conformation of α-helices (Izard, Evans et al. 2004). Talin VBS1, VBS2 and VBS3 have considerable variation in sequence, yet they bind the same site in Vh, albeit with different binding affinities (Table 4-1) (Izard and Vonrhein 2004).

A similar mechanism was found for the interaction between α-actinin and vinculin. The VBS domain in the central rod domain of α-actinin binds between helices H1 and H2 of the N-terminal helical bundle of Vh, and forces H1 into the Vh-Vt interface.

Similar to the VBSs of talin, the α-actinin VBS induces a helical bundle conversion in the N-terminal bundle of Vh, but the C-terminal bundle remains unaffected. However, the α-actinin VBS runs in opposite direction and is shifted compared to talin's VBSs and causes a unique structural change in Vh (Bois, Borgon et al. 2005). Binding of vinculin by either of the talin VBSs or by the α-actinin VBS results in a similar mode of vinculin activation, whereby the vinculin tail is displaced from a distance. The unique structural changes show flexibility in Vh that ensures distinct identities when bound to different ligands.

It is notable that the crystal structure of a region, consisting of two VBSs in IpaA, bound to Vh shows another mechanism of α-helix-helical bundle interaction besides helical bundle conversion. This mechanism is helix addition (Nhieu and Izard 2007). The C-terminus of IpaA contains two high affinity VBSs for vinculin, IpaA-VBS and IpaA-VBS2. IpaA-VBS binds between helices H1 and H2 of the N-terminal helical bundle in Vh and induces the helical bundle conversion described above. On the other hand, IpaA-VBS2 binds to the hydrophobic patch between helices H2and H3 of the C-terminal helical bundle. The structure of the C-terminal helical bundle is unaffected upon IpaA-VBS2 binding; a helix is simply added from IpaA-VBS2 to the vinculin C-terminal helical bundle. This addition by itself does not activate vinculin, but might be necessary to stabilize the IpaA-vinculin complex. A similar scenario is suggested for some of talin's VBSs. (Nhieu and Izard 2007).

Table 4-1 Binding affinities within vinculin and between vinculin and its ligands. Vh = vinculin head; Vt = vinculin tail (aa 884-1066).

Protein interaction	Binding	Literature
Vt-Vh (aa1-258)	~11.5 μM	(Cohen, Chen et al. 2005)
Vt-proteolytic Vh (aa1-858)	~50 nM	(Johnson and Craig 1994)
Vt-Vh (aa1-851)	~93 nM	(Cohen, Chen et al. 2005)
Vt-full length vinculin	<1 nM	(Bakolitsa, Cohen et al.
Talin VBS1 (aa607-636) – Vh (aa1-258)	~14.7 nM	(Izard and Vonrhein 2004)
Talin VBS2 (aa852-879) – Vh (aa1-258)	~32.8 nM	(Izard and Vonrhein 2004)
Talin VBS3 (aa1943-2157) – Vh (aa1-258)	~39 nM	(Bass, Patel et al. 2002)
Talin VBS3 (aa1944-1969) – Vh (aa1-258)	~3.1 nM	(Izard and Vonrhein 2004)
Talin VBS3 (aa1944-1969) – Vh, D1-3	~400 nM	(Bakolitsa, Cohen et al.
Vinculin-F-actin	>>50 μM	(Johnson and Craig 1995)
Vt-F-actin	~1 μM	(Johnson and Craig 1995)
α-actinin VBS – Vh (aa1-258)	~1.7 nM	(Bois, Borgon et al. 2005)
IpaA-VBS+VBS2 – Vh (aa1-258)	~3.1 nM	(Nhieu and Izard 2007)
IpaA-VBS2 – Vh (aa1-258)	~30.2 nM	(Nhieu and Izard 2007)

The objective of this study was to determine if the full length vinculin protein bundles actin filaments in a similar way as the vinculin tail domain (Vt) does by obtaining high resolution structural information using transmission electron microscopy. Vt comprises only 1/6 of the total molecular weight. One goal was to see where the rest of vinculin (~100kD) is located in the cross-linked F-actin and if it influences vinculin dimerization and subsequently affects actin bundle characteristics. I used the following VBS constructs to activate the full length vinculin protein in the presence of F-actin: talin's VBS2- and VBS3-domain, talin's VBS3-peptide, and α-catenin's CD3-region. In addition to wild-type vinculin, I also used the T19 vinculin mutant described previously (Cohen, Chen et al. 2005). In parallel with the use of full length vinculin, I also used a slightly shorter vinculin construct and determined its actin bundling characteristics. This construct, VΔ153, lacks the first 153 N-terminal amino acids and is therefore constituently active.

Experimental Procedures

Protein Preparation

Rabbit skeletal muscle actin was used from two different sources; it was generated as described in (Volkmann, Hanein et al. 2000) or provided by Cytoskeleton Inc (AKL99). Lab prepared actin was generally used within 2-3 weeks of preparation. His-tagged full length vinculin, kindly provided by Dr. R. Liddington, was recloned to remove the his-tag. The DNA sequence corresponding to the first 130 amino acids of chicken vinculin was made using primers 5'-catgccatgggcagca gcatgcctgtcttccacacacgcacc-3' and 3'-ccaggttgctgacagcggcctgcacggc cgacacg-5'. The product was amplified by PCR and cloned into vector pET15b containing the his-tagged vinculin construct using the Nco1-Eag1 restriction sites. The absence of his-tag and errors was confirmed by DNA sequencing. The vinculin mutant T19 (K1047A, R1049A and D1051A) was made using the QuikChange Multi Site-Directed Mutagenesis Kit and primers 5'-gaagcagcatccattgcgatagcaacagctgccggattcactctg-3' and 5'-cagagtgaatccggcagctgttgctat cgcaatggatgctgcttc-3'. Both vinculin proteins were expressed in *E.coli* strain BL21(DE3). Cell cultures were induced with 0.1 mM IPTG (16 hr,15ºC) and pellets frozen at -80ºC. Upon thawing, 2 mM PMSF, 1 protease inhibitor tablet [Roche] and 0.1% TWEEN-20 were added. Cells were homogenized at 15,000 psi, cell debris was removed by centrifugation. Purification of the proteins from cleared cell lysates was achieved by ion exchange chromatography on a 5 ml HiTrap Quaternary ammonium (Q Sepharose^{TM} HP) column (GE Healthcare) at pH 7.5 and pH 8.5, followed by purification on a 5 ml HiTrap Sulfopropyl (SP Sepharose ^{TM} HP) column (GE Healthcare) at pH 5.0 and 7.5.

Purified proteins was dialyzed against 20 mM Pipes, pH 7.5, 50 mM NaCl, 1 mM MgCl2 and stored at -80ºC until further use.

VΔ153 is a vinculin construct lacking the first 153 N-terminal amino acids and was kindly provided by Dr. R. Liddington as a His-tagged construct in pET-15GX. Due to its low binding affinity to nickel beads, VΔ153 was recloned into pGEX4T1 Ecor1/Not1 to obtain a GST-tagged construct. VΔ153 was expressed in *E.coli* strain BL21(DE3). The cell culture was induced with 0.1 mM IPTG (16 hr, 15ºC) and the pellet was frozen at -80ºC. Upon thawing, 0.1% TWEEN-20, 1 tablet of protease inhibitors, 1 mM DTT and 2 mM PMSF were added. Cells were homogenized at 15,000 psi, cell debris was removed by centrifugation. VΔ153 was purified from cleared cell lysates on a glutathione-sepharose affinity column (Amersham). The GST-tag was cleaved on the column by biotinylated thrombin and removed by streptavidin agarose. The purified protein was dialyzed against 20 mM Pipes, pH 7.5, 50 mM NaCl, 1 mM MgCl2 and stored at at -80ºC until further use.

The plasmids pET15b, which encodes amino acids 755-885, and pET151-DTOPO, which encodes amino acids 1843-1973 of mouse talin, called VBS2 and VBS3 respectively, were kindly provided by Dr. D. Critchley. The plasmid pET15b, which encodes amino acids 277-510 of mouse a-catenin, called CD3, was kindly provided by Dr. R. Liddington. VBS2, VBS3 and CD3 were expressed in *E.coli* strain BL21(DE3). Cells were grown to early log phase, induced with 1 mM IPTG (3 hrs, 37ºC) and the pellets frozen at -80ºC. Upon thawing, 2 mM PMSF, 1% Tween-20 and 1 tablet of protease inhibiters were added. Cells were homogenized at 15,000 psi, cell debris was removed by centrifugation. Purification of the proteins from the cleared cell lysate was achieved by metal chelate affinity chromatography on a 5 ml Hi-Trap

Nickel column (Amersham). The his-tag on VBS2 and CD3 was cleaved with biotinylated thrombin and removed with streptavidin agarose. They were further purified by ion-exchange chromatography on a 5 ml HiTrap Quaternary ammonium column (Amersham). The his-tag on VBS3 was cleaved with acTEV™ Protease (Invitrogen) and removed by rerunning the protein on a 5 ml Hi-Trap Nickel column. VBS2, VBS3 and CD3 were dialyzed into 20 mM Tris pH 7.5, 150 mM NaCl and stored at -80ºC until further use. The synthetic VBS3 peptide, corresponding to amino acids 1945-1970 of talin, was kindly provided by Dr. Satterthwait and Dr. Chen (BIMR).

Cosedimentation Assays

Binding and crosslinking of actin filaments by VΔ153 or vinculin in combination with VBS3, VBS2, CD3, or VBS3 peptide were characterized in cosedimenation assays using differential centrifugation in which the crosslinked actin filaments were recovered from low-speed pellets (20 krpm, 17,380 x g, 15 min), and filaments were recovered from high-speed pellets (80 krpm, 278,100 x g, 30 min). The samples were incubated with preformed actin filaments for 1 hr at 4ºC. (1 concentration unit is equal to 4 μM). All assays were performed in F-actin buffer (10mM Tris [pH 7.5], 50mM NaCl, 2mM DDT, and 2mM MgCl2). Pellets and supernatants were recovered using a Beckman TLA100 rotor at 4ºC at the respective speed. The samples were analyzed on 4%–20% Tris-Glycine gels. Each experiment was repeated at least once.

Size-exclusion chromatography

Complex formation of VBS3 and Vfl was analyzed by FPLC analysis using a Superdex^{TM} S200 10/300 GL size-exclusion column (GE Healthcare) on an ÄKTA-FPLC (UPC900/Frac920) with software package Unicorn 5.10 (GE Healthcare). Vfl and VBS3 were pre-spinned at 278,100 x g for 30 minutes at 4^{o}C. VBS3 was added to Vfl in a 20-fold molar excess and incubated for 30 minutes on ice before running the sample over the column.

Electron Microscopy

Actin-Vinculin-Activator Complexes

Actin was diluted to ~0.03 mg/ml with 50 mM Imidazole (pH 7.0), 100 mM NaCl, 10 mM MgCl2, 10 mM EGTA, 0.5 mM DTT, and 0.2 mM ATP and incubated with vinculin and activator in appropriate molar ratios for 10 minutes on ice. 5µl sample was absorbedto a glow-discharged ,400-mesh copper grid, coated with a carbon film. After a 1 min incubation in a humid chamber, the samples were stained with 2% uranyl acetate and air dried. Low-dose images were recorded with a Gatan 1k CCD camera on a Tecnai 12 electron microscope (FEI Electron Optics) at nominal magnifications of 52,000, 42,000 and 26,000 (all at 120 keV) and ~1.5 µm defocus for vinculin-activator complexes or with a Gatan 2k CCD camera on a Tecnai F20 electron microscope (FEI Electron Optics) at a nominal magnification of 13,500, at 200kV and ~4µm defocus for VΔ153 (electron dose ~10 e/Å2).

Actin-VΔ153 Arrays

Arrays were grown (24 hrs) at 4ºC on positively charged lipid layers consisting of a 3:7 w/w solution of di-lauryl-phosphatidylinositol and didodecyldimethylammonium bromide dissolved in chloroform (Taylor and Taylor, 1992; Volkmann et al., 2001). The lipid and surfactant mixture was layered over the polymerization buffer prior to the injection of G-actin (~0.1 mg/ml) for producing the arrays. The polymerization buffer contains 20 mM Na2PO4, 50 mM KCl, 1 mM ATP, 2 mMMgCl2, 1mMEGTA, 1mMDTT (pH 7.0) and ~0.06 mg/ml of VΔ153. The monolayers were transferred to 200-mesh copper grids coated with lacey carbon films. Specimens were stained with 2% uranyl acetate and air dried. Dual axis tomographic tilt series were recorded at magnifications of 29,000 (low dose) with tilt angles ranging from -60º to +60º and increments of 2º (at ~3.5 µm defocus) on a Tecnai TF20 (FEI Electron Optics) using the SerialEM 2.8.1 tomography package (Mastronarde 2005), the advanced tomography Holder from Fischione,PA, and a Gatan 2K CCD camera. The exposure on the sample was ~160 e/tomogram.

Analysis of Tomograms

The tomographic reconstructions were generated with IMOD (Kremer, Mastronarde et al. 1996). Two tilt series of the same sample, rotated 90º about the microscope axis, were aligned and then merged to reduce artifacts caused by the missing wedged data, which is especially visible in filamentous structures (chapter 2). This alignment was done by tracking 15nm gold fiducials that were deposited on one side of the sample. Densities of two adjacent actin filaments with a cross-linker between them were segmented from the tomographic reconstruction using a 3D watershed segmentation algorithm (Volkmann 2002).

Results

Vinculin activation by F-actin and talin VBSs

VBS2 is composed of amino acids 755-889, whereas VBS3 contains amino acids 1843-1973. The synthetic VBS3-peptide consists of the C-terminal α-helix of the VBS3 domain (aa 1945-1970). Fig. 4-1 shows the location of these regions within the talin protein.

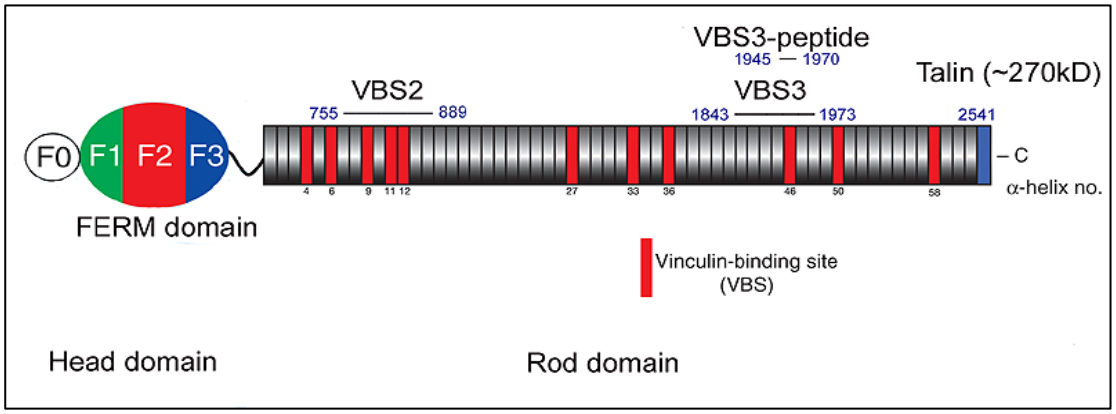

Fig. 4-1 Schematic representation of talin. The locations of the VBS2 and VBS3 domains and the VBS3-peptide are indicated.

Vinculin activation by F-actin and VBS3

Talin's VBS3 domain has a high binding affinity for vinculin head Domain 1 (~39 nM). 25-fold more VBS3 than vinculin was used to activate vinculin in the presence of actin filaments. To distinguish actin bundling form single filament binding, I performed an actin cosedimentation assay in which protein solutions were first centrifuged at low speed to isolate the actin bundles with their bound proteins and then centrifuged at low speed to recover the single actin filaments and bound proteins. Vinculin by itself induces a minimal amount of F-actin bundling, but mostly binds single actin filaments.

Addition of VBS3 induces more vinculin binding to actin filaments and a slight increase in F-actin bundling (Fig. 4-2).

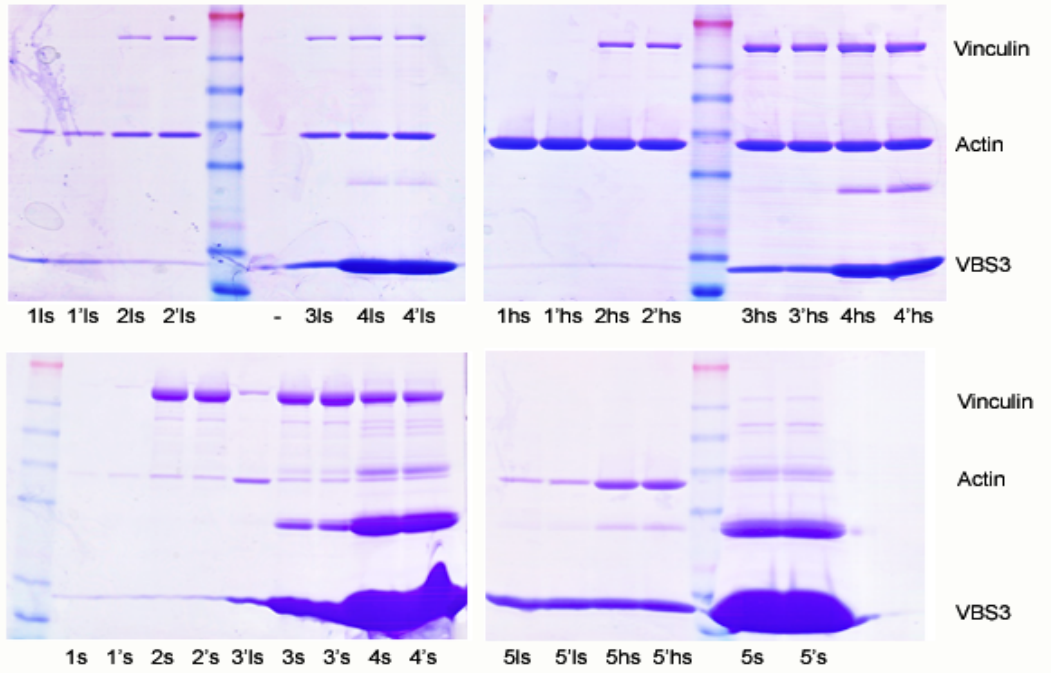

Fig. 4-2 Analysis of vinculin activation in the presence of F-actin and VBS3. Actin binding and bundling are detected by a co-sedimentation assay with vinculin and talin domain VBS3. ls: low speed pellet; hs: high speed pellet; s: supernatant. (1) actin = 4 μM; (2) actin:Vinculin = 4:1 μM; (3) actin:vinculin:VBS3 = 4:1:20 μM; (4) actin:vinculin:VBS3 = 4:1:500 μM; (5) actin:VBS3 = 4:500 μM.

Vinculin activation by F-actin and talin's VBS2 domain

Talin's VBS2 domain has a slightly higher binding affinity for vinculin head Domain 1 (~32 nM) than the VBS3 domain, and was suggested to be able to bind three vinculin proteins simultaneously (Fillingham, Gingras et al. 2005). I repeated the actin cosedimentation assay described for VBS3 to see if VBS2 might bind vinculin better and induce more actin bundling than VBS3. Addition of VBS2 causes more vinculin to bind single actin filaments and more actin bundling. VBS2 seems to induce

more actin bundling than VBS3. However, VBS2 by itself also induces bundle formation indicated by the appearance of a higher amount of actin in the low speed pellet when VBS2 is present than in the control (Fig. 4-3).

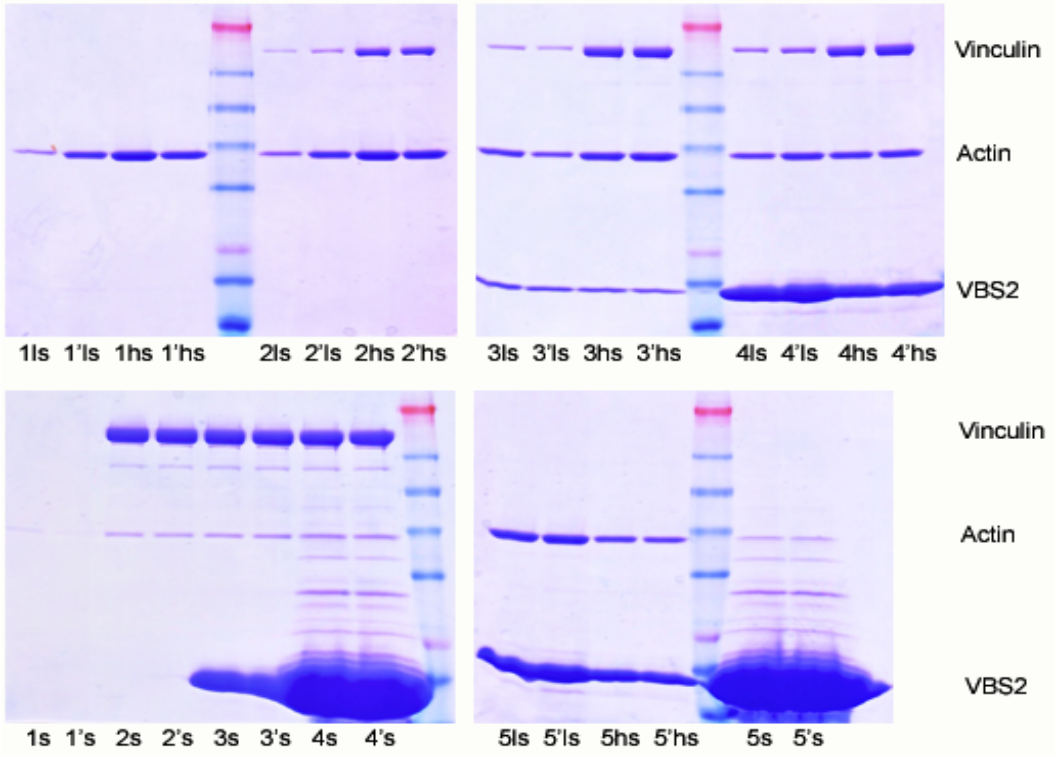

Fig. 4-3 Analysis of vinculin activation in the presence of F-actin and VBS2. Actin binding and bundling are detected by a co-sedimentation assay with vinculin and talin domain VBS2. ls: low speed pellet; hs: high speed pellet; s: supernatant. (1) actin = 4 μM; (2) actin:Vinculin = 4:1 μM; (3) actin:vinculin:VBS2 = 4:1:20 μM; (4) actin:vinculin:VBS2 = 4:1:500 μM; (5) actin:VBS2 = 4:500 μM.

Since VBS2 induces actin bundling formation by itself, I continued with the activator VBS3. Fig. 4-2 shows that, at 500-fold molar excess to vinculin, VBS3 induces some actin bundling. In fact, a 500-1000-fold molar excess to vinculin was suggested for VBS3 to activate vinculin (Cohen, Chen et al. 2005). A molar excess of VBS3 to vinculin of 50 was used for electron microscopy studies to image bundle

formation by vinculin and talin VBS3 (Fig. 4-4). Unfortunately, even at this concentration it is difficult to obtain images with a reasonable low background that will not interfere with image analysis (Fig. 4-4c). Fig. 4-4d shows that VBS3 by itself aggregates and interacts with F-actin.

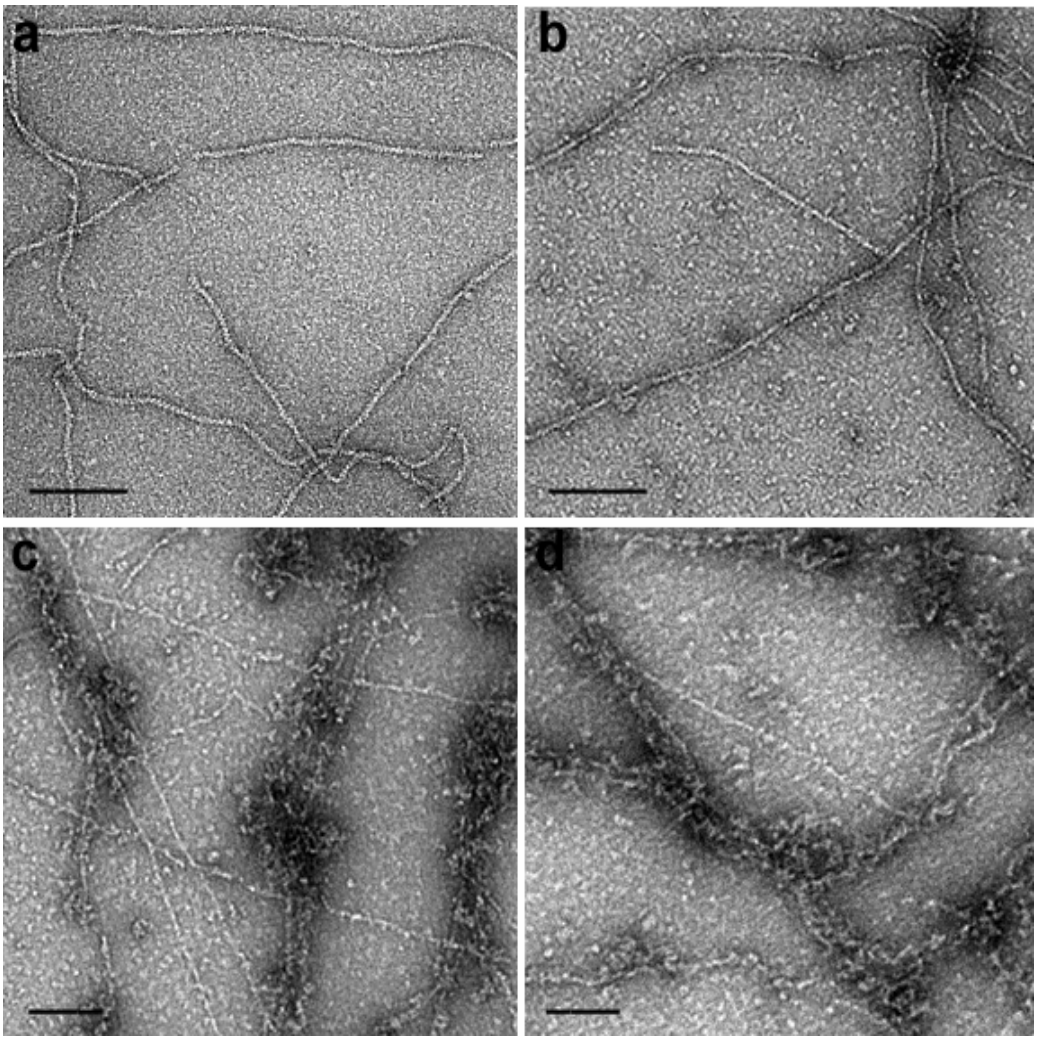

Fig. 4-4 Visualization of actin-vinculin-VBS3 assemblies. Electron microscopy images of negatively stained actin filaments alone (a), or in the presence of vinculin (b), vinculin and VBS3 (c), or in the presence of VBS3 alone (d). Scale bar is 100nm.

Increasing the VBS3 concentration is not a viable option due to the high amount of background it produces in the images. Lower concentrations of VBS3 do not seem to induce significantly more actin bundling, but according to Fig. 4-2 the amount of vinculin that binds F-actin is increased in the presence of a 20-fold excess of VBS3. In order to determine if VBS3 actually interacts with vinculin at this concentration, size exclusion chromatography was performed. Vinculin and VBS3 were incubated in a 1:20 molar ratio and run over a S200 10/300 sizing column (Fig. 4-5). Vinculin and VBS3 do not significantly bind each other at this ratio. In addition, VBS3 forms multimers. Even after high speed centrifugation to remove these multimers, no significant interaction was observed between vinculin and VBS3.

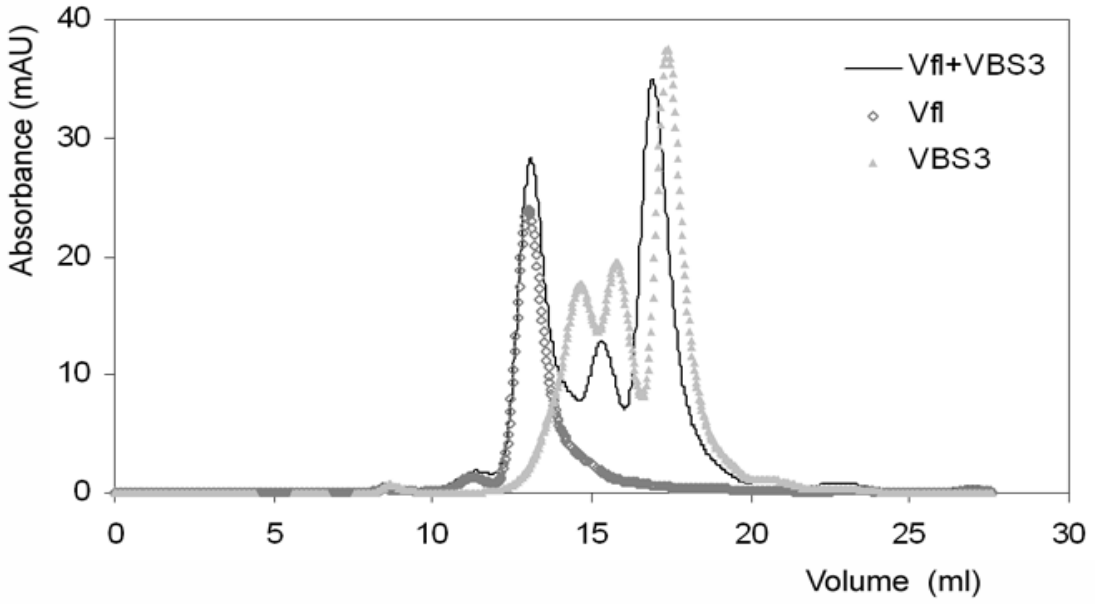

Fig. 4-5 Analysis of vinculin assemblies by size-exclusion chromatography. Overlay of chromatograms show that Vinculin and VBS3 do not form a complex in solution.

Vinculin activation by F-actin and talin's VBS3-peptide

In order to avoid the high background of particles in electron microscopy due to the high concentration and relatively large size (~14kD) of the talin VBS3 domain, I

decided to use a synthetic VBS3-peptide. The peptide is only ~2.9kD in size and has a binding affinity of ~3.1 nM for vinculin head domain 1 (Izard, Evans et al. 2004; Izard and Vonrhein 2004), and ~400 nM for vinculin head domain 1-3 (Bakolitsa, Cohen et al. 2004). Due to the smaller size, higher concentrations can be used without causing too much background in electron microscopy images.

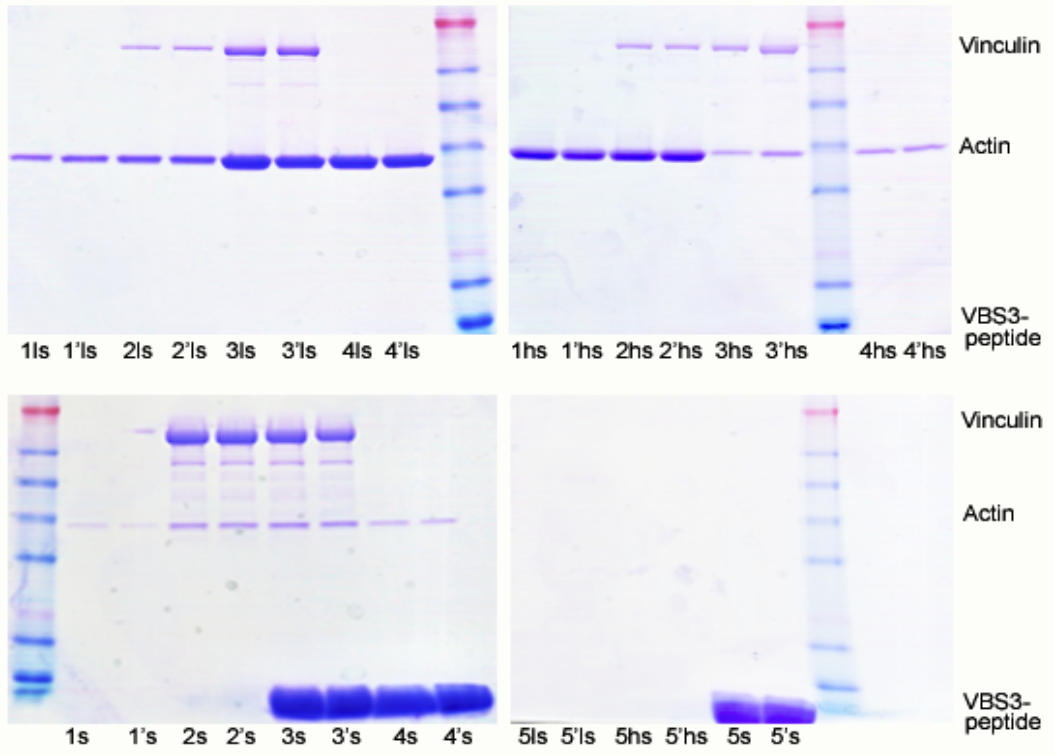

Fig. 4-6 Analysis of vinculin activation in the presence of F-actin and VBS3-peptide. Actin binding and bundling are detected by a co-sedimentation assay with vinculin and talin's VBS3-peptide. ls: low speed pellet; hs: high speed pellet; s: supernatant. (1) actin = 4 μM; (2) actin:Vinculin = 4:1 μM; (3) actin:vinculin:VBS3-peptide = 4:1:260 μM; (4) actin:VBS3-peptide = 4:260 μM; (5) VBS3-peptide 260 μM.

I originally started out with 1000-fold molar excess of VBS3-peptide. At this concentration the peptide heavily aggregates. After high speed centrifugation to remove aggregates, a 260-fold molar excess to vinculin could be reached. The

peptide induces substantially more vinculin binding to F-actin and more actin bundling. However, the same amount of actin bundling was obtained by VBS3-peptide alone (lane 4, Fig. 4-6).

Vinculin mutant T19 activation by F-actin and talin VBS2 or VBS3

In an effort to use a lower amount of activator and thus get less background in EM-images, I generated a vinculin T19 mutant (Fig. 4-7). The charge-to-alanine mutations (K1047A; R1049A; D1051A) in the basic patch of the base of the vinculin tail helical bundle increase the Kd for vinculin head binding by a factor of 42-fold, while still being able to bind F-actin (Cohen, Chen et al. 2005).

a

V_t sample	K_d	Fold increase
	μM	
WT	0.09	1
T8	0.55	6
T14	0.77	8.3
R976A	0.75	8.1
R978A	0.67	7.2
T12	>10	>100
T19	3.9	42
T8/19	9.2	98

b

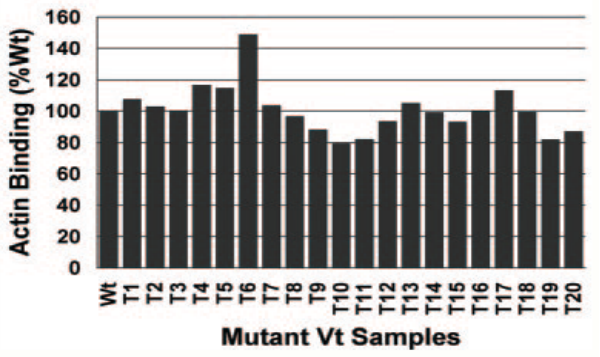

Fig. 4-7 Summary of analysis of several vinculin tail mutants. (a) Strength of the head-tail interaction and (b) actin binding activity of several vinculin tail mutants (Cohen, Chen et al. 2005).

Fig. 4-8 confirms loss of basic residues (lower pI) in the T19 mutant, but no increased exposure of Vt that would indicate activation. This is expected since the Vt-Domain 1 interaction is still intact.

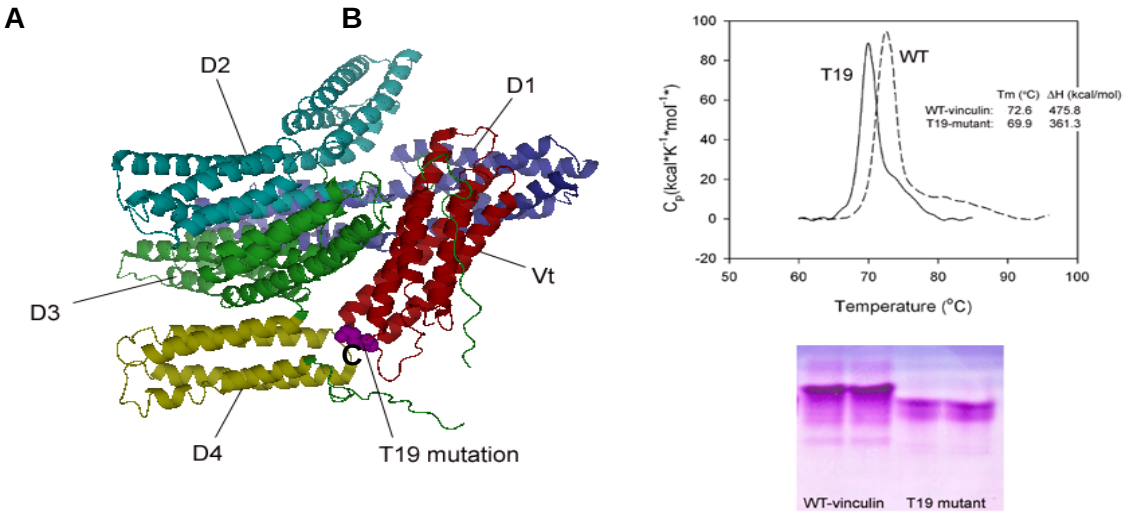

Fig. 4-8 Analysis of T19 vinculin mutant. The crystal structure of vinculin (A) indicates the location of the T19 mutations (K1047A; R1049A; D1051A) between the base of Vt and Domain 4. Differential scanning calorimetry shows that T19 is less stable than wt-vinculin (B) and an IEF gel (C) confirms loss of basic residues occurring in this mutant.

Activation of T19 in presence of F-actin and one of the talin VBS2 or VBS3 activators or VBS3-peptide was assessed by differential actin cosedimentation assays.

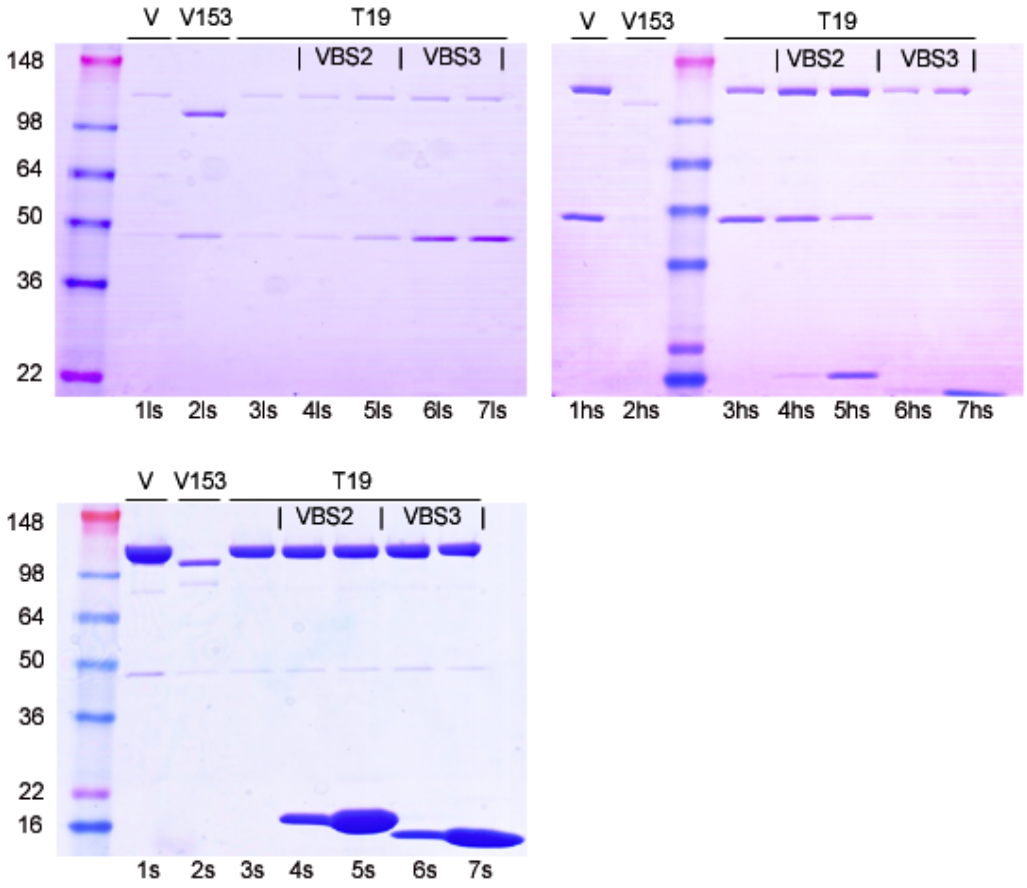

Fig. 4-9 Analysis of T19 activation in the presence of F-actin and VBS2 or VBS3. Actin binding and bundling were detected by a co-sedimentation assay with vinculin mutant T19 and talin's VBS2- and VBS3-domain. ls: low speed pellet; hs: high speed pellet; s: supernatant. (1) actin:vinculin = 4:1 µM; (2) actin:VΔ153 = 4:1 µM; (3) actin:T19 = 4:1 µM; (4) actin:T19:VBS2 = 4:1:5 µM; (5) actin:T19:VBS2 = 4:1:50 µM; (6) actin:T19:VBS3 = 4:1:5 µM; (7) actin:T19:VBS3 = 4:1:50 µM.

The vinculin mutant T19 binds significantly better to F-actin in the presence of VBS2. However, the reason for using a vinculin mutant was to reduce the activator concentration. At low concentrations of VBS2 F-actin bundling by T19 is not better than by wild-type vinculin. On the other hand, actin bundling is much improved in the presence of VBS3. However, in the presence of VBS3 the total amount of T19

binding to actin is much less than wild-type vinculin. I will use the VBS3-peptide to determine if this activator induces more T19 to bind F-actin and induces increased actin bundling.

Vinculin mutant T19 activation by F-actin and VBS3-peptide

Activation of the vinculin mutant T19 was also tested in the presence of the synthetic VBS3 peptide and F-actin. Fig. 4-10 shows the actin cosedimentation assay of these proteins.

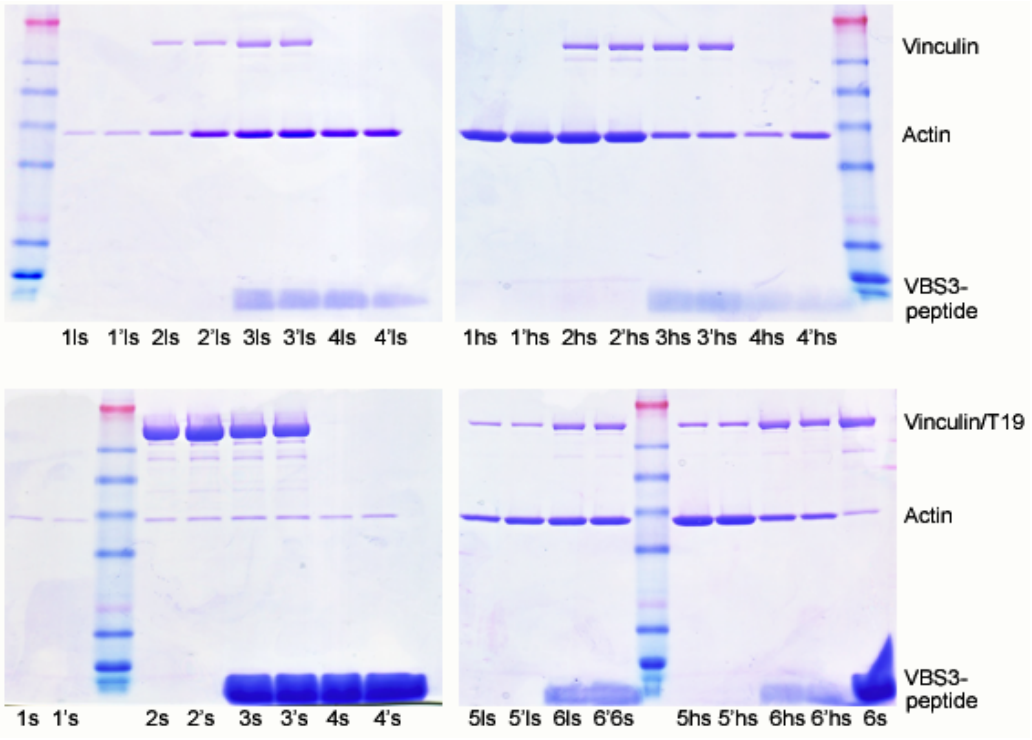

Fig. 4-10 Analysis of vinculin/T19 activation in the presence of F-actin and VBS3-peptide. Actin binding and bundling were detected by a co-sedimentation assay with vinculin or T19 and talin's VBS3-peptide. ls: low speed pellet; hs: high speed pellet; s: supernatant. . (1) actin = 4 μM; (2) actin:T19 = 4:1 μM; (3) actin:T19:VBS3-peptide = 4:1:260 μM; (4) actin:VBS3-peptide = 4:260 μM; (5) actin:vinculin = 4:1 μM; (6) actin:vinculin:VBS3-peptide = 4:1:260 μM.

As seen in the previous experiment with VBS2 as activator, T19 binds F-actin better than wt-vinculin (lane 3 and 6, Fig. 4-10). In presence of the VBS3-peptide, actin bundling is increased. However, there is no significant difference seen between wt-vinculin and the T19 mutant. As was shown for the VBS3 domain, the VBS3-peptide induces actin bundling or forms large aggregates (lane 4, Fig. 4-10). Since no significant difference was detected between wt-vinculin and T19 mutant activation and actin bundle formation, I decided to evaluate actin bundle formation by vinculin in the presence of the VBS3-peptide using electron microscopy. As can be seen in Fig. 4-11, the VBS3-peptide aggregates and induces actin bundles/aggregates on its own, even when vinculin is not present (as was also seen in the actin cosedimentation assays).

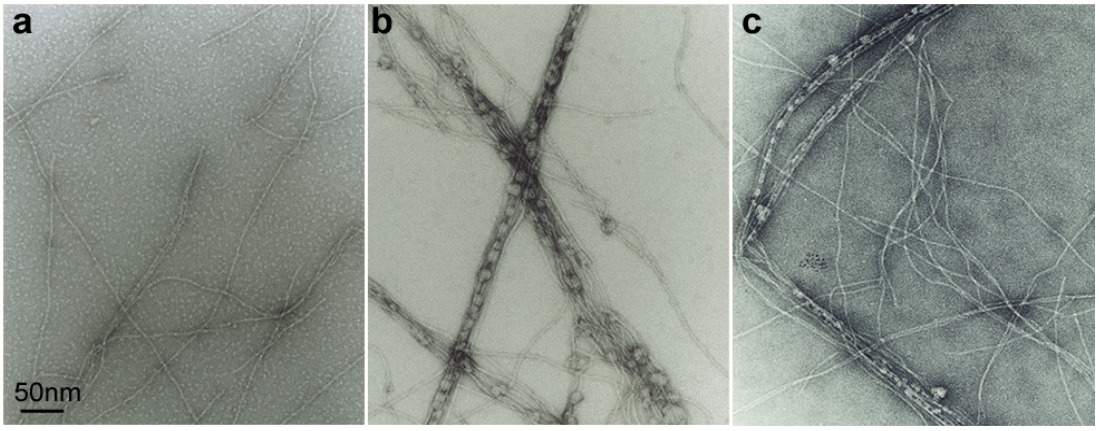

Fig. 4-11 Visualization of actin-vinculin-VBS3-peptide assemblies. Electron microscopy images of negatively stained actin filaments in the presence of vinculin (left), vinculin and VBS3-peptide (middle), and VBS3-peptide (right).

Vinculin activation by α-catenin's CD3-region

A region of α-catenin containing the vinculin binding site, CD3, was shown to bind vinculin very weakly (Yang, Dokurno et al. 2001; Bakolitsa, Cohen et al. 2004). In the

presence of F-actin this affinity increases significantly (Janssen, Kim et al. 2006). I repeated the actin cosedimentation assay with vinculin in the presence of CD3 (Fig. 4-12).

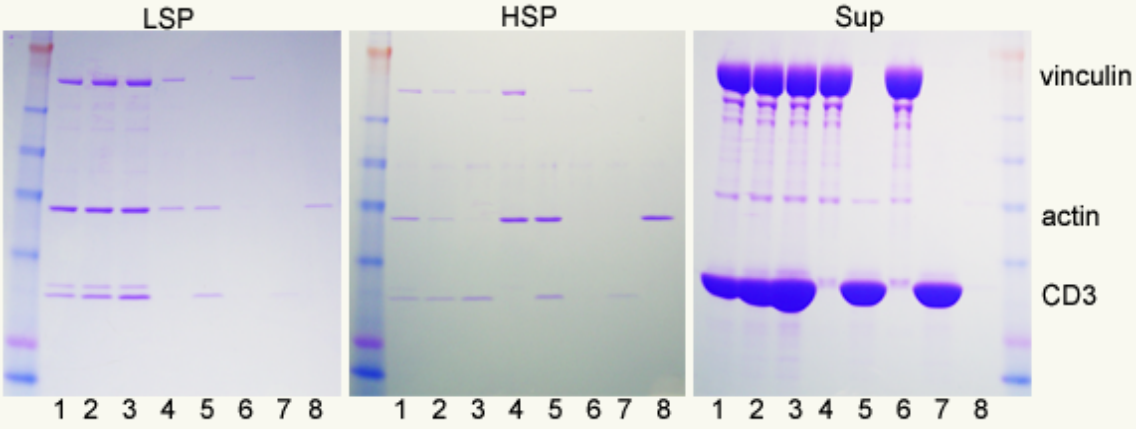

Fig. 4-12 Analysis of vinculin activation in the presence of F-actin and CD3. Actin binding and bundling are detected by a co-sedimentation assay with vinculin and α-catenin's CD3-domain. LSP: low speed pellet; HSP: high speed pellet; Sup: supernatant. (1) actin:vinculin:CD3 = 1:1:1 μM; (2) actin:vinculin:CD3 = 1:1:5 μM; (3) actin:vinculin:CD3 = 1:1:10 μM; (4) actin:vinculin = 1:1 μM; (5) actin:CD3 = 1:5 μM; (6) vinculin = 1 μM; (7) CD3 = 5 μM; (8) actin = 1 μM.

Compared to a mixture of vinculin and actin alone, in the presence of CD3 more vinculin is incorporated in actin bundles and actin bundling is increased. CD3 by itself does not induce actin bundling/aggregation. The increase of actin bundling in the presence of a 10-fold molar excess of CD3 is significant and suggests that CD3 is a better activator than talin's VBS2-, VBS3-domain, and VBS3-peptide.

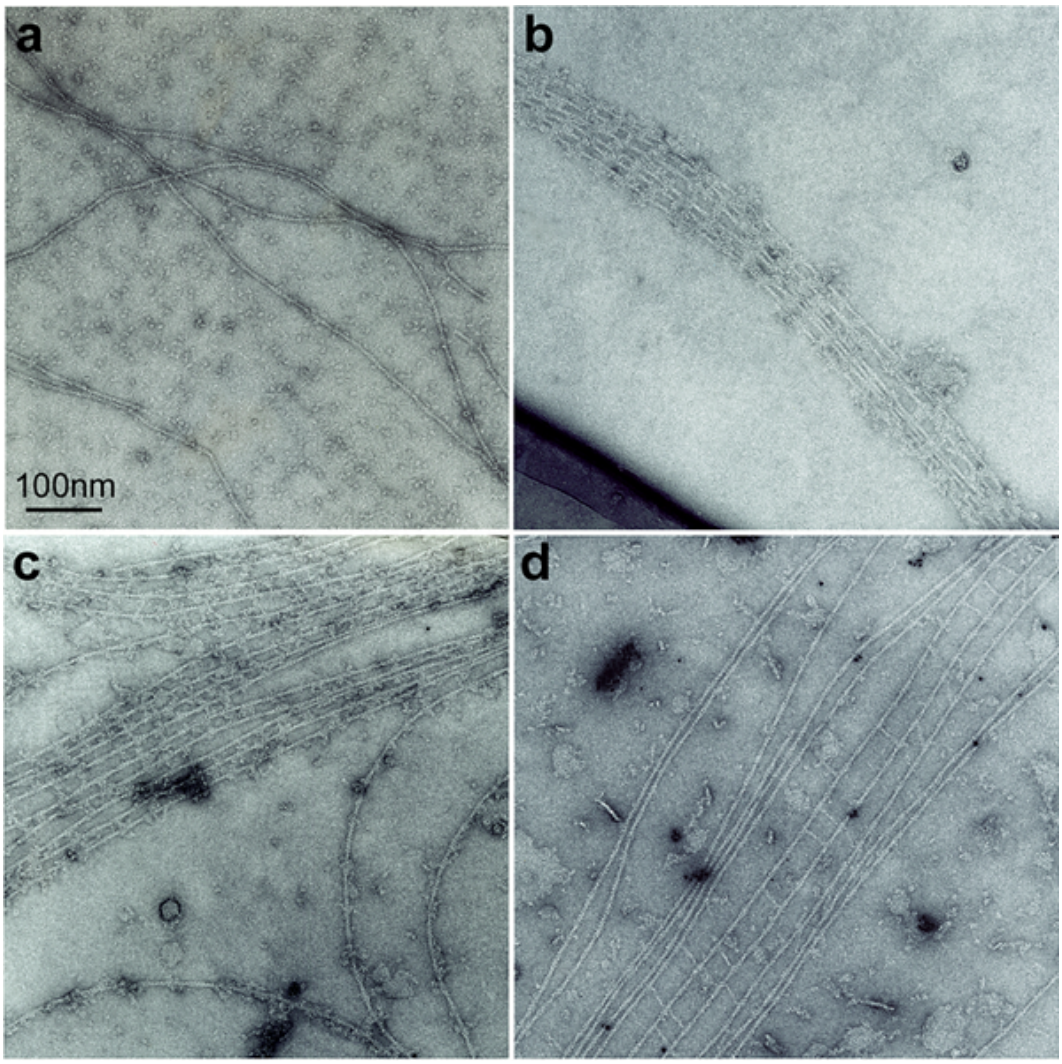

Fig. 4-13 Visualization of actin-vinculin-CD3 assemblies. Electron microscopic images show (a) actin in the presence of vinculin (1:1 molar ratio), actin in the presence of both vinculin and CD3 (1:1:10 molar ratio) (b-d) on lipid layers over holey formvar grids.

Fig. 4-13b-d show how vinculin cross-links actin filaments in the presence of CD3. The size of the densities between the actin filaments, which should correspond to vinculin and CD3, is irregular and so are the distances between adjacent filaments. The specimen mostly resembles the organization as seen in Fig. 4-13b-c. Only in few

places an assembly such as in Fig. 4-13d is seen. Optimization of this system is required to verify if the latter is a reproducable phenomenon.

Filamentous actin cross-linking by VΔ153

VΔ153 is a vinculin construct consisting of amino acids 154-1066. The region that includes the first 153 N-terminal amino acids of vinculin forms a major interface with the tail domain. Without this intramolecular interface the construct is likely to be constituently active. Indeed, in the presence of VΔ153 actin bundles are formed (Fig. 4-14), comparable to bundle formation by Vt (for Vt bundles see Fig. 5-10d).

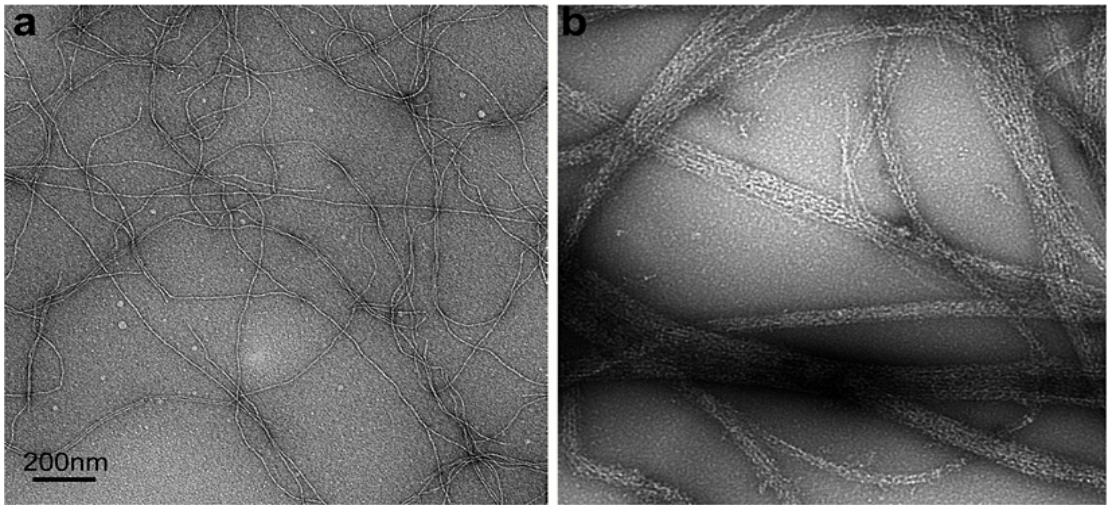

Fig. 4-14 Visualization of actin-VΔ153 assemblies. Electron microscopy images of actin (a) and actin in presence of VΔ153 (b) were taken at a defocus of -4μm and magnification of 11,000x.

In order to determine the structural details of how VΔ153 bundles actin filaments, I used electron microscopy to visualize two-dimensional arrays of actin cross-linked by V153. As previously explained (chapter 3), restraining the assembly process in the third dimension allows for high resolution analysis. Using dual axis electron tomography, 61 images were collected of different angles of such an array from -60^{o}

to 60^{o}, every 2^{o}, after which the sample was rotated 90^{o} and a second series was collected (Fig. 4-15).

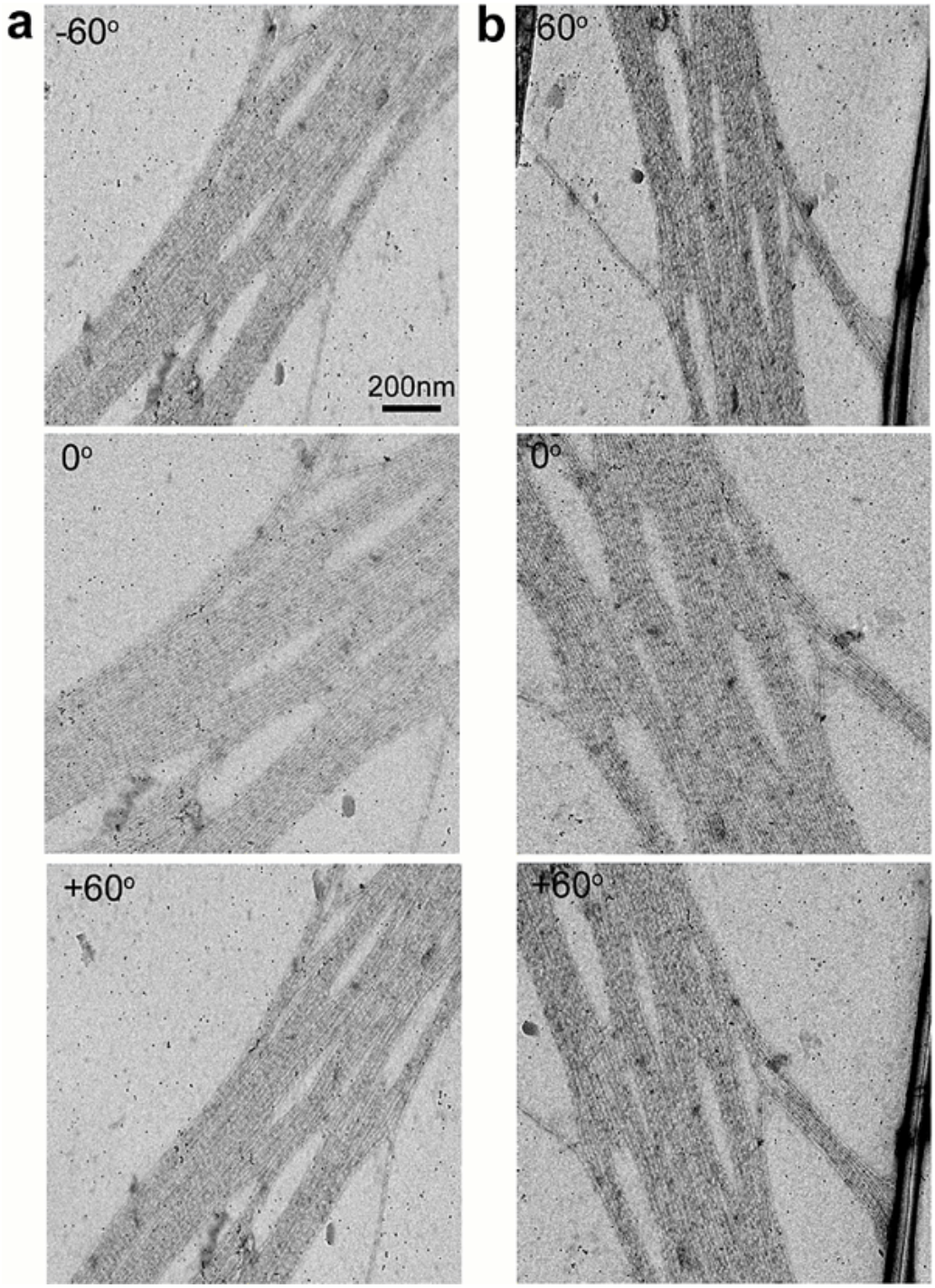

Fig. 4-15 Dual axis electron tomography of F-actin-VΔ153 arrays. Images were taken every 2° from -60° to 60°. (a) Three different angles of the first tomography series, (b) similar angles of the same sample but rotated over 90°. Data was collected at ~3.5µm defocus and a magnification of 29kx. Tilt axis was vertical in all images.

The 3D reconstruction of this array was calculated (Fig. 4-16).

Fig. 4-16 Tomographic reconstruction of a 2D actin array crosslinked by VΔ153. The red highlighted circle indicates some VΔ153 binding a single filament; the yellow highlighted area represents an area of organized actin filaments crosslinked by VΔ153.

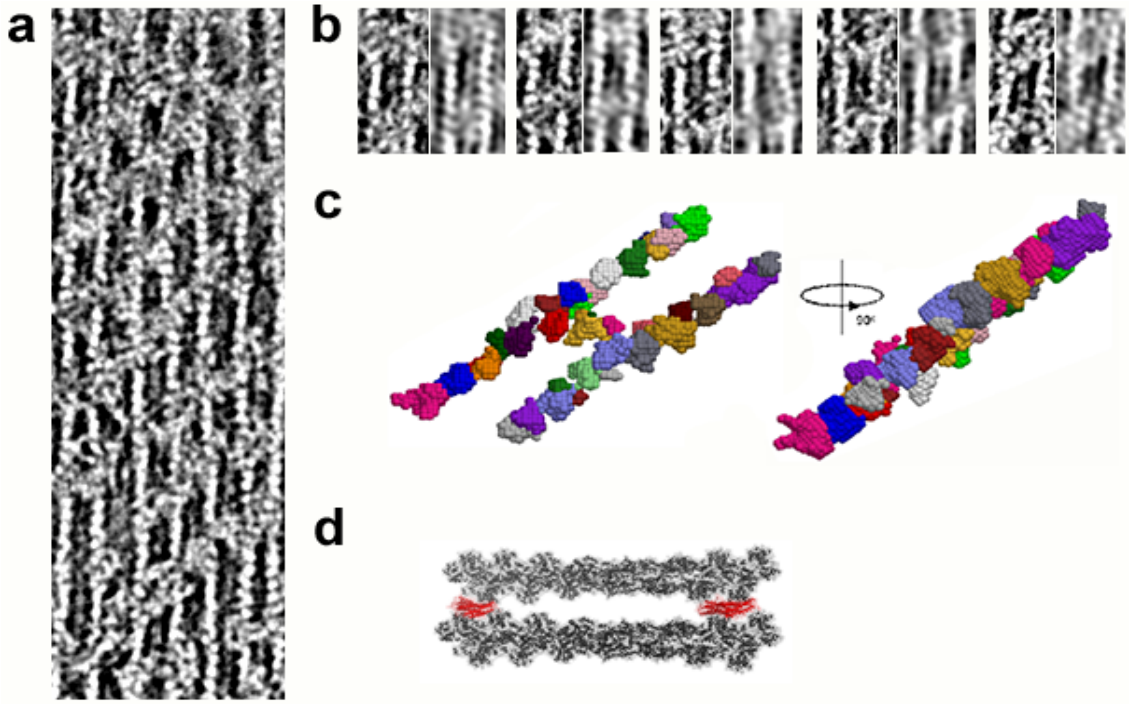

Fig. 4-17 Analysis of the actin-VΔ153 crosslink. (a) A small region of the tomographic reconstruction of actin cross-linked by VΔ153. (b) Five examples of individual VΔ153 crosslinks cut out of the tomogram (left sides) and filtered (right sides). (c) Example of watershed segmentation of one such VΔ153 crosslink from the front and rotated by 90^{o}. Actin monomers can be identified as different colored segments in two actin filament areas. The yellow/pink segment in between the two actin filaments can be attributed to VΔ153. (d) For comparison the Vt-actin crosslink is shown, see chapter 3.

Although VΔ153 does not crosslink filaments everywhere in the raft, the areas that are highly organized are crosslinked and show a preference for a slanted orientation (Fig. 4-16 and 4-17a). The distance between filaments crosslinked by VΔ153 is approximately 3 times larger than when F-actin is crosslinked by Vt. VΔ153 crosslinkers appear to be regularly spaced in the raft, however, there is variation in the distance between successive crosslinkers as seen in Fig. 4-17b. This might be due to the flexibility of the head domain. Paired up with these individual crossbridges are their filtered images. These show about 13 actin subunits between successive

crosslinkers (Fig. 4-17b). Fig. 4-17c shows an example of an isolated VΔ153 crosslinker. The segment in yellow/pink that is located between the two actin filaments can be attributed to VΔ153. The size of the cross-linker roughly corresponds to one VΔ153 molecule (~100kD). In order to obtain more structural information on the position and orientation of actin filaments cross-linked by VΔ153, I analyzed several diffraction patterns from regions of negatively-stained arrays (Fig. 4-18). The paracrystalline order of the arrays is poorer than the arrays cross-linked by Vt (see chapter 3). As was true for Vt, the diffraction pattern of the VΔ153-actin arrays shows a single meridonal reflection at a height corresponding to the actin cross-over repeat (1/38 nm). This corresponds to the image in Fig.4-18a which also shows a single cross-linker per actin cross-over. In addition, actin filaments cross-linked by VΔ153 run unipolar as is deducted from the distance between the diffraction spots in relation to the filament distance. This is consistent with actin filaments cross-linked by Vt and with observations in cells (Geiger, Yehuda-Levenberg et al. 1995). The inter-filament distance in the array is ~13.3nm, which is about 3-fold larger than the spacing between filaments that are crosslinked by Vt.

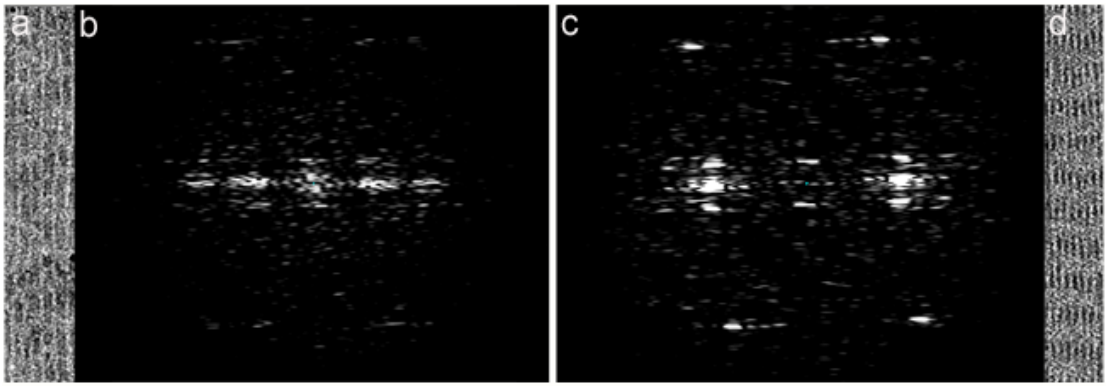

Fig. 4-18 Comparison of diffraction patterns of VΔ153 and Vt. (a) 2D actin array cross-linked by VΔ153 and (b) its corresponding diffraction pattern. (c) Diffraction pattern of an actin-Vt array and the actin-Vt raft (d) for comparison.

Discussion

Full length vinculin activation

In the previous chapter I determined the structural details of vinculin tail cross-linking actin filaments. Here, I extended this study and determined the structural details of actin bundling by full length vinculin. Several protein constructs were used to activate vinculin in the presence of F-actin. The talin VBS3 domain is shown to activate vinculin only at concentrations of 500-1000-fold molar excess to vinculin (Cohen, Chen et al. 2005). Here, I also showed that, at a 500-fold molar excess to vinculin, the VBS3-domain of talin induces more vinculin to bind single actin filaments. However, there is only a slight increase in actin bundling as compared to the control sample without the VBS3-domain. The VBS2-domain of talin contains three vinculin binding sites, instead of only one in the VBS3-domain (Fillingham, Gingras et al. 2005). For this reason an increase of vinculin activation and subsequent actin bundling was expected. Indeed, the VBS2-domain induces increased actin bundle formation. However, it induces the same amount of actin bundling when vinculin is not present. The large amount of background in electron microscopy images due to the large excess of activator (VBS3-domain) makes it difficult to analyze these images. In addition, the VBS3-domain does not interact with vinculin at a lower molar ratio such as 1:20 (vinculin to VBS3). To circumvent this problem I used a VBS3-peptide which is only ~2.9kD in size and should be less visible in electron microscopy when added in large quantities. This peptide induced increased vinculin binding to actin filaments and a higher degree of actin bundling compared to the larger VBS3-domain, but as was the case for the VBS2-domain, the VBS3-peptide induces actin bundling on its own, even when vinculin is not present.

Since this peptide consists of only the vinculin binding region it was not expected to bundle actin filaments so heavily. An increase in salt concentration from 50 to 300mM NaCl did not lower non-specific binding of this peptide to actin or lower actin bundling/aggregation.

In order to use lower amounts of activator and make it easier to activate vinculin, a vinculin mutant with decreased binding affinity between the head and tail domains was used. Several vinculin tail domain mutants were shown to have less affinity for the head domain, but are still able to bind actin (Cohen, Chen et al. 2005). One of these is the K1047;R1049;D1051A mutant (T19), which was chosen because it increases the Kd of the head-tail interaction 42-fold and its mutations are farthest from the actin binding sites (Cohen, Chen et al. 2005). Activation of T19 in the presence of the VBS2- or VBS3-domain of talin did not result in significantly better actin bundling than when wt-vinculin is activated. The talin VBS3-peptide also did not result in increased bundling formation as compared to wt-vinculin. This study showed that the talin constructs do not significantly induce actin bundling through vinculin.

The most efficient activator of vinculin is α-catenin's CD3 construct, which bundles actin filaments at a 10-fold molar excess. Optimizing this system and eventually using electron cryo-tomography might allow characterization of F-actin bundling by full length vinculin in the presence of a second ligand. A possible explanation for the ability to activate vinculin in the presence of α-catenin's construct, but not by talin's constructs might involve their structure and destination. α-Catenin might induce a slightly different conformational change in the vinculin head domain than talin and is able to activate vinculin in the presence of F-actin, thereby forming stable cell-cell contacts. On the contrary, an additional step might be required prior to activation of

vinculin by talin in the presence of F-actin. Vinculin is known to be highly phosphorylated in nascent focal adhesion sites, but is much less phosphorylated in mature focal adhesions (Mohl, Kirchgessner et al. 2009). Phosphorylation might induce initial activation of vinculin after which ligands such as F-actin and talin stabilize its conformation and induce formation of stable focal contacts. On the other hand, vinculin phosphorylation might weaken the head-tail interaction just enough for talin and F-actin to fully activate vinculin.

Cross-linking of actin filaments by VΔ153

Parallel to the study of full length vinculin activation, a constituently active vinculin construct was used, called VΔ153. This construct does not need the presence of an activator, but instead lacks the first 153 N-terminal amino acids necessary for the high affinity between vinculin's head and tail domain. Highly ordered actin-VΔ153 arrays were obtained and showed that VΔ153 crosslinks F-actin into slanted arrays and that it binds actin filaments once every crossover and crosslinks them in a unipolar manner. The latter is consistent with how Vt crosslinks actin filaments (chapter 3) and how vinculin bundles actin in the cell (Geiger, Yehuda-Levenberg et al. 1995). Furthermore, VΔ153 seems to bind two neighboring actin subunits along the filament similar to Vt. To confirm this more analysis is required. Data of VΔ153 bound to F-actin can be collected and a 3D reconstruction can then be generated to verify that the actin binding sites are still similar to Vt. Another observation was that, although the VΔ153 crossbridges seem to appear at regular distances from each other in the raft, a closer look revealed some variation in these distances. This might be due to the vinculin head domain which is connected to the tail domain via a flexible region.

The head domain might be positioned in different orientations, which might make up for the discrepancy in the distances between two successive VΔ153 crosslinks. Averaging enough VΔ153-actin crosslinks can provide better insight into the flexibility of vinculin's head domain.

The distance between filaments is ~13.3nm which is approximately 3-fold larger than when filaments are crosslinked by Vt. Since there are only two actin binding sites identified in vinculin (both in the tail domain) an explanation would be that VΔ153 cross-links F-actin by dimerization, like the vinculin tail, but that a large part of the molecule might not be located in the same plane of the actin filaments. Instead, most of the head domain of vinculin could be located above or below the plane of the actin array, while only the tail domain and a small part of the head domain of two VΔ153 molecules are located in between the filaments. During the segmentation process, in which density corresponding to the sample was carved out and isolated form the noise, too much density might have been removed. Furthermore, to allow for a larger interfilament distance, a conformational change could occur in the dimerization site that increases the distance between actin binding site and dimerization site. The five-helix bundle might partially unfurl. Unfurling of this domain has been observed in electron microscopy studies described in (Molony and Burridge 1985) and (Winkler, Lunsdorf et al. 1996). In order to get a more accurate 3D reconstruction of the VΔ153 cross-linker itself, more data should be obtained and averaged. In addition, the atomic model of Vt-F-actin should be docked into isolated VΔ153-F-actin crossbridges to determine if this model easily coincides with VΔ153-F-actin crosslinking. Determination of the structural details of VΔ153-actin cross-linking can be improved using cryo-electron tomography. In this technique, VΔ153-actin

arrays can be visualized in their native state, circumventing staining effects such as interaction with the sample, gap-filling and flattening effects due to drying of uranyl acetate stain. It might give a more realistic indication of the localization of the VΔ153-head domain.

References

Bakolitsa, C., D. M. Cohen, et al. (2004). "Structural basis for vinculin activation at sites of cell adhesion." Nature **430**(6999): 583-6.

Bass, M. D., B. Patel, et al. (2002). "Further characterization of the interaction between the cytoskeletal proteins talin and vinculin." Biochem J **362**(Pt 3): 761-8.

Bass, M. D., B. J. Smith, et al. (1999). "Talin contains three similar vinculin-binding sites predicted to form an amphipathic helix." Biochem J **341 (Pt 2)**: 257-63.

Bois, P. R., R. A. Borgon, et al. (2005). "Structural dynamics of alpha-actinin-vinculin interactions." Mol Cell Biol **25**(14): 6112-22.

Cohen, D. M., H. Chen, et al. (2005). "Two distinct head-tail interfaces cooperate to suppress activation of vinculin by talin." J Biol Chem **280**(17): 17109-17.

Fillingham, I., A. R. Gingras, et al. (2005). "A vinculin binding domain from the talin rod unfolds to form a complex with the vinculin head." Structure **13**(1): 65-74.

Geiger, B., S. Yehuda-Levenberg, et al. (1995). "Molecular interactions in the submembrane plaque of cell-cell and cell-matrix adhesions." Acta Anat (Basel) **154**(1): 46-62.

Gingras, A. R., W. H. Ziegler, et al. (2005). "Mapping and consensus sequence identification for multiple vinculin binding sites within the talin rod." J Biol Chem **280**(44): 37217-24.

Goksoy, E., Y. Q. Ma, et al. (2008). "Structural basis for the autoinhibition of talin in regulating integrin activation." Mol Cell **31**(1): 124-33.

Izard, T., G. Evans, et al. (2004). "Vinculin activation by talin through helical bundle conversion." Nature **427**(6970): 171-5.

Izard, T. and C. Vonrhein (2004). "Structural basis for amplifying vinculin activation by talin." J Biol Chem **279**(26): 27667-78.

Janssen, M. E., E. Kim, et al. (2006). "Three-dimensional structure of vinculin bound to actin filaments." Mol Cell **21**(2): 271-81.

Johnson, R. P. and S. W. Craig (1994). "An intramolecular association between the head and tail domains of vinculin modulates talin binding." J Biol Chem **269**(17): 12611-9.

Johnson, R. P. and S. W. Craig (1995). "F-actin binding site masked by the intramolecular association of vinculin head and tail domains." Nature **373**(6511): 261-4.

Kremer, J. R., D. N. Mastronarde, et al. (1996). "Computer visualization of three-dimensional image data using IMOD." J Struct Biol **116**(1): 71-6.

Mastronarde, D. N. (2005). "Automated electron microscope tomography using robust prediction of specimen movements." J Struct Biol **152**(1): 36-51.

Mohl, C., N. Kirchgessner, et al. (2009). "Becoming stable and strong: the interplay between vinculin exchange dynamics and adhesion strength during adhesion site maturation." Cell Motil Cytoskeleton **66**(6): 350-64.

Molony, L. and K. Burridge (1985). “Molecular shape and self-association of vinculin and metavinculin.” J Cell Biochem **29**(1): 31-6.

Nhieu, G. T. and T. Izard (2007). "Vinculin binding in its closed conformation by a helix addition mechanism." Embo J **26**(21): 4588-96.

Volkmann, N. (2002). "A novel three-dimensional variant of the watershed transform for segmentation of electron density maps." J Struct Biol **138**(1-2): 123-9.

Winkler, J., H. Lunsdorf, B.M. Jockusch (1996). “The ultrastructure of chicken gizzard vinculin as visualized by high-resolution electron microscopy.” J Struct Biol **116**(2): 270-7.

Yang, J., P. Dokurno, et al. (2001). "Crystal structure of the M-fragment of alpha-catenin: implications for modulation of cell adhesion." Embo J **20**(14): 3645-56.

Chapter 5

A 68 amino acid insert changes an actin bundling protein into an actin severing protein: actin organization by vinculin and metavinculin

Summary

Vinculin and metavinculin are two splice variants that connect the actin cytoskeleton to the cell membrane. The single difference between the two isoforms is a 68 amino acid acidic insert in the tail domain of metavinculin. Since the tail domain also contains the actin binding domains, vinculin and metavinculin could potentially organize actin filaments differently. Here it is shown for the first time that while the vinculin tail domain (Vt) bundles actin filaments in vitro, the metavinculin tail domain (MVt) instead severs actin filaments. Electron microscopy and image analysis suggest that the location of the MVt insert prevents dimerization. Kinetic and fluorescence microscopy assays demonstrate that actin severing is concentration dependent and that MVt also stabilizes filaments. In addition, this study shows that a larger metavinculin construct bundles F-actin like vinculin does. Together, these data suggest a model in which metavinculin bundles actin filaments unless the acidic insert is exposed and can therefore sever filaments. Furthermore, the cardiomyopathy-related R975W-MVt mutant functions similar to wild-type MVt, suggesting that this mutation does not affect actin binding sites or dimerization site in MVt.

Introduction

Vinculin is a highly conserved, 116kDa protein, which links actin filaments to cadherins and integrins in the cell membrane via α-catenin and talin in cell-cell and cell-matrix adhesion junctions respectively (Burridge and Mangeat 1984; Weiss, Kroemker et al. 1998). It plays a crucial role in brain and heart development, where it is required for the formation of normal cell-cell and cell-matrix adhesive complexes (Xu, Baribault et al. 1998; Zemljic-Harpf, Miller et al. 2007). In order to link the actin cytoskeleton to the cell membrane, vinculin interacts with a large number of proteins, such as VASP (Brindle, Holt et al. 1996), vinexin (Kioka, Sakata et al. 1999), ponsin (Mandai, Nakanishi et al. 1999), α-actinin (Kroemker, Rudiger et al. 1994), talin (Johnson and Craig 1994), PIP2 (Johnson, Niggli et al. 1998) and paxillin (Turner, Glenney et al. 1990). However, most of these ligand binding sites are masked by an intermolecular interaction between the vinculin head and tail domains and renders the protein inactive. The crystallographic models of vinculin determined by Dr. Liddington's lab and Dr. T. Izard's lab show the structural details of this interaction (Bakolitsa, Cohen et al. 2004; Borgon, Vonrhein et al. 2004). A combinatorial activation mechanism was proposed in which vinculin can be activated by simultaneously binding two or more of its ligands (Bakolitsa, Cohen et al. 2004; Janssen, Kim et al. 2006).

The existence of a second vinculin isoform was recognized nearly three decades ago (Feramisco, Smart et al. 1982). While extensive research has been done on vinculin, the function of the larger isoform, metavinculin, remains elusive. Vinculin is expressed ubiquitously, but metavinculin is mainly expressed in smooth and cardiac muscle tissue (Feramisco, Smart et al. 1982; Glukhova, Kabakov et al. 1986; Belkin,

Ornatsky et al. 1988). A small fraction of metavinculin also occurs in skeletal muscle tissue (Belkin, Ornatsky et al. 1988) and platelets (Turner and Burridge 1989), which is interesting since platelets also contain an abundance of the contractile proteins actin and myosin despite their non-muscle origin (Hathaway D.R. 1979). Both isoforms co-localize in dense plaques, intercalated disks, and costameres where they are thought to function in force transduction. The percentage of the two vinculin isoforms depends on tissue type, but was reported to vary between 20% metavinculin of the total vinculin pool in human cardiac tissue to more than 50% in human stomach and bladder smooth muscle tissue (Belkin, Ornatsky et al. 1988). In addition, metavinculin expression is closely related to differentiation of muscle cells. The metavinculin fraction (of the total vinculin pool) increases during development from 5% in fetuses to 44% in adults (Koteliansky, Belkin et al. 1991). In-vitro experiments showed metavinculin expression in 4-5 day cultured cells, but hardly any after 24 hours (Saga, Hamaguchi et al. 1985). These data suggest that metavinculin is important for force transduction since metavinculin expression appears to be directly correlated to the ability of differentiated muscle cells to contract.

The sole structural difference between the two vinculin isoforms is a 68aa acidic insert in the C-terminal tail domain of human metavinculin (Gimona, Small et al. 1988; Byrne, Kaczorowski et al. 1992). Three mutations are found in the insert region that are associated with dilated and hypertrophic cardiomyopathy (Olson, Illenberger et al. 2002). The affect of these mutations on actin organization was studied by light microscopy (Olson, Illenberger et al. 2002). They showed that the mutations in the insert of MVt cause MVt to bundle actin filaments like Vt. The most dramatic effect was exerted by the R975W-mutation.

These specific mutations indicate a specific function for the insert region. Several serine doublets and a tyrosine containing region have been identified in the insert (Gimona M. 1988). The presence of a number of potential phosphorylation sites corresponds to the eight fold greater phosphorylation of metavinculin as compared to vinculin (Siliciano and Craig 1982). However, the function of this phosphorylation is not understood yet. To date, no explicit binding protein for this insert has been reported. Since the tail domains of both isoforms include the actin binding domain, it has been suggested that the metavinculin tail insert influences the filamentous organization of actin (Rudiger, Korneeva et al. 1998). Studies on the organization of actin filaments by different vinculin isoforms were performed at a resolution too low to yield conclusive results (Rudiger, Korneeva et al. 1998; Olson, Illenberger et al. 2002). On the other hand, the insert region was proposed to affect metavinculin's intramolecular head-tail interaction by lowering its association constant as compared to the head-tail interaction in vinculin (Witt, Zieseniss et al. 2004). The specific function of metavinculin's insert still remains unsolved.

In the present study, I used the tail domains of vinculin and metavinculin because these contain the actin binding sites and the insert (for metavinculin). In addition, using these constructs circumvents the problem of (meta)vinculin activation. Here, the influence of Vt and MVt on actin organization is compared in order to determine the effect of the additional insert in MVt. In contrast to Vt, which induces the formation of large highly ordered actin bundles (Janssen, Kim et al. 2006), this study shows that the presence of the insert prevents actin bundling, and instead makes it a severing protein. Besides severing in a concentration dependent manner in vitro, MVt also stabilizes actin filaments. This combination of severing and stabilization is not shown

before, since severing proteins generally have a capping and/or (de)polymerization function in addition to their severing activity (Ono 2007). Electron microscopy was used to show that the insert does not affect the actin binding itself, although tryptophan fluorescence experiments indicate a lower actin binding affinity for MVt than for Vt. Together, a new function for MVt is proposed and a model for the mechanism of actin organization by the full length metavinculin protein. Furthermore, the effect of the MVt mutant R975W on actin organization is evaluated and compared to wild-type MVt.

Experimental Procedures

Protein Preparation

Skeletal muscle actin was either available in our laboratory or bought from Cytoskeleton Inc. Vt was purified as described in chapter III. The DNA sequence of the tail domain of chicken metavinculin (MVt), corresponding to amino acids 879-1134, was kindly provided by Dr. Liddington. The metavinculin tail mutant MVt-R795W was made using the QuikChange Multi Site-Directed Mutagenesis Kit and primers 5'-gcgccgagtcaggaacgtaacccttcggtg-3' and 5'-cgcggctcagtccttgcattgggaa gccac-3'. MVt and MVt-R975W were expressed in *E.coli* strain BL21(DE3). Cell cultures were induced with 0.1 mM IPTG (16 hr,15ºC) and pellets frozen at -80ºC. Upon thawing, 2 mM PMSF, 1 protease inhibitor tablet and 0.1% TWEEN-20 were added. Cells were homogenized at 15,000 psi, cell debris was removed by centrifugation. Purification of the proteins from the cleared cell lysates was achieved by a 40% ammonium sulfate cut, and its pellet was dissolved in 50 mM Tris-HCl, 50 mM NaCl, 1 mM EDTA, 2 mM DTT. Purification was continued using ion exchange

chromatography on a 5 ml HiTrap Quaternary ammonium (Q Sepharose^{TM} HP) column (GE Healthcare) at pH 8.0, followed by purification on a 5 ml HiTrap Sulfopropyl (SP Sepharose ^{TM} HP) column (GE Healthcare) at pH 7.0. Purified proteins were dialyzed against 20 mM Tris-HCl, pH 7.5, 150 mM NaCl and stored at -80ºC until further use. MVΔ153, corresponding to amino acids 154-1135 of chicken metavinculin, was constructed out of full length metavinculin (kindly provided by Dr. Liddington) using primers 5'-ctgtggcagaagtagtagagcatatggaggatttggtgacat-3' and 3'-gacaccgtcttcatcatct cgtatacctcctaaaccactgta-5'. The product was amplified by PCR and cloned into vector pET28a into the Nco1-Eag1 restriction sites. The absence of errors was confirmed by DNA sequencing. MVΔ153 was expressed in *E.coli* strain BL21(DE3). A cell culture was induced with 0.1 mM IPTG (~16 hrs, 16ºC) and pellets frozen at -80ºC. Upon thawing, 2 mM PMSF, 1 protease inhibitor tablet and 0.1% TWEEN-20 were added. Cells were homogenized at 15,000 psi, cell debris was removed by centrifugation. Purification was done using metal chelating chromatography on a 5 ml HiTrap Nickel column (GE Healthcare), followed by ion exchange chromatography on a 5 ml HiTrap Quaternary ammonium column. The His-tag was subsequently removed by incubation with biotinylated thrombin (Novagen) for 4 hours at 4ºC, after which the thrombin was captured with streptavidin agarose (Novagen) and the tag removed during dialysis into 20 mM Tris-HCl, pH 7.5, 150 mM NaCl. MVΔ153 was stored at-80ºC until further use. VΔ153 was prepared as described in chapter 4.

Actin Cosedimentation Assays

Standard actin binding assay

G-actin was polymerized in F-actin buffer (10 mMTris pH 7.5, 50 mM NaCl, 2 mM DDT, 0.5mM ATP and 2 mM MgCl2) for 1 hour at RT. Proteins (MVt, R975W-MVt or Vt) were added to the F-actin in a 2:1 and 1:2 molar ratio and incubated for 45 minutes on ice. The samples were centrifuged (TLA100, Beckman Coulter) at low speed (17,380x g, 15 minutes, 4ºC) to pellet bundled F-actin and the supernatant was subsequently centrifuged at high speed (278,100x g, 30 minutes, 4ºC) to pellet single actin filaments. Pellets and supernatants were analyzed on 4-20% Tris-Glycine gels. Assays were performed in F-actin buffer.

The actin cosedimentation assay in the presence of both MVt and Vt was performed as described above, with the exception that Vt was added 15 minutes after MVt was added to F-actin and vise versa.

Cosedimentation assay for measuring actin depolymerization

G-actin was polymerized in F-actin buffer for 1 hour at RT. 4 µM F-actin was then incubated at RT with buffer or increasing amounts of MVt. After 60 minutes, samples were centrifuged at 312,530x g at 4ºC for 20 minutes. Pellets and supernatants were analyzed on 4-20% Tris-Glycine gels.

Cosedimentation assay for measuring G-actin sequestering

4 µM G-actin was incubated with buffer or increasing amounts of MVt for 15 minutes at RT. 10x Initiation-buffer (500 mM KCl, 10 mM EGTA, 20 mM $MgCl_2$, 5 mM ATP)

was subsequently added and polymerization was allowed for 60 minutes at RT. Samples were centrifuged at 312,530x g at 4ºC for 20 minutes. Pellets and supernatants were analyzed on 4-20% Tris-Glycine gels.

Isoelectric focusing gel-electrophoresis

Vt, MVt, VΔ153 and MVΔ153 were pre-spinned at 278,100 x g for 30 min at 4^{o}C and diluted to 0.5 mg/ml. Proteins were loaded on a 3-10pH IEF-gel (Criterion/Bio-Rad) and run for 1 hour at 100V, 1 hour at 250V and 30 min at 500V. Gels were stained using the IEF gel staining solution (Bio-Rad).

Kinetics studies using Tryptophan fluorescence assay

Binding kinetics between F-actin and Vt, and between F-actin and MVT, were measured using the naturally occurring tryptophans near the actin binding sites in Vt and MVt. The tryptophans were excited at 290 nm and emission was measured at 330 nm using a fluorescence spectrophotometer (MOS-250 Biologic Science Instruments), the stopped-flow tool SFM-20 (Bio-Logic), and software package Biokine 32 (V4.07). Titration of actin binding proteins was performed by adding 0-11 μM Vt or MVt to 3 μM F-actin in 20 mM Pipes pH 7.5, 50 mM NaCl, 1 mM $MgCl_2$, 0.2 mM ATP. In a control experiment Vt or MVt was added to buffer solution without F-actin. The binding constants were calculated using SigmaPlot, with equation (2) of (Bobkov, Muhlrad et al. 2002): $\Delta F = 0.5\Delta F max A^{-1}[(A+C+Kd)-\{(A+C+Kd)^2-4AC\}^{0.5}]$, where ΔF is the fluorescence change, ΔF_{max} is the maximum fluorescence change (at a complete saturation of actin with MVt/Vt), and A and C are the concentrations of actin and MVt/Vt, respectively.

Depolymerization fluorescence assay

Unlabeled G-actin and pyrene-labeled G-actin were mixed in G-buffer (0.2 mM $CaCl_2$, 10 mM Tris-HCl pH 8.0) to produce an actin stock of 3% labeled actin (3.1 µM). G-actin was polymerized in F-actin buffer for 30 minutes at RT. Increasing amounts of MVt or buffer were incubated with F-actin for 30 minutes at RT. Samples were diluted to 0.5 µM F-actin in G-buffer to start the assay. Pyrene fluorescence was measured (excitation 344 nm, emission > 385 nm) on a spectrofluorometer using BioKine32. Time between the addition of G-buffer and start of fluorometer data collection was estimated to be about 10 seconds for each measurement.

Polymerization fluorescence assay

Unlabeled G-actin and pyrene-labeled G-actin are pre-spinned for 1 hour at 80 krpm (TLA100) at 4ºC. 1µM unlabeled G-actin is polymerized overnight on ice by adding 10x Initiation Buffer. Add Cofilin, MVt or buffer to 50 µl 1µM F-actin in increasing molar ratios, gently mix and incubate for 10 minutes at RT (these conditions will be used as ‘seeds’). For the final reaction mix G-buffer, 1µM seeds, 1.2µM 3.4% pyrene-labeled G-actin, and 20x KME-buffer (2M KCl, 40mM $MgCl_2$, 4mM EGTA). Pyrene fluorescence (λ_{ex} = 344nm, λ_{em} =>385nm) is being measured on a spectrofluorometer using BioKine32. Time between the addition of fresh pyrene-G-actin and start of fluorometer data collection was estimated to be about 10 seconds for each measurement.

Electron Microscopy

Electron microscopy of actin-MVt assemblies for image reconstruction

Actin filaments decorated with MVt were prepared at 4ºC on positively charged lipid layers consisting of a 3:7 w/w solution of di-lauryl-phosphatidylinositol and didodecyldimethylammonium bromide dissolved in chloroform (Taylor and Taylor 1992; Volkmann, DeRosier et al. 2001). G-actin (~0.05 mg/ml) was injected through the lipid layer, which was deposited on top of the polymerization buffer (20 mM Na2PO4, 50 mM KCl, 1 mM ATP, 2 mM MgCl2, 1 mM EGTA, 1 mM DTT (pH 7.0) and ~0.07 mg/ml of MVt). The actin concentration was low enough to promote growth of single actin filaments bound by MVt on lipid layers. Samples were transferred to 200-mesh copper grids coated with lacey carbon films. Specimens were stained with 2% uranyl acetate and air dried. Low-dose images were recorded with a Gatan 1k CCD camera on a Tecnai 12 electron microscope (FEI Electron Optics) at a nominal magnification of 52,000 (at 120 keV) and ~1.5 µm defocus (electron dose ~10 e^2/A^2). A total of 46 micrographs were digitized with a SCAI scanner (Z/I Imaging Corporation) with an effective pixel size of 0.3 nm at the sample.

Image Analysis of actin filaments bound by MVt

A hybrid procedure (Volkmann, Liu et al. 2005) that combines single-particle reconstruction approaches with helical symmetry (Egelman 2000) was used to obtain the reconstructions. A total of 14,396 small, overlapping segments of MVt-decorated actin filaments were selected from the micrographs. The data were then split into two arbitrary halves for independent analysis. Each set was phase corrected after fitting

of the contrast transfer function with EMAN (Ludtke, Baldwin et al. 1999). Our atomic model for undecorated F-actin was used as a starting model (Volkmann et al. 2005). For each of the half-data sets, about 10 iterations were performed until convergence was achieved. An analysis of the Fourier shell correlation between the reconstructions from the independent half sets shows that the curve drops below the 0.5 threshold at a resolution of 2.1 nm.

*Electron microscopy of actin-VΔ153, actin-MV*Δ153, *actin-MVt, actin-R975W and actin-Vt assemblies*

F-actin was diluted to ~0.03 mg/ml with 50 mM Imidazole (pH 7.0), 100 mM NaCl, 10 mM MgCl2, 10 mM EGTA, 0.5 mM DTT, and 0.2 mM ATP and mixed with VΔ153, MVΔ153, MVt, R975W, or Vt. Samples were incubated for 10 minutes on ice and applied to glow-discharged , 400-mesh copper grids, coated with carbon film. They were incubated on the grid for 1 min in a humid chamber. The samples were stained with 2% uranyl acetate for 1 min and air dried. Low-dose images were recorded with a Gatan 1k CCD camera on a Tecnai 12 electron microscope (FEI Electron Optics) at a nominal magnification of 52,000 (at 120 keV) and ~1.5 µm defocus.

Light Microscopy

Severing assay using fluorescence microscopy

Actin was polymerized for 1 hour at RT in F-actin buffer. F-actin (2 µM) and increasing ratios of MVt were incubated for 10 minutes at RT. An equal volume of Alexa-488 Phalloidin (Invitrogen A12379) in F-actin buffer was added to the mixture in a 1:1 molar ratio with F-actin and incubated for 15 minutes at RT. The sample was

then diluted 50x with H_2O. Samples (5µl) were absorbed to 0.01% poly-L-lysine coated coverslips and visualized on a Nikon Eclipse TE2000-u, using a 100x 1.4 numerical aperture objective. Images were acquired with a Hamamatsu charged-coupled device camera using Metamorph software. Filament length was measured using ImageJ. About 6 images (2 images/3 different samples) were analyzed per condition, and all filaments having two distinguishable ends (~1200 filaments/condition) were measured.

Dual color filament assay using fluorescence microscopy

Actin was polymerized for 1 hour in F-actin buffer and subsequently incubated with MVt at a molar ratio of 1:2, actin to MVt for 10 minutes at RT. Rhodamine-labeled phalloidin (Sigma P1951) was added in a 1:1 molar ratio to actin and incubated for 10 minutes on ice. Samples were diluted 10-fold with 0.5 µM alexa-488 labeled G-actin, incubated for 5 minutes at RT, and diluted 2-fold in F-actin buffer. Samples (5µl) were absorbed to 0.01% poly-L-lysine coated coverslips and visualized on a Nikon Eclipse TE2000-u, using a 100x 1.4 numerical aperture objective. Images were acquired with a Hamamatsu charged-coupled device camera using Metamorph software.

Results

Differences in the modes by which Vt and MVt organize filamentous actin

Since metavinculin has an additional 68 amino acid acidic insert region in the tail domain, which also contains the actin binding sites, I hypothesized that the two vinculin isoforms organize actin filaments differently. Consistent with previous studies showing that full length vinculin and also the truncated form, Vt, induce actin bundle

formation (Jockusch and Isenberg 1981; Janssen, Kim et al. 2006), actin co-sedimentation assays show that Vt is a strong actin bundler (Fig. 5-1g). In the presence of Vt all actin ends up in the low speed pellet, which is an indication of heavy actin bundling. On the contrary, in the presence of MVt, most actin ends up in the high speed pellet, indicating that MVt is not an actin bundler but mostly binds single actin filaments (Fig. 5-1g).

Visualizing these assemblies using fluorescence microscopy, shows heavy actin bundling when Vt was present, but interestingly, in the presence of MVt, the actin filaments were significantly shorter than control actin filaments (Fig. 5-1d to 5-1f). These same mixtures of F-actin-Vt and F-actin-MVt were also imaged using transmission electron microscopy (Fig. 5-1a to 5-1c), again showing that Vt organizes actin filaments into large, highly-ordered bundles and, as seen in fluorescence microscopy, MVt induces the formation of short actin filaments. These images show that MVt not only shortens filaments, but also bind the filament sides (Fig. 5-1c).

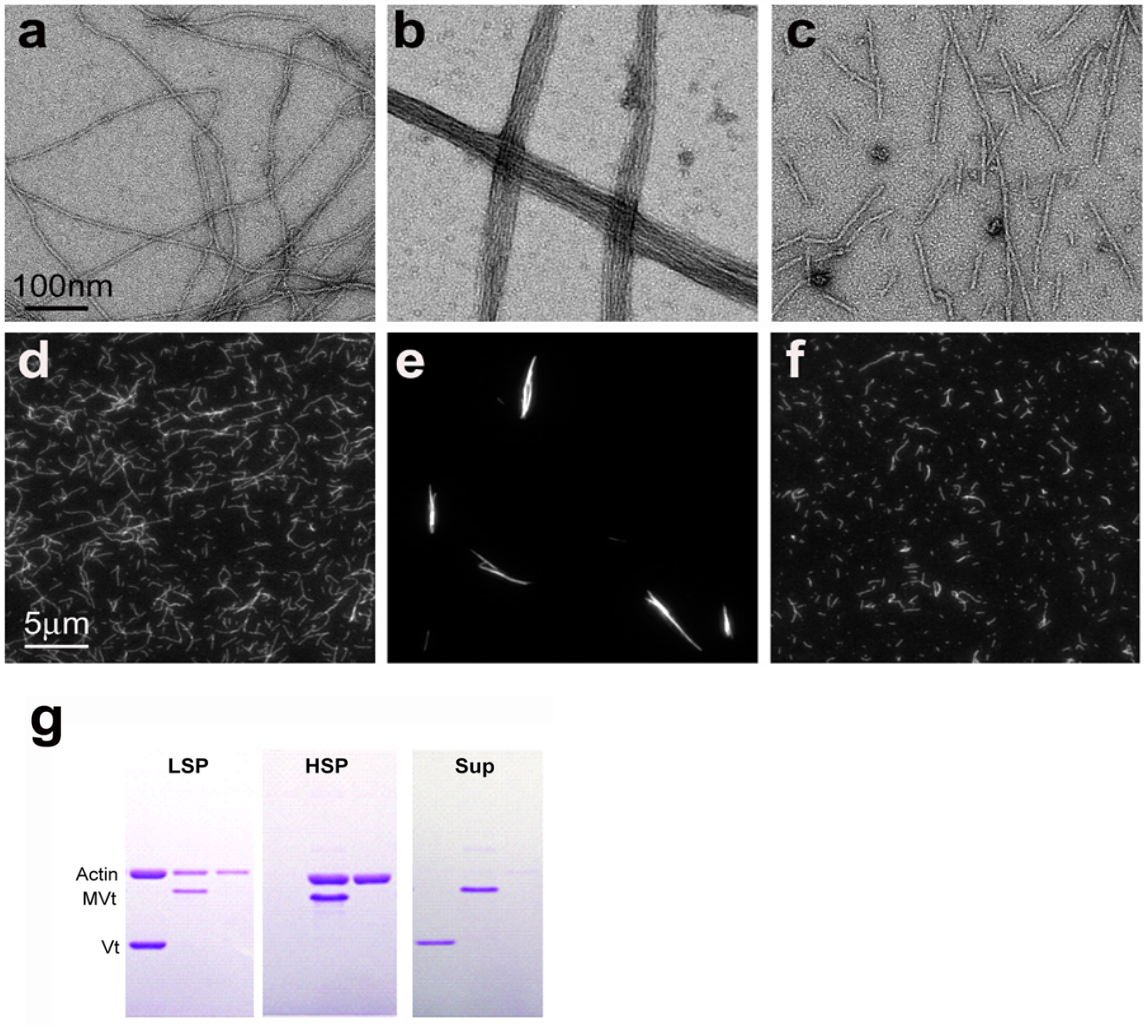

Fig. 5-1 Influence on actin filament organization by both vinculin tail isoforms. Molar ratio of F-actin to vinculin tail isoform is 1:2. (a-f) Electron and fluorescence microscopy images of filamentous actin structures show that actin filaments are organized into bundles by the vinculin tail (b,e) and into short fragments by the metavinculin tail (c,f). (g) A differential actin cosedimentation assay confirms actin bundling by the vinculin tail and shows actin filament binding of the metavinculin tail.

The F-actin-MVt interaction is weaker than the F-actin-Vt interaction

To further investigate differences between Vt and MVt binding to F-actin, I determined their binding constants for actin by making use of their intrinsic tryptophan fluorescence. In a stopped-flow tryptophan fluorescence assay I made use of two tryptophans located in the vinculin C-terminal tail domain that contribute to the level of quenching (Bakolitsa, de Pereda et al. 1999). Increasing concentrations of MVt or Vt were titrated at room temperature into a solution of F-actin. To determine the equilibrium dissociation constant (Kd) for both MVt and actin and for Vt and actin, a stoichiometric binding between the proteins was assumed. The changes in fluorescence upon addition of one of the vinculin tail isoforms were fitted in equation II (see materials and methods). F-actin saturated faster in the presence of Vt. The dissociation constant for Vt and F-actin was calculated to be ~40-fold higher than for MVt and F-actin (Fig. 5-2). MVt has a higher overall fluorescence signal, which can be due to a difference in environment of the tryptophans in each molecule or due to the extra tryptophan present in the insert. In addition, the change in fluorescence signal is larger for MVt, suggesting either a larger conformational change in MVt upon F-actin binding or a greater contribution due to the additional tryptophan in MVt.

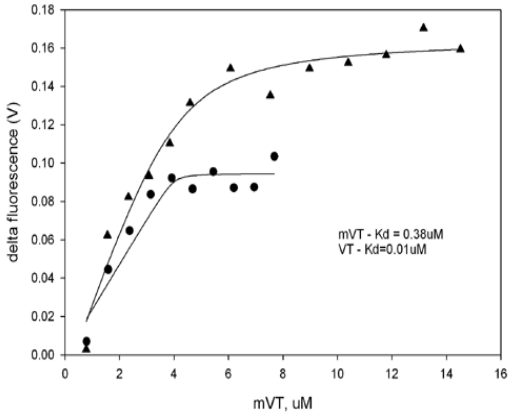

Fig. 5-2 Dissociation constants of Vt and MVt. A tryptophan assay shows that Vt (●) has a ~40x higher Kd than MVt (▲).

Reconstructions of F-actin-Vt and F-actin-MVt assemblies suggest why MVt does not bundle actin filaments

The presence of the additional 68 amino acid stretch in the C-terminal domain of metavinculin led me to believe that the insert prevents actin bundling either by interfering with actin binding or with (meta)vinculin dimerization. To answer this issue, I wished to map the insert by collecting high resolution data on the MVt-F-actin complex and compare this to the Vt-F-actin data we have obtained previously (Janssen, Kim et al. 2006). Electron microscopy and helical reconstruction techniques were used to generate two independent, 3D density maps of MVt bound to F-actin. They were subsequently used for cross-validation purposes. Analysis of the Fourier shell correlation shows a resolution of 2.1nm at the 0.5 criterion. A comparison between the electron density maps of Vt-F-actin and MVt-F-actin suggests that Vt and MVt bind F-actin similarly, and attach to the filament in the same orientation (Fig. 5-3a and 5-3b). In a filament in which the barbed end is directed upwards, both tail domains bind the upper actin monomer of two consecutive monomers at the bottom

of subdomain 1 and the lower actin monomer at the top of subdomain 1, see also (Janssen, Kim et al. 2006). Fig. 5-3b shows an additional density in the region that was suggested to coincide with the dimerization site in the Vt-F-actin model (Janssen, Kim et al. 2006).

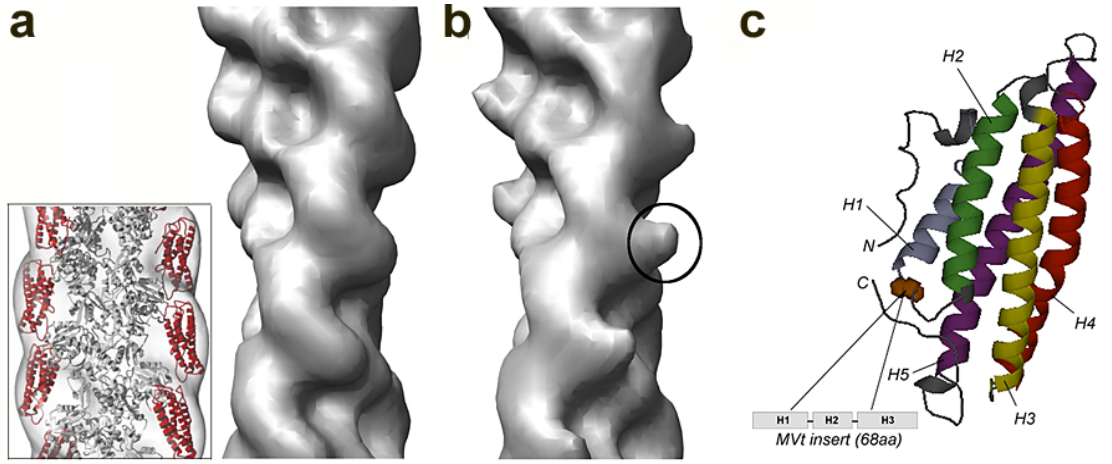

Fig. 5-3 Comparison between the 3D reconstructions of an actin filament decorated with vinculin tail and with metavinculin tail. (a) Electron density map of F-actin-Vt complex at 2nm resolution. The inset shows the atomic models of F-actin and vinculin tail docked into the density map. (b) Electron density map of F-actin-MVt complex at 2nm resolution, showing extra density near the dimerization site, which can be attributed to the metavinculin tail insert. (c) Schematic representation of the location of the insert between helix 1 and 2 in the C-terminal tail domain of metavinculin. The Vt model was adopted from (Bakolitsa, de Pereda et al. 1999).

MVt is an actin severing protein

The appearance of shorter actin filaments can be caused by several mechanisms, such as severing, F-actin depolymerization and/or actin monomer sequestering. To determine if MVt induces depolymerization of actin filaments, I added increasing amounts of MVt to preformed F-actin and checked the supernatants for the presence of G-actin after centrifugation. The gel in Fig. 5-4a does not show any increased amount of actin in the supernatant after adding an increasing concentration of MVt,

suggesting that MVt does not shorten F-actin by inducing filament depolymerization. Fig. 5-4b shows an experiment in which we added increasing amounts of MVt to G-actin before starting the polymerization process. No increased amount of actin was found in the supernatant, indicating that MVt does not retain G-actin in the supernatant. This supports the idea that MVt is neither a depolymerization nor an actin monomer sequestering protein.

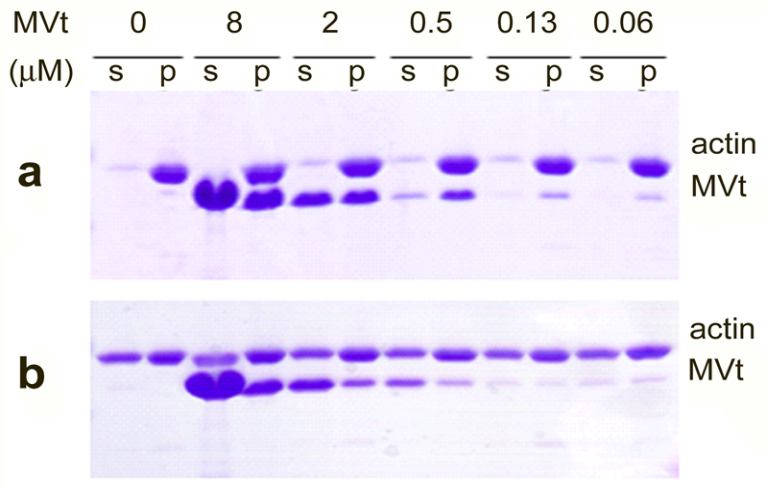

Fig. 5-4 Co-sedimentation assay of actin in presence of increasing amounts of MVt. (a) Effect of MVt on F-actin depolymerization. Abbreviations are as follows: s, supernatant; p, pellet. The gel shows there is no actin depolymerization upon MVt increase. (b) Effect of MVt on G-actin sequestering. The gel shows that MVt does not sequester actin monomers.

F-actin severing by MVt was established using pyrene fluorescence in a polymerization assay. The experiment starts with either F-actin seeds or F-actin-MVt seeds. Adding fresh pyrene-labeled G-actin results in actin polymerization, which increases in pyrene fluorescence. If the short actin filaments in presence of MVt are produced by severing as opposed to depolymerization, more filament ends will be

available for nucleation upon addition of new pyrene-labeled G-actin. This in turn will result in a higher initial polymerization rate, giving a faster increase in pyrene fluorescence signal. Fig. 5-5a shows how the pyrene fluorescence changes upon addition of increasing MVt concentrations. Indeed, the initial polymerization rate in presence of MVt is higher than in the control, suggesting that more filament ends are available for nucleation. The optimal severing concentration in this experiment is at a molar ratio of 2:1, actin: MVt. In addition, F-actin severing seems to have a biphasic MVt concentration dependency (Fig. 5-5b). Compared to cofilin, MVt is a rather efficient severing protein (Fig. 5-5).

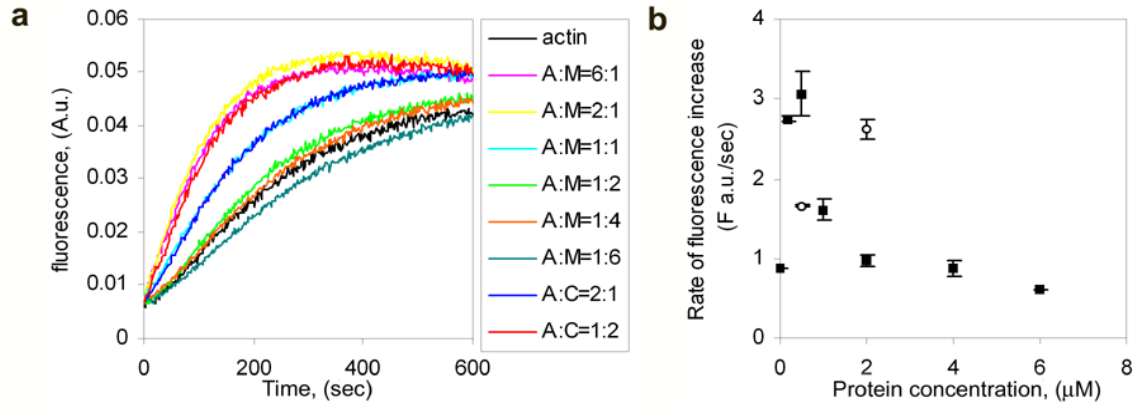

Fig. 5-5 Effect of MVt on the initial actin polymerization rate. (a) The initial actin polymerization rate is dependent on the amount of actin filament ends available for nucleation, which in turn is dependent on MVt concentration (■). Cofilin is used for comparison (□). Abbreviations are as follows: A, actin; M, MVt; C, cofilin. (b) Rate of pyrene fluorescence increase as function of protein concentration. The optimal F-actin severing occurs at a subsaturating MVt concentration. Error bars were compiled from independent experiments.

I determined how actin filament length depends on MVt concentration using fluorescence microscopy. MVt was incubated with F-actin before stabilizing and visualizing filaments with fluorescently-labeled phalloidin. This way, any stabilizing effect of phalloidin on actin that could alter or prevent the severing activity of MVt can

be avoided. Fig. 5-6 shows that actin filament length depends on MVt concentration. We found that filaments were, on average, more than twice as short when the MVt:actin molar ratio was 2:1. At a MVt:actin molar ratio of 1:2, filaments were almost 4 times shorter and ~64% of the filaments were < 0.5μm long (as compared to ~20% in the actin control). This experiment shows again a biphasic MVt concentration dependency for F-actin severing and the optimal severing condition at a sub-stoichiometric MVt concentration (Fig. 5-6F).

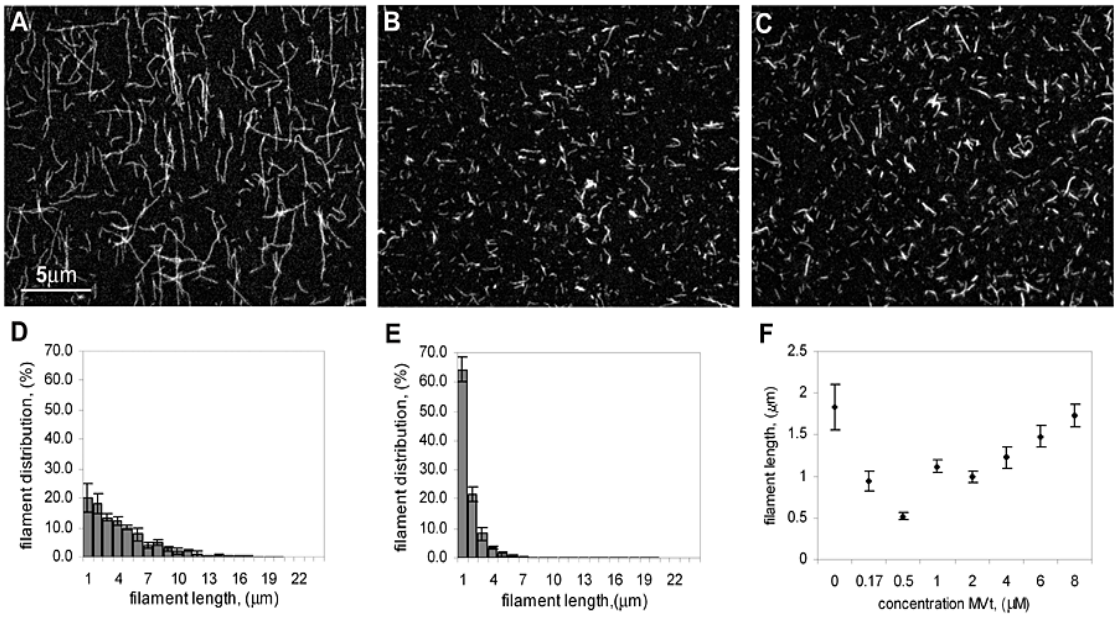

Fig. 5-6 Length distribution of actin filaments in presence of MVt. (A) Fluorescence microscopy image of actin filaments, (B) of MVt and actin filaments at a molar ratio of 1:2, and (C) MVt and phalloidin-stabilized actin filaments at a molar ratio of 1:2. (D) Filament length distribution of F-actin alone. (E) Filament length distribution of MVt and F-actin at a molar ratio of 1:2, showing that F-actin is about 4x as short as in the actin control. (F) Average filament length as function of MVt concentration. The graph shows that F-actin severing has a biphasic MVt concentration dependency. Error bars were compiled from 3 different experiments.

When actin filaments are stabilized with phalloidin before addition of MVt, filaments have an average length of 0.7μm at the same sub-stoichiometric MVt

concentration of 2:1. This means that phalloidin either decreases MVt severing or phalloidin prevents further depolymerization after severing (Fig. 5-6C).

MVt binding stabilizes individual actin filaments

Another approach in identifying actin severing is a pyrene fluorescence depolymerization assay. Actin severing creates more filament ends, which will result in faster initial filament depolymerization upon sample dilution below the critical concentration of actin. This in turn will show a drastic decrease in pyrene fluorescence signal. Surprisingly however, F-actin alone depolymerizes faster than F-actin in the presence of MVt. Increasing MVt concentrations result in decreasing depolymerization rates (Fig. 5-7A). This suggests that MVt, in addition to severing, also prevents actin from depolymerization and has a stabilizing activity. Fig. 5-7B shows that MVt is bound to the sides of severed actin filaments.

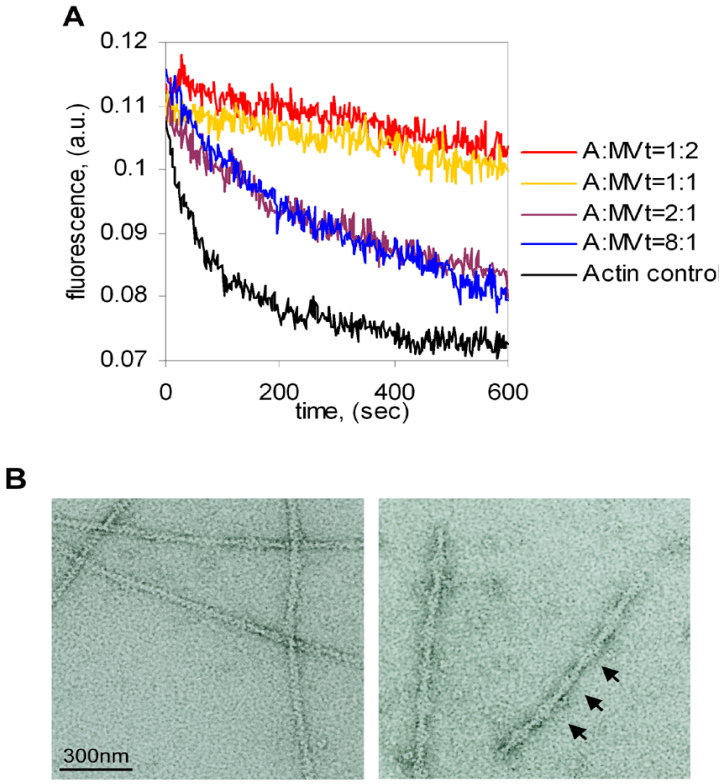

Fig. 5-7 MVt stabilizes severed actin filaments. (A) A pyrene fluorescence depolymerization assay shows the concentration dependent F-actin stabilization by MVt. (B) Electron microscopy images of negatively stained filaments show that the severed actin filaments are fully decorated by MVt.

Actin stabilization by MVt was further examined by dual color fluorescence to determine if this stabilization is due to binding to filament sides or to actin filament capping. Actin filaments severed by MVt were stabilized by rhodamine-phalloidin. Fresh alexa-488 G-actin was added to observe actin growth from both filament ends. Fig. 5-8 shows that, after actin severing by MVt, new actin still adds to both filament ends, suggesting that actin stabilization seen in (Fig. 5-7) is caused by filament side binding and not by capping.

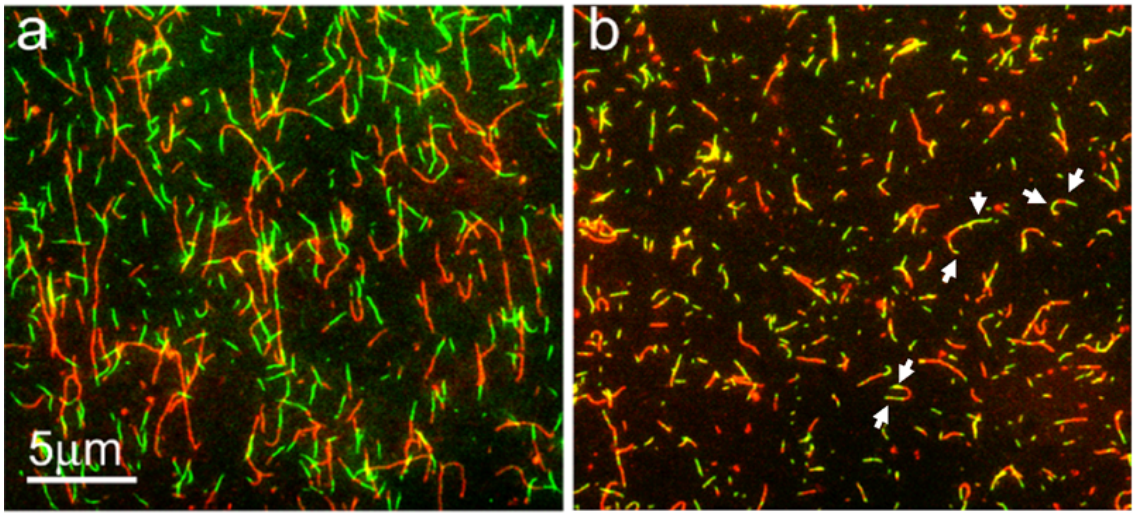

Fig. 5-8 Dual color fluorescence to determine actin filament capping. New actin (green) grows from the ends of existing (red) actin filaments in the control (a) but also when severed by MVt (b). MVt severed actin filaments are diluted 4-fold to better distinguish filament ends. White arrows indicate examples of new actin growth from both pointed and barbed ends.

MVΔ153 bundles actin filaments

To determine if full length metavinculin exerts the same function as the tail domain of metavinculin, I generated the metavinculin deletion mutant, MVΔ153. This mutant lacks the first 153 N-terminal amino acids, which would otherwise obscure the actin binding sites in the full length, auto-inhibited metavinculin protein. I visualized a suspension of actin filaments in the presence of MVΔ153 using transmission electron microscopy. Surprisingly, MVΔ153 does not sever F-actin, but organizes the filaments into bundles just like Vt (Fig. 5-9A). I hypothesized that the insert in metavinculin has to be available for the severing activity. In MVt the insert is available (Fig. 5-3B), but in MVΔ153 the insert might be (partially) obscured by the head domain.

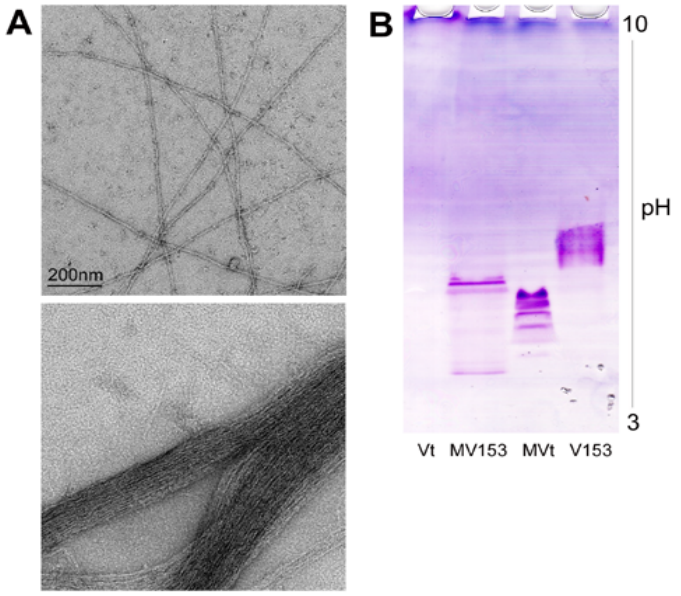

Fig. 5-9 Actin organization by MVΔ153. (A) Electron microscopy images of negatively stained actin filaments alone (top) and actin filaments bundled by MVΔ153 (bottom). (B) The isoelectric focusing gel compares Vt, MVΔ153, MVt, and VΔ153. MVΔ153 runs higher than expected, suggesting that the acidic insert might be occluded.

To test this hypothesis, I compared the isoelectric focusing point of Vt, MVt, VΔ153, and MVΔ153 (Fig. 5-9B). This gel shows that the isoelectric focusing point of MVΔ153 runs higher than that of MVt, while in theory it should have been lower than that of MVt. This suggests that the acidic insert in shielded by the head domain of the construct.

The R975W mutation in MVt causing does not affect actin organization

An actin cosedimentation assay shows that the mutant R975W MVt behaves like wild-type MVt (Fig. 5-10). R975W MVt predominantly sediments together with actin in the high speed pellet, indicating that R975W MVt binds single actin filaments. In

addition, R975W MVt induces some actin bundling, similar to MVt but to a much lesser extent than Vt.

Electron microscopy also shows that the mutant R975W MVt behaves similar to wild-type MVt (Fig. 5-10). The same samples were used as in the actin cosedimentation assay above. Electron microscopy shows that Vt forms highly organized actin bundles, as was already discussed in chapter 3. Actin in the presence of the mutant R975W appears as very short filaments, similar to the ones in the presence of wild-type MVt. This suggests that R975W also severs actin filaments.

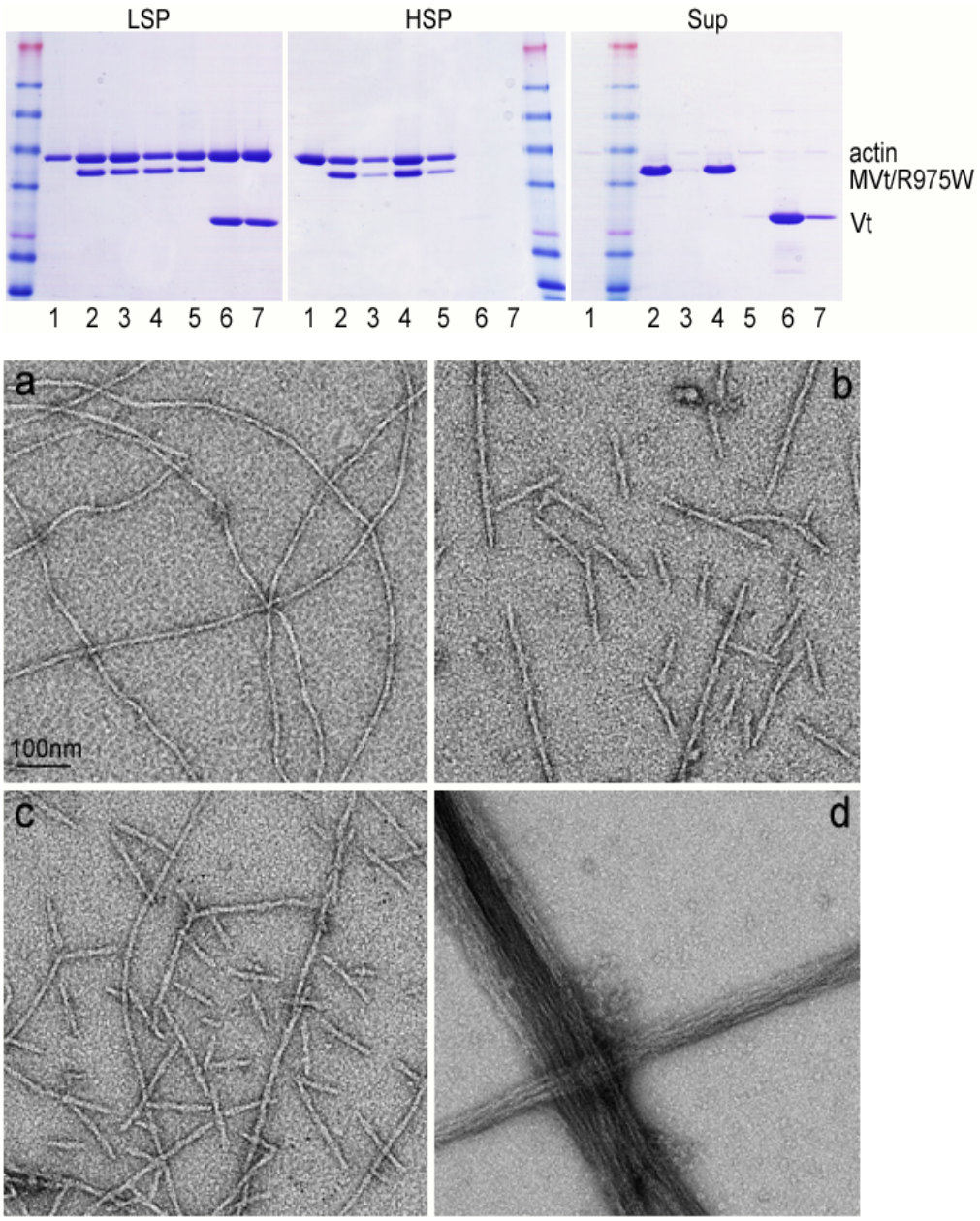

Fig. 5-10 Effect of the R975W mutation on actin organization. (Top) Coomassie stained gels of an actin cosedimentation assay with the R975W-MVt mutant, compared to MVt and Vt. LSP: low speed pellet; HSP: high speed pellet; Sup: supernatant. (1) actin; (2) actin:MVt = 6:12 μM; (3) actin:MVt = 6:3 μM; (4) actin:R975W = 6:12 μM; (5) actin:R975W = 6:3 μM; (6) actin:Vt = 6:12 μM; (7) actin:Vt = 6:3 μM. (Bottom) Electron microscope images of actin alone (a), actin in the presence of MVt (b), actin in the presence of the MVt mutant R975W (c), and actin in the presence of Vt (d) show that the mutant R975W severs actin filaments similar to wild-type MVt.

Actin organization in the presence of both MVt and Vt

Since vinculin and metavinculin were found to colocalize in muscle tissue (Feramisco, Smart et al. 1982; Belkin, Ornatsky et al. 1988; Witt, Zieseniss et al. 2004), it would be interesting to see whether both MVt and Vt form heterodimers and how they influence actin organization when they are both present in the same mixture. Analytical ultracentrifugation was used to determine if the tail domains of both isoforms heterodimerize. Although this technique was able to show some minor MVt- and Vt-homodimerization, it could not distinguish MVt-Vt heterodimerization from homodimerization. Size-exclusion chromatography on the other hand was better suited and showed two single peaks in the MVt-Vt mixture that correspond to the peaks of Vt and MVt alone. No additional peak that would correspond to MVt-Vt heterodimers was seen (Fig. 5-11).

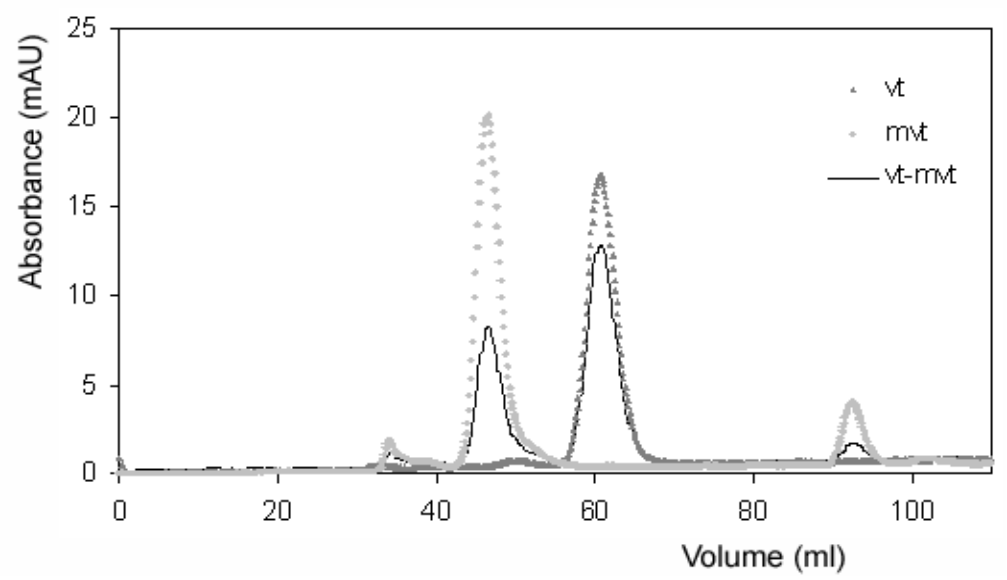

Fig. 5-11 Analysis of MVt-Vt complex formation by size-exclusion chromatography. Similar peaks for Vt and MVt are seen for the MVt-Vt mixture as for MVt and Vt alone. No additional peak for MVt-Vt dimers was detected, suggesting MVt and Vt do not heterodimerize.

A cosedimentation assay was performed to determine what happens to the actin organization when both MVt and Vt are added to F-actin (Fig. 5-12). Adding both isoforms at the same time results in actin bundling similar to the bundling that happens in the presence of Vt alone. This is not surprising, since the Kd of Vt for F-actin is ~40-fold higher than the Kd of MVt for F-actin (Fig. 5-2). Adding MVt to a mixture of F-actin and Vt does not make a difference, MVt does not seem to affect the actin bundling by Vt. Adding Vt to a mixture of F-actin and MVt results in bundling or formation of other large actin assemblies.

Electron microscopy was used to visualize these assemblies. Fig. 5-12 shows that there is still formation of actin bundles, but actin bundles are less tight. Furthermore, the mutant R975W-MVt also behaves similar to the wild-type MVt in the presence of Vt.

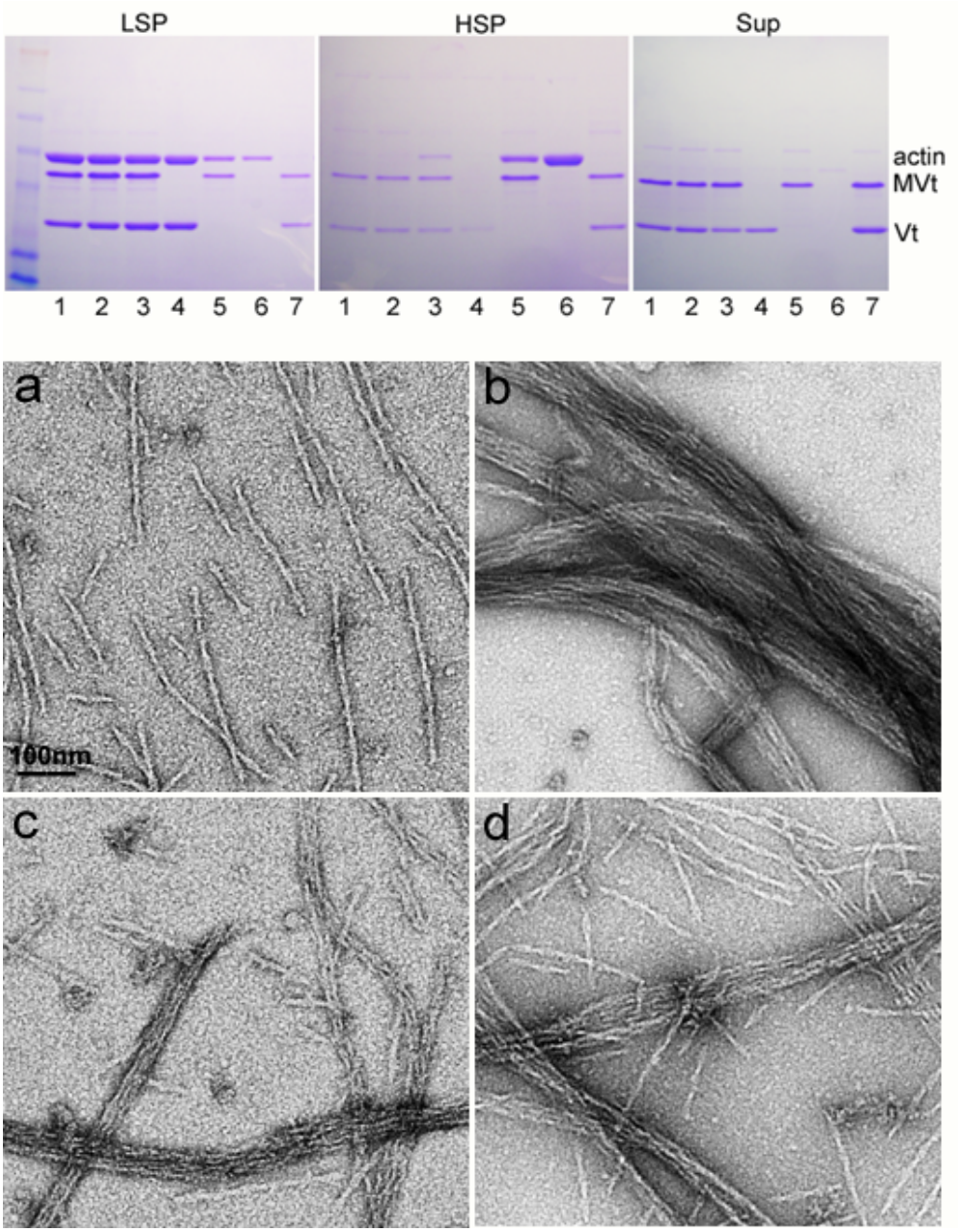

Fig. 5-12 Actin in the presence of both Vt and MVt. (Top) Coomassie stained gels of an actin cosedimentation assay with Vt and MVt. LSP: low speed pellet;HSP: high speedpellet; Sup: supernatant. (1) actin:Vt:MVt=1:1:1 μM; (2) actin:Vt=1:1 μM, 1 μM MVt is added after 10 minutes; (3) actin:MVt=1:1 μM, 1 μM Vt is added after 10 minutes; (4) actin:Vt=1:1 μM; (5) actin:MVt=1:1 μM; (6) actin alone; (7) MVt:Vt=1:1 μM. (Bottom) Electron microscopy images show actin severing by MVt (a), actin bundling by Vt (b) and less severe bundling by both Vt and MVt together (c) or R975W-MVt and Vt together (d).

Discussion

Prevention of actin bundling by MVt

Muscle specific isoforms of actin regulating proteins are common in mammals. UNC-60B, an ADF/cofilin family actin binding protein of *Caenorhabditis elegans*, is specific for muscle tissue, whereas its splice variant, UNC-60A, is expressed in various tissues. UNC-60B has a stronger actin severing activity and induces faster pointed-end depolymerization than UNC-60A (Yamashiro, Mohri et al. 2005). Also, the expression of twinfilin isoform Twf2b is restricted to striated muscle, whereas Twf2a is expressed in most non-muscle tissues. The difference between these isoforms is that Twf2a has a higher affinity for ADP-G-actin than Twf2b. (Nevalainen, Skwarek-Maruszewska et al. 2009). However, no other isoforms of actin binding proteins are known to display such a dramatic change on actin organization as happens with Vt and MVt.

The C-terminal domain of metavinculin contains the 68 amino acid acidic insert as well as the actin binding sites (Gimona, Small et al. 1988; Janssen, Kim et al. 2006). The insert is located between Trp912 and Ser913 in the loop between helix 1 and 2 of the tail domain (Gimona, Small et al. 1988). This location does not directly interfere with the actin binding sides or the proposed dimerization site (Janssen, Kim et al. 2006), but because of their close proximity I hypothesized that metavinculin influences actin organization in a manner different than vinculin. The data in this work indeed show a large difference in F-actin organization by both isoforms. Vt induces formation of large, highly organized actin bundles, whereas MVt exhibits no actin bundling activity. F-actin bound by MVt is significantly shorter than control actin filaments. The electron microscopy reconstructions indicate that the insert most

probably prevents actin bundling due to its location near the N-terminal strap, which was suggested to play a role in dimerization (Janssen, Kim et al. 2006). A recent study showed reduced MVt dimerization after PIP_2 induction as compared to Vt. But it was suggested that this was caused by the negative charges of the insert affecting initial PIP_2 binding to the hydrophobic finger (Witt, Zieseniss et al. 2004). This study indeed suggests that the insert prevents MVt dimerization. Although the insert does not physically seem to disrupt either of the actin binding sites, its proximity to the lower binding site might also explain the lower dissociation constant for F-actin that we see in our kinetics study.

Mechanism of actin severing by MVt

In this study, MVt is shown to have a double activity: actin severing and stabilization. Many severing proteins have multiple activities like F-actin depolymerization, nucleation, G-actin sequestering and/or filament end capping (Ichetovkin, Han et al. 2000; Harris, Li et al. 2004; Andrianantoandro and Pollard 2006; Moseley, Okada et al. 2006; Revenu, Courtois et al. 2007; Klaavuniemi, Yamashiro et al. 2008). Several assays were used to show that the appearance of short actin filaments in the presence of MVt is a result of F-actin severing as opposed to F-actin depolymerization or G-actin sequestering. Stabilization of actin filaments is most probably due to the binding of MVt to the sides of F-actin. Pointed end capping would be another way in which MVt could stabilize these filaments. Recently, vinculin was suggested to partially cap barbed ends of filaments in the presence of the C-terminal domain of the Shigella secretion protein IpaA (Ramarao, Le Clainche et al. 2007). There is no direct evidence available to support the hypothesis that MVt caps

F-actin. I showed that actin is still able to add to both actin filament ends. However, to determine if MVt is a leaky pointed end capper, gelsolin or capZ can be added to cap barbed ends. Pyrene fluorescence polymerization assays can subsequently show at what rate filaments are able to grow from the pointed ends, which would show if MVt is a leaky capper or not. Stabilization of severed actin filaments could provide very stable short filaments that can be readily incorporated into new actin structures.

Like cofilin (Pavlov, Muhlrad et al. 2007), MVt promotes F-actin fragmentation most efficiently at substoichiometric concentrations. In addition, MVt severing has a biphasic concentration dependency. It first increases and then decreases upon adding MVt. This suggests a severing mechanism in which sparsely bound MVt is able to alter the helical twist of actin filaments, like cofilin (Andrianantoandro and Pollard 2006); (McGough, Pope et al. 1997). Changing the twist of an actin filament by binding to it is a common mechanism by which many severing proteins act (Galkin, Orlova et al. 2003; Prochniewicz, Janson et al. 2005). However, the 3D reconstruction of MVt bound to F-actin did not show any alteration in filament twist. A change in twist would have resulted in a change in F-actin crossover length (McGough, Pope et al. 1997). Actin flexibility seems to affect the actin severing ability of MVt. Actin filaments tethered to a glass surface or an electron microscopy grid were not severed by MVt. Like gelsolin (Dawson, Sablin et al. 2003), the filaments have to be freely available in solution for MVt to sever them. Cofilin acts in an opposite manner since actin filament flexibility has to be restricted for optimal severing (Pavlov, Muhlrad et al. 2007). Thus, MVt might sever mainly at pre-existing bends in the actin filament. In this mechanism, actin filaments are mechanically disrupted by intercalation of MVt between two adjacent actin monomers within the

filament. This process depends on the bending-flexibility of F-actin, which is in turn dependent on the bound divalent cation (Ca^{2+} or Mg^{2+}) and nucleotide (ATP or ADP) (Rebello and Ludescher 1998).

Two motifs are known within the actin severing protein group of gelsolin, villin, fragmin and severin that are involved in actin severing. These motifs are GFKHV and LDDYLGG (Southwick FS 1995; McLaughlin, Gooch et al. 1993). I could not find any sequence similarity between the first motif and the MVt insert sequence. Part of the second motif, DDY, was an exact match with a region in the insert and is also highly conserved among species. Furthermore, the sequences LKSKM and DAIKKKL are basic actin binding motifs that are found in cofilin. They do not show any sequence similarities with the MVt insert. However, peptides containing these motifs compete for actin binding with a gelsolin peptide containing helix DESGAAIVQLDDYL (McLaughlin, Gooch et al. 1993). This actin binding helix in gelsolin binds actin between subdomains 1 and 3 (Burtnick and Urosev et al. 2004). The sequence of this motif shows 58% similarity with a region in the MVt insert (Kalign, gap open penalty 11.0, gap extension penalty 0.85, terminal gap penalty 0.45) (Lassmann and Sonnhammer 2005):

AA I FTVQ - - - MDDYL

A**A**G**F**P**V**PP**DM**E**DDYE**

Again, the similarities (underlined) involve mainly conserved residues (in bold). It may be that this represents a third, weaker actin binding site within the MVt insert. If an actin filament bends just enough to expose some additional surface, this MVt region

could potentially bind between subdomains 1 and 3 and sever actin filaments by intercalation. It would be informative to test if mutation of the DDY sequence affects MVt severing of actin filaments.

Actin organization by full length metavinculin

Vinculin has to be activated in order to unmask its ligand binding sites, meaning that the intramolecular interaction between the head and tail domains has to be relieved (Bakolitsa, Cohen et al. 2004). The vinculin tail forms a large, intramolecular hydrophobic contact with the N-terminus of domain 1, a smaller contact with the C-terminus of domain 4, and a smaller, polar contact with the domain 1-3 interface (Bakolitsa, Cohen et al. 2004). These contacts all contribute to the high affinity (<1nM) of Vt for Vh. It was shown that metavinculin is also regulated by an intramolecular head-tail interaction, but that there is a decreased affinity of the vinculin head domain for MVt as compared to Vt (Witt, Zieseniss et al. 2004). There is no atomic model for full length metavinculin, but we assumed that the residues in the head domain that help maintain this intramolecular interaction are similar for both vinculin isoforms. To determine if the full length metavinculin protein functions similar as MVt, but at the same time avoiding any potential problems linked to metavinculin activation, we designed MVΔ153, which lacks the first 153 N-terminal amino acids that are crucial for the high affinity of the head-tail interaction. In contrast to MVt, MVΔ153 bundles but does not sever actin filaments. The isoelectric focusing point experiment suggests that the acidic insert is partially obscured by the head domain of MVΔ153. It suggests that metavinculin is a severing protein when the insert is fully exposed and a bundling protein when the protein is only partially activated. In

summary, the data presented here reveals a new function for metavinculin in vitro. The fact that MVt severs and stabilizes actin filaments, suggests a very efficient way to reorganize F-actin. Older filaments can be severed and the resulting short F-actin can then be readily incorporated into new actin bundles, enabling a fast reaction to sudden force generations needed in muscle tissue and platelets.

R975W-MVt affects actin organization in a manner similar to wild-type MVt

R975 in the metavinculin-specific exon of vinculin is a highly conserved residue and the missense mutation R975W leads to both dilated and hypertrophic cardiomyopathy (Vasile, Will et al. 2006). It was previously shown by light microscopy that the R975W mutation in MVt causes actin bundling like Vt (Olson, Illenberger et al. 2002). Here, however, it is shown that R975W-MVt does not bundle actin filaments, but actually severs them like wild-type MVt. This study shows no difference in actin organization between R975W-MVt and wild-type MVt. It is interesting to note that in the study of Olson et al. a different R975W-MVt construct was used (aa 858-1134 versus aa 879-1134 in this study). Our construct lacks the proline-rich region interspaced with some arginine and lysine residues that could potentially form electrostatic interactions with the acidic insert in MVt. Hence, the acidic insert in MVt in this study is probably exposed and gives MVt its actin severing activity, whereas the insert in the other construct might be shielded by the proline-rich region. The observation that MVΔ153 (includes the proline-rich region) does not sever but bundles actin filaments, makes this hypothesis now plausible. It also supports the notion that metavinculin has a dual function: an actin severing protein when fully

activated (and the insert is exposed) and a bundling protein when only partially activated.

Actin organization in the presence of both Vt and MVt

The isoforms vinculin and metavinculin co-localize in muscle tissue in dense plaques, intercalated disks and costameres (Feramisco, Smart et al. 1982; Belkin, Ornatsky et al. 1988; Witt, Zieseniss et al. 2004). In addition, immunoprecipitates indicate that both isoforms are present in the same complex (Witt, Zieseniss et al. 2004). Here, I showed that MVt and Vt do not form heterodimers in solution. However, they are able to heterodimerize after Vt is activated by PIP2 (Witt, Zieseniss et al. 2004). Vt was found to homodimerize after F-actin binding induces a conformational change in the Vt C-terminal region (Janssen, Kim et al. 2006). It may be that the isoforms can heterodimerize after similar conformational changes occur in each isoform upon binding to F-actin.

Actin filaments in the presence of both MVt and Vt induce formation of actin bundles, but bundles are less compact than those formed solely in the presence of Vt. The Kd of Vt for F-actin is ~40-fold higher than the Kd of MVt for F-actin, thereby suggesting that MVt does not compete with Vt for actin binding. The precise mechanism is still unclear, but a high concentration of fully activated metavinculin that severs actin filaments might be beneficial in generating short stable actin filaments that can be readily incorporated into new actin bundles. In this scenario activation of vinculin and metavinculin has to be tightly regulated and interdependent. Another mechanism is one in which metavinculin severs Vt-F-actin assemblies and generates

short actin bundles. This phenomenon was sporadically observed in the electron microscopy images, but not enough to be conclusive.

Chapter 5, in part is currently being prepared for submission for publication of the material. Mandy Janssen, Hongjun Liu, Robert Jeng, Larnele Hazelwood, Niels Volkmann and Dorit Hanein. Janssen and Hanein conceived the project, designed the experiments and will finalize the write up of the paper. Janssen performed most of the experiments. Jeng provided some of the reagents and technical help. Hazelwood provided some of the EM samples, Liu assisted and provided some of the image analysis studies, Bobkov assisted with pyrene fluorescence experiments, Volkmann provided significant input on image analysis.

References

Andrianantoandro, E. and T. D. Pollard (2006). "Mechanism of actin filament turnover by severing and nucleation at different concentrations of ADF/cofilin." Mol Cell **24**(1): 13-23.

Bakolitsa, C., D. M. Cohen, et al. (2004). "Structural basis for vinculin activation at sites of cell adhesion." Nature **430**(6999): 583-6.

Bakolitsa, C., J. M. de Pereda, et al. (1999). "Crystal structure of the vinculin tail suggests a pathway for activation." Cell **99**(6): 603-13.

Belkin, A. M., O. I. Ornatsky, et al. (1988). "Immunolocalization of meta-vinculin in human smooth and cardiac muscles." J Cell Biol **107**(2): 545-53.

Bobkov, A. A., A. Muhlrad, et al. (2002). "Structural effects of cofilin on longitudinal contacts in F-actin." J Mol Biol **323**(4): 739-50.

Borgon, R. A., C. Vonrhein, et al. (2004). "Crystal structure of human vinculin." Structure **12**(7): 1189-97.

Brindle, N. P., M. R. Holt, et al. (1996). "The focal-adhesion vasodilator-stimulated phosphoprotein (VASP) binds to the proline-rich domain in vinculin." Biochem J **318 (Pt 3)**: 753-7.

Burridge, K. and P. Mangeat (1984). "An interaction between vinculin and talin." Nature **308**(5961): 744-6.

Byrne, B. J., Y. J. Kaczorowski, et al. (1992). "Chicken vinculin and meta-vinculin are derived from a single gene by alternative splicing of a 207-base pair exon unique to meta-vinculin." J Biol Chem **267**(18): 12845-50.

Dawson, J. F., E. P. Sablin, et al. (2003). "Structure of an F-actin trimer disrupted by gelsolin and implications for the mechanism of severing." J Biol Chem **278**(2): 1229-38.

Egelman, E. H. (2000). "A robust algorithm for the reconstruction of helical filaments using single-particle methods." Ultramicroscopy **85**(4): 225-34.

Feramisco, J. R., J. E. Smart, et al. (1982). "Co-existence of vinculin and a vinculin-like protein of higher molecular weight in smooth muscle." J Biol Chem **257**(18): 11024-31.

Galkin, V. E., A. Orlova, et al. (2003). "ADF/cofilin use an intrinsic mode of F-actin instability to disrupt actin filaments." J Cell Biol **163**(5): 1057-66.

Gimona, M., J. V. Small, et al. (1988). "Porcine vinculin and metavinculin differ by a 68-residue insert located close to the carboxy-terminal part of the molecule." Embo J **7**(8): 2329-34.

Gimona M., S. J. V., Moeremans M., van Damme J., Puype M., Vandekerckhove J. (1988). "Molecular domain structure of porcine vinculin and metavinculin." protoplasma **145**: 133-140.

Glukhova, M. A., A. E. Kabakov, et al. (1986). "Meta-vinculin distribution in adult human tissues and cultured cells." FEBS Lett **207**(1): 139-41.

Harris, E. S., F. Li, et al. (2004). "The mouse formin, FRLalpha, slows actin filament barbed end elongation, competes with capping protein, accelerates polymerization from monomers, and severs filaments." J Biol Chem **279**(19): 20076-87.

Hathaway D.R., A. R. S. (1979). "Human platelet myosin light chain kinase requires the calcium-binding protein calmodulin for activity." Proc Natl Acad Sci U S A **76**(4): 1653-1657.

Ichetovkin, I., J. Han, et al. (2000). "Actin filaments are severed by both native and recombinant dictyostelium cofilin but to different extents." Cell Motil Cytoskeleton **45**(4): 293-306.

Janssen, M. E., E. Kim, et al. (2006). "Three-dimensional structure of vinculin bound to actin filaments." Mol Cell **21**(2): 271-81.

Jockusch, B. M. and G. Isenberg (1981). "Interaction of alpha-actinin and vinculin with actin: opposite effects on filament network formation." Proc Natl Acad Sci U S A **78**(5): 3005-9.

Johnson, R. P. and S. W. Craig (1994). "An intramolecular association between the head and tail domains of vinculin modulates talin binding." J Biol Chem **269**(17): 12611-9.

Johnson, R. P., V. Niggli, et al. (1998). "A conserved motif in the tail domain of vinculin mediates association with and insertion into acidic phospholipid bilayers." Biochemistry **37**(28): 10211-22.

Kioka, N., S. Sakata, et al. (1999). "Vinexin: a novel vinculin-binding protein with multiple SH3 domains enhances actin cytoskeletal organization." J Cell Biol **144**(1): 59-69.

Klaavuniemi, T., S. Yamashiro, et al. (2008). "Caenorhabditis elegans gelsolin-like protein 1 is a novel actin filament-severing protein with four gelsolin-like repeats." J Biol Chem **283**(38): 26071-80.

Koteliansky, V. E., A. M. Belkin, et al. (1991). "Developmental changes in expression of adhesion-mediating proteins in human aortic smooth muscle." Biochem Soc Trans **19**(4): 1072-6.

Kroemker, M., A. H. Rudiger, et al. (1994). "Intramolecular interactions in vinculin control alpha-actinin binding to the vinculin head." FEBS Lett **355**(3): 259-62.

Lassermann T. and E. L. L. Sonnhammer (2005). “Kalign – an accurate and fast multiple sequence alignment algorithm.” BMC Bioinformatics **6**:298.

Ludtke, S. J., P. R. Baldwin, et al. (1999). "EMAN: semiautomated software for high-resolution single-particle reconstructions." J Struct Biol **128**(1): 82-97.

Maciver, S. K., H. G. Zot, et al. (1991). "Characterization of actin filament severing by actophorin from Acanthamoeba castellanii." J Cell Biol **115**(6): 1611-20.

Mandai, K., H. Nakanishi, et al. (1999). "Ponsin/SH3P12: an l-afadin- and vinculin-binding protein localized at cell-cell and cell-matrix adherens junctions." J Cell Biol **144**(5): 1001-17.

McGough, A., B. Pope, et al. (1997). "Cofilin changes the twist of F-actin: implications for actin filament dynamics and cellular function." J Cell Biol **138**(4): 771-81.

McLaughlin, P. J., J. T. Gooch, et al. (1993). “Structure of gelsolin segment 1-actin complex and the mechanism of filament severing.” Nature **364**(6439): 685-92.

Moseley, J. B., K. Okada, et al. (2006). "Twinfilin is an actin-filament-severing protein and promotes rapid turnover of actin structures in vivo." J Cell Sci **119**(Pt 8): 1547-57.

Nevalainen, E. M., A. Skwarek-Maruszewska, et al. (2009). "Two biochemically distinct and tissue-specific twinfilin isoforms are generated from the mouse Twf2 gene by alternative promoter usage." Biochem J **417**(2): 593-600.

Olson, T. M., S. Illenberger, et al. (2002). "Metavinculin mutations alter actin interaction in dilated cardiomyopathy." Circulation **105**(4): 431-7.

Ono, S. (2007). "Mechanism of depolymerization and severing of actin filaments and its significance in cytoskeletal dynamics." Int Rev Cytol **258**: 1-82.

Pavlov, D., A. Muhlrad, et al. (2007). "Actin filament severing by cofilin." J Mol Biol **365**(5): 1350-8.

Prochniewicz, E., N. Janson, et al. (2005). "Cofilin increases the torsional flexibility and dynamics of actin filaments." J Mol Biol **353**(5): 990-1000.

Ramarao, N., C. Le Clainche, et al. (2007). "Capping of actin filaments by vinculin activated by the Shigella IpaA carboxyl-terminal domain." FEBS Lett **581**(5): 853-7.

Rebello, C. A. and R. D. Ludescher (1998). "Influence of tightly bound Mg2+ and Ca2+, nucleotides, and phalloidin on the microsecond torsional flexibility of F-actin." Biochemistry **37**(41): 14529-38.

Revenu, C., M. Courtois, et al. (2007). "Villin severing activity enhances actin-based motility in vivo." Mol Biol Cell **18**(3): 827-38.

Rudiger, M., N. Korneeva, et al. (1998). "Differential actin organization by vinculin isoforms: implications for cell type-specific microfilament anchorage." FEBS Lett **431**(1): 49-54.

Saga, S., M. Hamaguchi, et al. (1985). "Expression of meta-vinculin associated with differentiation of chicken embryonal muscle cells." Exp Cell Res **156**(1): 45-56.

Siliciano, J. D. and S. W. Craig (1982). "Meta-vinculin--a vinculin-related protein with solubility properties of a membrane protein." Nature **300**(5892): 533-5.

Southwick, F. S. (1995). “Gain-of-function mutations conferring actin-severing activity to human macrophage Cap G”. J Biol Chem **270**(1): 45-8.

Taylor, K. A. and D. W. Taylor (1992). "Formation of 2-D paracrystals of F-actin on phospholipid layers mixed with quaternary ammonium surfactants." J Struct Biol **108**(2): 140-7.

Turner, C. E. and K. Burridge (1989). "Detection of metavinculin in human platelets using a modified talin overlay assay." Eur J Cell Biol **49**(1): 202-6.

Turner, C. E., J. R. Glenney, Jr., et al. (1990). "Paxillin: a new vinculin-binding protein present in focal adhesions." J Cell Biol **111**(3): 1059-68.

Vasile, V. C., M. L. Will, et al. (2006). Identification of a metavinculin missense mutation, R975W, associated with both hypertrophic and dilated cardiomyopathy. Mol Genet Metab. **87:** 169-74.

Volkmann, N., D. DeRosier, et al. (2001). "An atomic model of actin filaments cross-linked by fimbrin and its implications for bundle assembly and function." J Cell Biol **153**(5): 947-56.

Volkmann, N., H. Liu, et al. (2005). "The structural basis of myosin V processive movement as revealed by electron cryomicroscopy." Mol Cell **19**(5): 595-605.

Weiss, E. E., M. Kroemker, et al. (1998). "Vinculin is part of the cadherin-catenin junctional complex: complex formation between alpha-catenin and vinculin." J Cell Biol **141**(3): 755-64.

Witt, S., A. Zieseniss, et al. (2004). "Comparative biochemical analysis suggests that vinculin and metavinculin cooperate in muscular adhesion sites." J Biol Chem **279**(30): 31533-43.

Xu, W., H. Baribault, et al. (1998). "Vinculin knockout results in heart and brain defects during embryonic development." Development **125**(2): 327-37.

Yamashiro, S., K. Mohri, et al. (2005). "The two Caenorhabditis elegans actin-depolymerizing factor/cofilin proteins differently enhance actin filament severing and depolymerization." Biochemistry **44**(43): 14238-47.

Zemljic-Harpf, A. E., J. C. Miller, et al. (2007). "Cardiac-myocyte-specific excision of the vinculin gene disrupts cellular junctions, causing sudden death or dilated cardiomyopathy." Mol Cell Biol **27**(21): 7522-37.

Chapter 6

Conclusion and future directions

Mechanism of actin bundling by the vinculin tail domain

Cell adhesions, whether cell-cell or cell-matrix adhesion sites, determine structural integrity of the cell, sense mechanical forces exerted by the environment, and are involved in processes such as migration, contraction, differentiation and proliferation. Among the many proteins that are involved in formation of these adhesion sites, vinculin and its isoform metavinculin are key players. It was shown that vinculin null fibroblasts have fewer and smaller focal adhesions, but their turnover is faster (Xu, Baribault et al. 1998). Although vinculin is not necessary for the formation of focal adhesions, it plays a major role in their stabilization. Vinculin forms a platform for many binding ligands, such as paxillin, PIP2, Arp2/3 and VASP (Zamir and Geiger 2001; DeMali, Barlow et al. 2002). The essential role that vinculin plays in generating stable cell adhesions by connecting the actin cytoskeleton to integrins or cadherins via talin or α-catenin (Burridge and Mangeat 1984; Weiss, Kroemker et al. 1998) led me to study the mechanism of actin organization by vinculin.

The vinculin tail domain was shown to bind and bundle actin filaments, and to contain both the actin binding sites and the dimerization site (Johnson and Craig 1995; Johnson and Craig 2000; Subauste, Pertz et al. 2004). However, the exact positions of these sites had not been determined and nothing was known about the nature of this interaction. This led to the first aim of this study, namely the determination of an atomic model of how the vinculin tail binds to and bundles actin

filaments. No large conformational changes have been detected upon F-actin binding (Bakolitsa, de Pereda et al. 1999). In this study, two distinct actin binding sites in the vinculin tail domain were shown to interact with two actin monomers along a filament. One site is located at the top of helices H2 and H3, and the is at the base of helix H3 and includes some residues near the C-terminus. The upper binding site is partially occluded by head domain D1 in full length vinculin, whereas the lower site is fully exposed, explaining the low affinity of vinculin for F-actin and the possible role of F-actin in the combinatorial input activation hypothesis.

Although no large conformational change in the vinculin tail was detected upon F-actin binding, 3D reconstructions of Vt-cross-linked F-actin filaments showed severe clashes between the C-terminal loop of one Vt molecule and the N-terminal strap of another. A mutagenesis study confirmed the involvement of these regions in dimer formation. This led to the proposed mechanism in which binding of Vt to F-actin triggers a conformational change in the C-terminal loop and N-terminal strap of Vt, exposing its dimerization site and enabling Vt to dimerize with another F-actin-bound Vt molecule. Crosslinking actin filaments at sites where talin and α-catenin link F-actin to integrins and cadherins, respectively, might greatly enhance the stabilization of these structures.

Evaluating the combinatorial input hypothesis to activate vinculin

The vinculin tail is an excellent system for studying the detailed mechanism by which it binds and bundles actin its. However, to gain a more complete picture of how vinculin regulates the formation of actin assemblies, the full length vinculin has to be studied. Most of vinculin's ligand binding sites are masked by an intramolecular head-

tail interaction (Johnson and Craig 1994; Johnson and Craig 1995). This interaction has to be relieved in order to activate vinculin and expose its ligand binding sites. The major contacts the tail domain makes with the head domain are the N-terminal bundle of head domain D1 and the neck region (top of D4 and part of D3) (Bakolitsa, Cohen et al. 2004). Vinculin was suggested to be activated by a combinatorial input of two or multiple ligands binding vinculin simultaneously (Bakolitsa et al. 2004). As shown in chapter 3, the upper actin binding site in vinculin is partially shielded by vinculin head domain D1, but the lower binding site is exposed. To bind F-actin tightly, vinculin must be activated. However, since vinculin binds actin filaments weakly in its inactive conformation, F-actin could be one of the potential activators in the combinatorial input hypothesis. This led to the second aim of this work, in which I studied the activation of vinculin in the presence of F-actin and vinculin binding domains of either talin or α-catenin. The fact that the talin constructs do not activate vinculin but α-catenin's CD3-region does, might mean that a different activation mechanism is employed. For example, α-Catenin might induce a slightly different conformational change in the vinculin head domain compared to that induced by talin, and this would enable vinculin to be activated by a combinatorial input of α-catenin and F-actin forming stable cell-cell contacts. Alternatively, activation by talin and F-actin might not fully activate vinculin and an additional step would be required. Since the talin constructs did not activate vinculin in the presence of F-actin, phosphorylation of vinculin might weaken its head-tail interaction just enough for talin and F-actin to fully activate vinculin. Vinculin is known to be highly phosphorylated in nascent focal adhesion sites and focal adhesion sites of highly motile cells, while it is phosphorylated at low levels in mature focal adhesions (Mohl, Kirchgessner et al.

2009). Phosphorylation might induce initial activation of vinculin after which ligands such as F-actin and talin stabilize its conformation and induce formation of stable, mature focal contacts.

Although CD3 appeared to be the most promising activator of vinculin in the presence of F-actin, generation of 2D paracrystalline actin arrays, crosslinked by CD3-activated vinculin, remains a challenge. Different structural actin-vinculin assemblies were observed in the 2D arrays. Anti-vinculin antibodies should be used to confirm the presence of vinculin in these assemblies. If vinculin is indeed present, cryo-electron microscopy and image reconstruction techniques should provide a molecular model of how vinculin crosslinks F-actin in the presence of CD3. To somewhat simplify the system, I used VΔ153, a slightly smaller, constituently active vinculin construct. This construct lacks the first N-terminal four-helix bundle, and hence the major head-tail interface is absent and VΔ153 is considered active. VΔ153 was shown to bundle actin filaments in solution, and 2D actin arrays crosslinked by VΔ153 show that the structural details of actin filaments in these arrays are similar to those cross-linked by the vinculin tail domain: the filaments run in a unipolar direction and do not show any rotational or translational shift relative to each other. The polarity is consistent with how Vt crosslinks actin filaments (chapter 3) and how vinculin bundles actin in the cell (Geiger, Yehuda-Levenberg et al. 1995). However, the distance between filaments is larger, ~13.3nm as compared to 10.5nm for Vt (9nm for F-actin by itself). This distance would fit the tail domains and part of the head domains of two VΔ153 molecules. VΔ153 seems to crosslink F-actin in the array once every crossover (~every 13 actin subunits) and binds two neighboring actin subunits along the filament similar to Vt. To confirm this binding mode more analysis is

required. Images of VΔ153 bound to F-actin should be recorded to yield a 3D reconstruction to determine if the actin binding sites are still similar to Vt. Although the VΔ153 crossbridges seem to appear at regular distances in the raft, close inspection revealed some variation, which is possibly due to the vinculin head domain that connects the tail domain via a flexible linker. The head domain might adopt a variety of different orientations, and this might explain the discrepancy in the distances separating two successive VΔ153 crosslinks.

The observation that the distance between successive actin filaments crosslinked by VΔ153 is almost three times as large as when crosslinked by the vinculin tail, suggests the possibility of a different dimerization site in VΔ153 (since the actin binding sites likely remain the same). This can be verified by mutating the original dimerization site in the tail domain to see if VΔ153 still crosslinks F-actin. Alternatively, a conformational change in the dimerization site might be caused by the presence of the large head domain in combination with its binding to F-actin. To allow for an increased interfilamental spacing, the distance between the actin binding site and dimerization site has to be increased. This requires a conformational change. Other groups have shown that the vinculin tail domain adopts an elongated conformation, which suggests unfurling of the five-helix bundle (Molony and Burridge 1985; Winkler, Lunsdorf et al. 1996). The tail domain might partially unfurl to allow actin crosslinking by the full length protein. This can be determined by generating high resolution density maps using cryo-electron microscopy and fitting the atomic models of F-actin and the vinculin domains into these maps. Once the structural details of vinculin-actin crosslinking in the 2D arrays are known, this should be

extrapolated towards 3D actin bundles using the bonding rules obtained from the arrays.

Recently, a study showed that Shigella invasion protein, IpaA, binds to vinculin and activates its binding to actin, which then induces vinculin-dependent partial barbed end capping (Ramarao, Le Clainche et al. 2007). The structural changes in the vinculin head domain in complex with IpaA's binding region are similar to those observed upon activation with a talin VBS-construct (Izard, Evans et al. 2004; Izard and Vonrhein 2004; Nhieu and Izard 2007). This implies that leaky, barbed-end capping might be also a function of vinculin when it is bound to talin or possibly other ligands in adhesion sites. Polymerization assays using pyrene fluorescence can be used to determine actin filament growth from barbed ends.

Filamentous actin organization by metavinculin

The presence of the highly conserved acidic insert in MVt, which is located in the same domain as the actin binding sites, led me to study metavinculin's affect on actin organization. At the time I conducted these studies, only one group had published on the actin organization in the presence of metavinculin tail (Witt, Zieseniss et al. 2004). They showed that the metavinculin tail does not bundle actin filaments in contrast to the vinculin tail, which induces formation of highly ordered bundles. My goal was to determine why the metavinculin tail affects actin organization differently. It was hypothesized that this difference was caused by the location and nature of the acidic insert, and so we used electron microscopy and 3D image reconstruction methods to study F-actin bound by vinculin and by metavinculin tails. The resulting reconstructions show that the insert does not affect the actin binding sites, since both

tail domains bind similar sites on the actin filament and are oriented similarly. Furthermore, the location of the insert was determined by comparing both reconstructions. The extra density shown in the actin-MVt reconstruction, attributed to the presence of the insert in MVt, is located near the N-terminal strap of the tail domain. This region was suggested to be part of the dimerization site (determined in the actin-vinculin tail model) and might interfere with metavinculin tail dimerization, and hence prevent actin bundling.

Interestingly, an exciting new function of the tail domain was discovered: Metavinculin tail severs actin filaments in a concentration dependent manner. As this result was entirely unexpected, I set out to verify actin severing and confirm that filaments were not appearing shorter due to increased depolymerization and/or actin monomer sequestering. Severing was shown to be most efficient at substoichiometric concentrations of MVt and when filaments are freely available in solution. A mechanism can be suggested in which this protein severs F-actin by binding to the filament sides, which are then mechanically disrupted by intercalation of a potential actin binding region in the insert between two adjacent actin monomers in the curvature of a filament. This potential actin binding region maps to a conserved stretch of amino acids (McLaughlin, Gooch et al. 1993) and it would be informative to learn if mutations in the DDY motif prevent MVt from severing actin filaments. Furthermore, filament bending is dependent on nucleotide state and the bound divalent cation of F-actin (Rebello and Ludescher 1998). A severing preference by MVt of ADP- or Mg^{2+}-actin filaments over ATP- or Ca^{2+}-actin filaments might indicate that MVt favors severing within filament curvatures. In addition to actin severing, the metavinculin tail stabilizes filaments. It prevents actin depolymerization after diluting

actin below its critical concentration. This is most probably due to its binding to the sides of straight actin filaments and not to filament end capping. Stabilization of short, severed actin filaments might be beneficial because they can be readily incorporated into new actin structures that are necessary to withstand transduction forces.

The fact that the earlier study did not observe an actin severing activity for MVt might be due to the larger construct that was used (Witt, Zieseniss et al. 2004). Their protease cleaved metavinculin tail construct starts at aa858 and contains the proline-rich region, whereas the construct used in this study starts at aa879. In addition, this work shows that the larger, constituently-activated metavinculin construct, MVΔ153, also does not sever filaments, but does bundle actin filaments. The highly hydrophobic, proline-rich region, containing the basic residues arginine and lysine, in both MVΔ153 and the protease cleaved metavinculin tail construct, might shield the acidic insert and prevent actin severing. Isoelectric focusing showed that MVΔ153 has a higher pI than expected, suggesting that the acidic insert is indeed shielded in this construct. Together, this implies that metavinculin has a dual function: actin severing in fully activated state, when the insert is completely exposed, and actin bundling in partially activated state. However, this severing function might be an artifact of using only the tail domain. In other words, this function might not be a biological relevant activity of full length metavinculin. *In vivo* experiments aimed at probing the relevance of the MVt severing activity might be complicated by the presence of other (severing) proteins or compensatory mechanisms. In addition, using the full length metavinculin protein is complicated by its requirement to be activated. Therefore MVΔ153 is most promising to study its dual function. The hypothesis would be that MVΔ153 is opened up enough to be able to expose both

actin binding sites in addition to the already exposed dimerization site in order to induce actin bundling, but that an additional conformational change is necessary to reveal the insert. Generation of an x-ray crystallographic model of MVΔ153 would reveal if and how the insert is shielded. Knowing that the R975W-mutation in the metavinculin tail did not make a difference concerning actin organization, this mutation could potentially affect the intramolecular head-tail interaction, influencing the conformational change required to expose the insert.

Like vinculin, full length metavinculin is present in an auto-inhibited conformation due to an intramolecular head-tail interaction. However, it was shown that the affinity of the metavinculin tail domain for the head domain is lower than that of the vinculin tail domain, possibly facilitating activation (Witt, Zieseniss et al. 2004). It would be informative to see whether metavinculin can be activated by similar binding ligands, such as talin and α-catenin, and if only one activator is sufficient or if a similar combinatorial input mechanism is required. Furthermore, it would be interesting to determine the significance of the 8-fold increase in phosphorylation of metavinculin compared to vinculin (Siliciano and Craig 1982; Gimona M. 1988). Phosphorylation might potentially facilitate activation of the protein.

Another topic left unexplored is the reason for both vinculin isoforms to be co-expressed. This study touched it briefly, demonstrating that the tail domains do not heterodimerize in solution and that the presence of MVt causes weaker bundling by Vt. Since MVt was shown to dimerize with PIP2-activated Vt (Witt, Zieseniss et al. 2004), MVt might also dimerize when bound to F-actin with F-actin-bound Vt. I tried to use an antibody against the insert of MVt to determine if MVt was present in actin arrays formed in the presence of both the vinculin and the metavinculin tail.

Unfortunately, this antibody was usable in ELISA's and Western blots, but it failed to recognize native MVt in solution (as confirmed by size-exclusion chromatography and native gel electrophoresis). A tagged MVt construct would be more helpful for detection. Vt is shown to be able to homodimerize after a conformational change induced upon F-actin binding, in which the C-terminal region of the tail domain is suggested to move away to expose the dimerization site. If this would also be true for MVt, a vinculin and a metavinculin tail construct that both lack their C-terminal region might be able to interact. Even more interesting would be to determine what would happen to F-actin in the cell adhesion sites in the presence of increasing concentrations of metavinculin. However, although vinculin and metavinculin were localized in the same cellular complex, it is not known if they actually interact with each other. Fusion constructs of cyan fluorescent protein-vinculin tail and yellow fluorescent protein-metavinculin tail could be used to determine Förster resonance energy transfer (FRET) if and when vinculin and metavinculin tails interact in the cell. Together, this would allow us to understand more about the necessity of a second vinculin isoform.

References

Bakolitsa, C., D. M. Cohen, et al. (2004). "Structural basis for vinculin activation at sites of cell adhesion." Nature **430**(6999): 583-6.

Bakolitsa, C., J. M. de Pereda, et al. (1999). "Crystal structure of the vinculin tail suggests a pathway for activation." Cell **99**(6): 603-13.

Burridge, K. and P. Mangeat (1984). "An interaction between vinculin and talin." Nature **308**(5961): 744-6.

DeMali, K. A., C. A. Barlow, et al. (2002). "Recruitment of the Arp2/3 complex to vinculin: coupling membrane protrusion to matrix adhesion." J Cell Biol **159**(5): 881-91.

Gimona, M., J. V. Small, et al. (1988). "Porcine vinculin and metavinculin differ by a 68-residue insert located close to the carboxy-terminal part of the molecule." Embo J **7**(8): 2329-34.

Gimona M., S. J. V., Moeremans M., van Damme J., Puype M., Vandekerckhove J. (1988). "Molecular domain structure of porcine vinculin and metavinculin." protoplasma **145**: 133-140.

Izard, T., G. Evans, et al. (2004). "Vinculin activation by talin through helical bundle conversion." Nature **427**(6970): 171-5.

Izard, T. and C. Vonrhein (2004). "Structural basis for amplifying vinculin activation by talin." J Biol Chem **279**(26): 27667-78.

Johnson, R. P. and S. W. Craig (1994). "An intramolecular association between the head and tail domains of vinculin modulates talin binding." J Biol Chem **269**(17): 12611-9.

Johnson, R. P. and S. W. Craig (1995). "F-actin binding site masked by the intramolecular association of vinculin head and tail domains." Nature **373**(6511): 261-4.

Johnson, R. P. and S. W. Craig (2000). "Actin activates a cryptic dimerization potential of the vinculin tail domain." J Biol Chem **275**(1): 95-105.

McLaughlin, P. J., J. T. Gooch, et al. (1993). “Structure of gelsolin segment 1-actin complex and the mechanism of filament severing.” Nature **364**(6439): 685-92.

Mohl, C., N. Kirchgessner, et al. (2009). "Becoming stable and strong: the interplay between vinculin exchange dynamics and adhesion strength during adhesion site maturation." Cell Motil Cytoskeleton **66**(6): 350-64.

MolonyL., K. Burridge (1985). "Molecular shape and self-association of vinculin and metavinculin." J Cell Biochem **29**(1): 31-6.

Nhieu, G. T. and T. Izard (2007). "Vinculin binding in its closed conformation by a helix addition mechanism." Embo J **26**(21): 4588-96.

Ramarao, N., C. Le Clainche, et al. (2007). "Capping of actin filaments by vinculin activated by the Shigella IpaA carboxyl-terminal domain." FEBS Lett **581**(5): 853-7.

Rebello, C. A. and R. D. Ludescher (1998). "Influence of tightly bound Mg2+ and Ca2+, nucleotides, and phalloidin on the microsecond torsional flexibility of F-actin." Biochemistry **37**(41): 14529-38.

Siliciano, J. D. and S. W. Craig (1982). "Meta-vinculin--a vinculin-related protein with solubility properties of a membrane protein." Nature **300**(5892): 533-5.

Subauste, M. C., O. Pertz, et al. (2004). "Vinculin modulation of paxillin-FAK interactions regulates ERK to control survival and motility." J Cell Biol **165**(3): 371-81.

Weiss, E. E., M. Kroemker, et al. (1998). "Vinculin is part of the cadherin-catenin junctional complex: complex formation between alpha-catenin and vinculin." J Cell Biol **141**(3): 755-64.

Winkler, J., H. Lunsdorf, B.M. Jockusch (1996). "The ultrastructure of chicken gizzard vinculin as visualized by high-resolution electron microscopy." J Struct Biol **116**(2): 270-7.

Witt, S., A. Zieseniss, et al. (2004). "Comparative biochemical analysis suggests that vinculin and metavinculin cooperate in muscular adhesion sites." J Biol Chem **279**(30): 31533-43.

Xu, W., H. Baribault, et al. (1998). "Vinculin knockout results in heart and brain defects during embryonic development." Development **125**(2): 327-37.

Zamir, E. and B. Geiger (2001). "Components of cell-matrix adhesions." J Cell Sci **114**(Pt 20): 3577-9.